Supplementary Materials for

Whole-genome analyses resolve early branches in the tree of life of modern birds

Erich D. Jarvis,* Siavash Mirarab, Andre J. Aberer, Bo Li, Peter Houde, Cai Li, Simon Y. W. Ho, Brant C. Faircloth, Benoit Nabholz, Jason T. Howard, Alexander Suh, Claudia C. Weber, Rute R. da Fonseca, Jianwen Li, Fang Zhang, Hui Li, Long Zhou, Nitish Narula, Liang Liu, Ganesh Ganapathy, Bastien Boussau, Md. Shamsuzzoha Bayzid, Volodymyr Zavidovych, Sankar Subramanian, Toni Gabaldón, Salvador Capella-Gutiérrez, Jaime Huerta-Cepas, Bhanu Rekepalli, Kasper Munch, Mikkel Schierup, Bent Lindow, Wesley C. Warren, David Ray, Richard E. Green, Michael W. Bruford, Xiangjiang Zhan, Andrew Dixon, Shengbin Li, Ning Li, Yinhua Huang, Elizabeth P. Derryberry, Mads Frost Bertelsen, Frederick H. Sheldon, Robb T. Brumfield, Claudio V. Mello, Peter V. Lovell, Morgan Wirthlin, Maria Paula Cruz Schneider, Francisco Prosdocimi, José Alfredo Samaniego, Amhed Missael Vargas Velazquez, Alonzo Alfaro-Núñez, Paula F. Campos, Bent Petersen, Thomas Sicheritz-Ponten, An Pas, Tom Bailey, Paul Scofield, Michael Bunce, David M. Lambert, Qi Zhou, Polina Perelman, Amy C. Driskell, Beth Shapiro, Zijun Xiong, Yongli Zeng, Shiping Liu, Zhenyu Li, Binghang Liu, Kui Wu, Jin Xiao, Xiong Yinqi, Qiuemei Zheng, Yong Zhang, Huanming Yang, Jian Wang, Linnea Smeds, Frank E. Rheindt, Michael Braun, Jon Fjeldsa, Ludovic Orlando, F. Keith Barker, Knud Andreas Jønsson, Warren Johnson, Klaus-Peter Koepfli, Stephen O'Brien, David Haussler, Oliver A. Ryder, Carsten Rahbek, Eske Willerslev, Gary R. Graves, Travis C. Glenn, John McCormack, Dave Burt, Hans Ellegren, Per Alström, Scott V. Edwards, Alexandros Stamatakis, David P. Mindell, Joel Cracraft, Edward L. Braun, Tandy Warnow,* Wang Jun,* M. Thomas P. Gilbert,* Guojie Zhang*

*Corresponding author. E-mail: jarvis@neuro.duke.edu (E.D.J.); tandywarnow@gmail.com (T.W.); mtpgilbert@gmail.com (M.T.P.G.); wangj@genomics.cn (W.J.); zhanggj@genomics.cn (G. Z.)

This PDF file includes:
> Supplementary Text SM1 to SM13
> Figs. S1 to S29
> Tables S2 to S15
> Appendices
> Full Reference List

Other Supplementary Material for this manuscript includes the following:
(available at www.sciencemag.org/content/346/6215/1320/suppl/DC1)
> Tables S1, S16, and S17

Author contributions

Supplemental Acknowledgments

Contents

SM1 Rationale for selection of species, sex, tissue sources, and bird collection details

Erich D Jarvis, M. Thomas P. Gilbert, Guojie Zhang, Jason Howard, Jon Fjeldså, Knud Andreas Jønsson, Ludovic Orlando, Mads Bertelsen, Michael Bunce, Frank Keith Barker, Frederick Sheldon, Elizabeth Derryberry, Stephen O'Brien, David Haussler, Oliver Ryder, Klaus Koepfli, Warren Johnson, Peter Houde, Scott Edwards, Joel Cracraft, Gary Graves.

In mid-2010 we brought together four research consortia that were engaged in planning to, or active in sequencing of avian and reptile genomes (**Table S1, column C**): 1) Individuals sequencing a genome at their own institution [3 avian genomes, the budgerigar and bald eagle, led by Jarvis and Warren, and Hoatzin by Houde; and the alligator by Green, Ray, and Braun]; 2) individuals collaborating with BGI on species-specific genome projects [8 avian genomes; and the green sea turtle genome]; 3) the genome 10,000 (G10K) group who were collaborating with BGI to produce a set of 101 high quality vertebrate genomes [of which 11 were avian genomes, including the hoatzin] (http://ldl.genomics.org.cn/page/bgi-g10k.jsp) and with the National Institutes of Health to sequence the bald eagle genome at Washington University; and 4) a group based at the Natural History Museum of Denmark (Copenhagen) collaborating with BGI to sequence avian genomes for the purpose of resolving Neoavian phylogeny [25 low coverage avian genomes]. At the time of merging efforts, each group (particularly the G10K-BGI and Copenhagen-BGI collaborations) modified their list of species until we had at least one species per order of Neognathae (*36, 37*) and two Palaeognathae orders as defined in the International Ornithology Congress (IOC) list in 2011 Version 2.10 generated on 2011-10-20 (*103*). The inclusion of multiple species for specific orders enabled the targeting of non-phylogeny based questions that specific collaborators wished to address.

We sequenced or obtained the genome sequences of one species of each known waterbird order (except sequenced 2 penguins, and did not obtain a stork) that were thought to belong to separate orders. In the interim, the Howard and Moore 2013 classification of birds was published (*36, 37*), where they grouped 4 of the 10 Neoaves waterbird orders into one, which they called Pelecaniformes (**Figs. 1, S1**). This makes it appear as if this part of the tree is over-represented with waterbirds from Pelecaniformes, when in fact our sampling covers a representative of each of the problematic lineages believed by some to make the traditionally defined orders non-monophyletic. Given the relatively ancient divergences of these waterbird lineages before 50 MYA, comparable to the divergence time for a number of other orders, they may deserve reclassification as separate orders. However, doing so would require additional taxa sampling in this part of the tree to be more certain.

For the G10K species selection, additional criteria included: 1) that the species is studied by a well-established biological community; 2) can be used in biological applications for science, comparative medicine or society; 3) the species is a popular image, recognition or utility (e.g. domesticated species, conservation targets, national animals, wildlife icons); and 4) there exists an explicit scientific value in studying the selected species historically and for the future.

In terms of specific scientific questions, one we focused on was choosing species to answer questions on genetics of vocal learning. Vocal learning is a critical behavior for spoken language in humans and only a few rare groups of birds have vocal learning behavior and the neural circuitry for it (*38*). Thus we chose representative species of the three well-known vocal learning lineages (oscine songbirds, parrots, and hummingbirds) and their closest vocal non-

learning relatives, according to phylogenies from different sources (*15, 17, 18, 24, 26, 29, 38, 39*). Although Hackett et al 2008 (*17*) for the first time brought together Psittaciformes and Passeriformes as sisters, the support was relatively weak (77%) compared to the support we obtained. Moreover, they did not mention the implications for the evolution of vocal learning. After we sequenced the selected species, Suh et al 2011 (*29*) used TEs to support this relationship and interpreted the findings for understanding the evolution of vocal learning, but there were a number of polytomies in their tree which did not resolve the position of hummingbirds. Several other recent nuclear gene studies *(26-27)* also supported Psittaciformes-Passeriformes monophyly, but contemporaneous morphological and mitochondrial phylogenies rejected this relationship (*14, 15, 18*). We also generated genome sequences of some species for branches that would break up deep nodes in the Caprimulgiformes (oilbird and potoo genomes) discovered midway through the project and that would also contribute to questions on origins of vocal learning. The sequencing and assembly of these genomes were conducted by the Brazilian consortium part of our collaboration, although these were not completed in time to be included in the current study. They will be included in future investigations.

In terms of choosing which sex to sequence, different groups had different rationales. The G10K group and individual collaborators with BGI chose to sequence mostly males based on advice from those that had sequenced the chicken genome, where it was difficult to assemble the sex chromosomes in the heterogameotic (ZW) female; males in birds are homogametic (ZZ). In contrast, for the dataset predominantly assembled by the Copenhagen collaboration, we chose to focus on females, in case new computational tools would allow us to assemble the sex chromosomes and study sex chromosome evolution. The result was that of the 45 new genomes, 21 were female. As hoped, we developed a new computational analysis tool for sex chromosome assembly and analyses of females and were able to generate novel findings on sex chromosome evolution in a companion study (*104*).

In summary, the final collection of avian genomes in this collaboration was 48 species (*44*), including the three previously published genomes of chicken, turkey and zebra finch. In **Table S1** we list the tissue sources, source IDs, the persons and institutes responsible for the collection and DNA processing, and some information about each animal.

SM2 Identification and annotation of total evidence nucleotide and whole genome datasets

Bo Li, Erich D. Jarvis, Cai Li, Guojie Zhang, Brant C. Faircloth, Claudio Mello

We initially made several attempts to identify a total evidence nucleotide dataset useful for phylogenomic inference across the selected taxa using a host of standard tools, including TreeFam, dN/dS distances, and reciprocal BLAST. These were unsuccessful in identifying sufficient numbers of accurate orthologs across the taxa under study. The common problem was either that paralogs were observed to be annotated as orthologs or different exons of different splice variants were being pulled into the annotated genes from different species, although all species had all exons represented in the scaffolds or raw reads. This problem was contributed in part by the pre-existing chicken v3 and zebra finch v1 genome annotations, which had inconsistencies with each other (some exons included in one species, but not the other, or paralogs incorrectly identified as orthologs) and the annotation methods were not ideal. We also

tried to use transcriptome data representing 10 (*105*) of the 48 bird species, but found that different splice variants from different species caused differences in annotations. Thus, the objective of the annotation schemes below was to generate a more uniform reference chicken and zebra finch gene set utilizing human sequences, and then propagate those annotations to the other 46 species. This means that the annotations will change relative to the previously published genomes. Part of this process is also described in our companion comparative genomics paper (*44*), as we used this annotated set for comparative analyses. Missing from many of the protein coding gene annotations are 5' and 3' UTRs, as we wanted to generate a phylogeny based upon coding sequence only.

8251 protein-coding exon gene set

We started with the homology-based predicted 13,000-18,000 protein coding genes for all species reported in our companion study (*44*), which was based on sequence identity to the chicken, zebra finch, and human genomes. In that annotation pipeline, a large reference gene set of exons (predicted transcripts) from the three reference species was created, here of which we used 12,484 putative orthologs, consisting of 7,832 zebra finch and 4,652 chicken genes present in both species. The difference in the choice of species to use for a specific reference gene was based on which one (chicken or zebra finch) had the most complete annotated gene model.

We used this reference set to make the chicken and zebra finch annotations more uniform across the two species. For chicken, the 7,832 zebra finch_ORTH proteins were used as reference genes to run Genewise to re-annotate the corresponding orthologs in the chicken genome. For each orthologous gene pair, we used the re-predicted gene model to replace the chicken Ensembl gene model. Conversely, the 4,652 chicken_ORTH proteins were used as reference genes to re-annotate the corresponding orthologs in zebra finch, with the same procedure as that applied on chicken.

We found that several exons had overlapping coordinates in the chicken or zebra finch genomes and removed them, because counting the same sequence twice in phylogenomic analyses would bias the results. We also manually curated the protein coding genes that had the highest dN/dS values > 1 (~40 genes) among all birds, and found that several of them consisted solely of mis-annotated short exons without a start codon and in the antisense orientation to a protein coding exon or in intronic regions of a longer validated protein coding gene. We thus removed them. This filtering step reduced the number of orthologs from 8295 to 8251.

Next, we developed and used two methods to select among the putative orthologous genes those that were clearly syntenic between zebra finch and chicken, and took the union of the two. For the first method we used protein sequence alignments, and for the second we used the whole genome alignment to chicken, building pair-wise orthologs between chicken and another species (47 avian and 4 outgroup species).

1) Protein sequence alignment: We aligned protein sequences of the two gene sets to each other by BLASTP with a E-value cut-off of 1e-5, and combined local alignments with the SOLAR program (*106*) (download from http://treesoft.svn.sourceforge.net/viewrc/treesoft/). We filtered out those candidate orthologs with homologous block lengths of < 30% of length of the longest protein. In addition we filtered out candidate orthologs with identity < 50%.

2) Best-hit orthologs: We first identified reciprocal best hit (RBH) orthologs in all aligned gene pairs by using the same average coverage ratio (30%) and sequence identity (50%) cutoffs.

To save candidate orthologs from the strict RBH method, we identified RBH orthologs for the second and third round by masking known RBH genes.

3) Gene synteny orthologs: We placed best-hit gene pairs on their chromosomes according to chicken, and sorted them in order. One best-hit gene pair (A_1A_2; 1 and 2 denote chicken and another species) and its nearest best-hit gene pair (B_1B_2) were considered to have syntenic evidence if they met the following requirements : a) genes A1 and B1 are on same chromosome or scaffold; b) genes A2 and B2 are on same chromosome or scaffold; c) the number of genes between A1 and B1 < 5; d) the number of genes between A2 and B2 < 5. We also retained best-hit gene pair if one of their scaffolds only has one gene.

4) Candidate syntenic gene pairs based on genomic synteny: We placed coding regions in genomic syntenic blocks (Net files with AXT format from pairwise genome alignments between chicken and another species), identified syntenic gene pairs, and calculated gene-in-synteny ratio for each gene (synteny-region-length/total-coding-region-length) and syntenic ratio (syntenic length of the two genes/length of the shorter gene). We filtered out syntenic gene pairs with gene-in-synteny ratio < 0.3 or syntenic ratio < 0.3.

5) Candidate syntenic gene pairs filtering: In the whole genome alignment (WGA), a query may align onto more than one target genomic loci by using LASTZ. In this condition, a gene in target genome will have more than one ortholog (such as AB and AC; A, B, and C denote genes) by using step 4 above. We firstly generated species-chicken syntenic gene pairs from species-chicken WGA and used this syntenic ortholog set to determine which gene pair is real. We furthermore removed syntenic gene pairs with stricter cut offs (syntenic ratio < 0.5) where we can filter out a gene's false syntenic ortholog. Finally, we removed all genes with more than one syntenic ortholog.

6) Final orthologs: We built pair-wise orthologs between the chicken gene set and one gene set of each other species (47 avian and 4 outgroup species) by retaining orthologs supported by protein similarity (steps 1 and 2), gene synteny (step 3), and genome synteny (steps 4 and 5). We then constructed the orthologous genes of the 52 species through merging pair-wise orthologs according to the reference chicken gene set. The final result was that the 12,484 putative orthologs were reduced to a higher quality orthologous 8251 syntenic set of protein coding genes.

2516 intron gene set

We generated conserved orthologous introns from the 8251 protein coding genes among the 52 species using the following steps:

1) Determining exon/intron boundaries with GeneWise: From the pair-wise synteny-based orthologous exon sequence alignments of the 8251 genes, we extracted the intronic regions and 2000bp upstream and downstream. The extracted sequences and corresponding chicken protein sequences were applied to GeneWise (*40*) to generate exon-intron boundaries and gene models. The introns with conserved exon-intron boundaries between chicken and another species (±1 codon) were chosen as candidate pair-wise orthologous introns.

2) Filtering out introns with different boundaries and sequence lengths: We removed pair-wise orthologous introns in which another species (not chicken) had a different gene model generated by the synteny-based pair-wise orthologous method above and the Genewise protein coding gene predictions. We also filtered out introns with length < 50 bp or intron ratio > 1.5 between chicken and another species or another species and chicken.

7

3) Merging: We merged pair-wise orthologous introns according to the reference chicken gene set, which resulted in concatenated intron sequence of 2516 genes from the 8251 protein coding gene set.

3679 UCE locus set

To create a large set of unique UCE regions, we combined UCE loci previously identified as conserved among vertebrates (*107, 108*), removed duplicate and reciprocal duplicate loci from the candidate set, and designed sequence capture probes (120 nt) for *in silico* capture of these loci (*108*). We aligned sequence capture probes to each avian genome assembly using a parallel wrapper around LASTZ (*109, 110*) (**Appendix A**). We searched each gene assembly for shorter probe sequences designed from UCE loci rather than the entire length of each UCE locus to standardize the specificity of search parameters across probes (which are identical lengths) versus UCE loci (which are different lengths), increase the number of loci detected, and facilitate detection and removal of duplicated or partially duplicated UCE loci (see below).

Based upon match coordinates returned from LASTZ, we sliced each UCE probe position at ± 1000 bp of flanking sequence from individual genome assemblies (*44*). Where we recovered slices derived from multiple probes targeting the same locus, we re-assembled sequences back into full UCE loci using code (assemble_contigs_from_genomes.py) in the PHYLUCE package (v1.0; https://github.com/faircloth-lab/PHYLUCE). During the re-assembly process, we also removed contigs hit by probes designed from different UCE loci as well as contigs matching the source UCE loci from which we designed probes having multiple hits. At the end of the reassembly and locus-assignment process, we used another code (get_match_counts.py) to create a relational database of UCE loci we identified in each genome assembly. We used the relational database to generate a complete data matrix (no missing taxa) of UCE loci shared among all avian genome assemblies, and we generated a FASTA file containing sequence data for all UCE loci in the complete data matrix.

UCE loci are sometimes located in proximate clusters (*111*) such that reasonably long sequence slices centered on proximate UCEs may overlap, while the core, conserved regions of individual UCE loci do not. Compactness of avian genomes (see (*112*) for review) may increase the proximity of UCEs and, as a result, the count of UCEs within clusters. To identify and remove these clusters, we aligned chicken UCE loci in the complete data matrix to the chicken reference assembly (UCSC galGal v3, downloaded June 6, 2012) using LASTZ, converted LASTZ match coordinates to BED format, and identified UCE loci with overlapping flanks using BEDTOOLS (*113*). We removed overlapping UCE loci from the data set. To identify UCE loci overlapping exons, we used BEDTOOLS to intersect the coordinates of remaining loci with REFSEQ (*114*) exon coordinates for chicken, and removed all UCE loci overlapping known exons. To ensure UCE data did not overlap introns used in our other analyses (2516 intron gene set), we extracted the chicken sequence from each UCE alignment, converted the sequence to FASTA format, and aligned them to chicken introns using LASTZ and BLAT (*115*), and removed all UCE alignments that overlapped with our chicken intron sequences (>= 80% identity over >= 100 bp). We also removed all UCE loci containing sequence data with non-standard or ambiguous nucleotide representations (e.g. at least one or more "X" or "N"). We aligned the remaining loci using SATé+MAFFT, and filtered poorly aligned regions as described in SM3.

Using the above approach, we identified 9,821 UCE loci shared among vertebrates, and we designed 12,253 probes targeting these UCE loci. After aligning UCE probes to each genome assembly, filtering duplicate hits, removing overlapping UCEs in clusters, and creating a 100% complete data matrix (no missing data for any taxon), we identified 4,097 UCE loci shared among all taxa. We removed one alignment from the complete set of UCE loci because the chicken sequence did not adequately map back to the chicken reference genome. We identified and filtered out 335 UCE loci that overlapped with exons and 82 that overlapped with introns. This resulted in a final set of 3,679 putatively non-coding UCE loci.

Whole genome data set
We generated a pair-wise whole genome alignment. We downloaded the whole genome alignment (WGA) of human-chicken and chicken-zebra finch from the UCSC website. We carried out WGA between genomes of chicken and another species using LASTZ program with parameters of "--step=19 --hspthresh=2200 --gappedthresh=10000 --ydrop=3400 --inner=2000 --seed=12of19 --format=axt --scores=HoxD55" and Chain/Net package with parameters of " –minScore=5000" for axtChain program and default parameters for other programs. We furthermore used chainSwap and other Chain/Net programs to convert the chicken-species WGA (chicken as target genome) to a species-chicken WGA (another species as target). The two Net results with AXT format for each pair-wise species were used for further analysis. To prevent multiple hits from the whole genome alignment being used, we took the best hits from the reciprocal best hits, and filtered out multiple hits.

SM3 Alignments and their filtering
Siavash Mirarab, Tandy Warnow, Rute da Fonseca, M. Thomas P. Gilbert, Cai Li, Guojie Zhang, Brant C. Faircloth, Erich D. Jarvis

All multiple sequence alignments (MSA) (including those mentioned in the previous sections) were performed in two rounds. The first round was used to find contiguous portions of sequences that we identified as aberrant. These aberrant sequences were of two types: 1) portions of the alignment where only one species contributed to the alignment; and 2) portions of a sequence for one species that was aligned to other sequences but did not appear to be homologous to any other species in that part of the alignment (see below for criteria used to judge homology). These aberrant sequences reflect both real single species differences, as well as errors in assembly, annotation, or alignment. The first type (i.e. single species columns) could reflect real insertions in one species (or deletion in all the other taxa), but such single-species sites are not useful for tree estimation using standard substitution-based models, and removing these does not lead to loss of data. The remaining aberrant sequences reflect error in assembly, annotation, or alignment. These would introduce error in phylogenetic inference. Thus, once identified, aberrant sequences were removed, and a second MSA round was performed.

To minimize alignment error, we needed an aligner that generated the best balance of avoiding aligning non-homologous sequences (thus introducing false positives) and avoiding not aligning truly homologous sequences (thus introducing false negatives). After trying many MSA methods (MAFFT, Prank, Muscle, and SATé in combination with others) (*53, 116-118*) on a test set of over 200 randomly chosen exons and introns from the 8251 protein coding gene set, we

found SATé+Prank was superior in the first MSA round in leaving a large portion of aberrant sequences unaligned while still generating good alignments for the remaining "correct" sequences (based on visual inspection by multiple observers). SATé is a tool for iterative alignment and tree co-estimation, and uses other tools internally for aligning subsets of taxa, merging sub-alignments, and for estimating phylogenetic trees (*53, 54, 119, 120*). In addition to the choice of these tools, SATé is parameterized by subset size, stopping rule, decomposition size, and the choice of an initial tree. We set the algorithmic parameters for SATé differently based on the type of data and whether we were using SATé to do the first round (identifying the aberrant sequences) or the second round (obtaining an accurate alignment on the sequence dataset after the aberrant sequences were removed). SATé+Prank and SATé+MAFFT refer to versions of SATé that internally use Prank and MAFFT, respectively, for aligning subsets. For the second round, SATé+MAFFT was preferred if feasible, because we found, consistent with previous studies (*53, 54*), that this combination resulted in the best accuracy once aberrant sequences were no longer present.

SATé internally uses an external tool for merging alignments on subsets and multiple options were available for this merger step. The performance of these merger tools was impacted by the type of sequence data. MUSCLE was superior for merging amino acid alignments, while Opal (*119*) performed better with DNA. **Table S2** outlines SATé parameters used for different datasets and **Appendix B** provides the exact configurations used.

Sequences that were very short (i.e. individual 100-200bp segments for the whole genome alignment; see below) were handled using MAFFT alone instead of SATé+MAFFT. SATé uses iterations to estimate alignments, but where sequences are very short, iterations do not improve alignments compared to MAFFT. Furthermore, MAFFT was computationally less demanding (it required much less I/O), which is important when millions of segments are being aligned in a whole genome alignment.

Once the alignments were made, to filter the two types of aberrant sequences we developed our own scripts. We found that readily available programs, such as G-blocks (*120*), were too aggressive and resulted in many false negatives and thereby a highly conserved alignment that would bias phylogenetic inference. We also found that different types of genomic partitions (exon vs the rest of the genome) required different filtering parameters to minimize false positives and false negatives.

We performed a series of initial analyses by estimating trees with a subset of the 77 fastest evolving genes (all genes with average p-distance > 0.25), and found that: 1) the choice between alignment methods (SATé+MAFFT, SATé+Prank, and MAFFT only) mostly affected low support edges in the species tree (i.e. alignment errors not properly filtered out could change the topology of those edges); and 2) SATé+MAFFT alignment resulted in higher bootstrap support compared to other methods. When Prank was used for aligning subsets, due to computational challenges, we had to reduce the alignment subset size to 20%, so that each subset aligned by Prank was smaller. The following are the specific approaches used for each type of genomic partition.

Exon alignment and filtering
The first round of alignment was performed using SATé+Prank, and after filtering the second round was performed using SATé+MAFFT. Before alignment, we concatenated amino acid sequences of all exonic regions belonging to the same gene. We did not align individual exons

because SATé relies on phylogenetic estimation for guiding its alignment, and very short exons could result in poor phylogenetic estimation and therefore poor alignments. We used amino acid sequences to build the alignment, as they preserved the codon frame, and back translated into DNA using a custom Perl script that preserved reading frame. We used the default JTT model in SATé because we found it to fit our data best for most genes.

Filtering step: It was simple to filter out cases where only one species had sequence in an alignment site. To filter out over-aligned sequences, sections within individual sequences were determined to be aberrant or correct based on a model that uses the divergence between species for each column of the alignment. The values of the parameters of the model are based on manual annotation of the alignments of the randomly chosen 200 gene set. Based on this manual analysis, we determined that we needed to calculate four parameters per sequence per window (length 12) of the alignment, using the following algorithms:

1. The first parameter **A** is based on the probability of observing the amino acids (**AA**s) in a sequence in a given window of the alignment. The probability of observing amino acid **a** in position **i** in a sequence **S** in an alignment corresponds to the counts for that amino acid, $c(a_i^S)$, divided by the number of sequences **N**:

$$P(a_i^S) = \frac{c(a_i^S)}{N} \qquad (1)$$

The parameter **A** for a window of sequence **S** corresponds to the sum of these probabilities for each position of the window divided by the length of the window **L**:

$$A(S) = \sum_{i=1}^{L} \frac{P(a_i^S)}{L} \qquad (2)$$

2. The second parameter **B** is based on the smallest pairwise distance to another amino acid in that position calculated using blosum62 (*121*). The use of a column-by-column score lowers the probability of an orthologous sequence that shares high sequence similarity with different orthologs in different sites of the window to be labeled as "wrong". For each position **i** of the sequence **S**, a_i^S is compared to each of the amino acids on that position in the other sequences. The distance to amino acid **b_i** in another sequence **X** that has the smallest dissimilarity to a_i^S corresponds to the highest pairwise blosum62 distance:

$$d(a_i^S) = max\{D(a_i^S, b_i^X) : b \neq a , X \neq S\} \quad (3)$$

The **B** parameter corresponds to the average of those distances:

$$B(S) = \sum_{i=1}^{L} \frac{d(a_i^S)}{L} \qquad (4)$$

3-4. The two other parameters used in the model are the Z-scores of the A and B parameters, Z_A and Z_B.

The four parameters were used to train a logistic regression model using the R package (*122*) and the regions manually annotated as being outliers ($t = 1$) with all the others ($t = 0$). Sequence segments were discarded that had more than 40% gaps or $P(a_i^S) < 70\%$, indicative of very conserved sequences. The resulting model:

$$t = 1 + 2.21 * A + 0.36 * Z_B + 1.32 * Z_A + 0.06 * B - 1.5 * B * A -$$
$$0.70 * Z_A * A - 0.10 * Z_A * Z_B \quad (5)$$

was then used to calculate t for all the windows within each sequence of each alignment. Overlapping windows with $t > 0$ were merged, and if they contained at least one window with $t > 3$ they were tagged as potentially corresponding to misannotations or resulting from alignment problems ($t = 3$ was chose after evaluating the false negative and false positive rate using the manual annotations). We generated exon alignments both with (13,553,087 nucleotide sites) and without (13,294,276 sites) non-avian outgroups (human, lizard, turtle, and alligator).

Protein Model selection: Once the alignments were estimated, we used them to select the best amino acid substitution model for subsequent phylogenetic analyses. We selected a separate substitution model for each gene using a Perl script developed by Alexis Stamatakis (available at http://www.exelixis-lab.org/software/ProteinModelSelection.pl). This script first estimates a parsimony tree, and then scores the alignment based on a list of protein substitution models. It then reports the best scoring AA substitution model. The following models were considered: "DAYHOFF", "DCMUT", "JTT", "MTREV", "WAG", "RTREV", "CPREV", "VT", "BLOSUM62", "MTMAM", "DAYHOFFF", "DCMUTF", "JTTF", "MTREVF", "WAGF", "RTREVF", "CPREVF", "VTF", "BLOSUM62F", "MTMAMF". On our dataset, for 91% of the genes either JTT or JTTF were found as the best scoring model.

Intron alignment and filtering
The procedure used to align introns was similar to exons, but was simpler as there is no amino acid sequence evolution to model. Important differences from the exon procedure were that we used SATé+MAFFT for both rounds of alignment and we aligned each intron from the same gene individually instead of concatenating them. We found SATé+Prank on the long introns to be too computationally intensive, limiting its practicality for very long alignments (**Fig. S19** shows alignment lengths). Also, we were able to reliably align each intron individually since they were typically much longer than exons. To identify and filter out over-aligned sequences, we scanned for regions of >=36 bp window size (equivalent to the 12 amino acid criterion for exons) that have <55% sequence identity to all other species in the alignment with gaps allowed;

these were removed from the alignment. We tried sequence identity cut-off values from 25-60% (in 5% increments) and found 60% clearly resulted in too many false negatives and 50% in not enough true positives; so 55% was finally used. After filtering was done, we built a new SATé+MAFFT alignment and subsequently concatenated all introns belonging to the same gene using a custom Perl script. We generated intron alignments both with (19,530,152 sites) and without (19,258,311 sites) non-avian outgroups (human, lizard, turtle, and alligator).

UCE alignment and filtering
Both rounds of the alignment were done SATé+MAFFT. We filtered aberrant aligned sequences in the UCEs using the same code applied to the introns above. Using code (nexus_to_concatenated_phylip.py) available in the PHYLUCE package (v1.0; https://github.com/faircloth-lab/PHYLUCE), we prepared the 3,679 UCE alignments for gene tree and concatenated species tree analyses with (UCE+outgroup) and without (UCE) a non-avian outgroup (alligator). The UCE+outgroup concatenated alignment consisted of 9,251,694 sites, including 5,012,622 site patterns; and the UCE alignment without outgroups consisted of 9,229,346 sites, including 4,833,835 site patterns; the average length of a filtered UCE+outgroup alignments was 2,514 bp (95CI = 5.22; min=1,787; max=3,527; **Fig. S19**). The average length of filtered UCE without outgroup alignment was 2,508 bp (95CI = 5.31; min=1,803; max=3,561).

Whole genome alignment and filtering
Whole genome alignments were first created by a LASTZ+MULTIZ (*109, 123*) (http://www.bx.psu.edu/miller_lab/) pipeline across all 48 bird species and outgroups using individual chromosomes of the chicken genome as the reference (initial alignment 392,719,329 Mb). We only allowed a 1:1 mapping to the chicken sequence, choosing the hits with the highest identity, to reduce the probability of finding paralogs. MULTIZ alignment segments were roughly 100-200 bps long, with millions of such segments in the whole genome alignment. Segments with less than 42 avian species (> 5 missing bird species) were removed to eliminate bias of species that are more closely related to the chicken reference genome, and to allow missing non-assembled data of at least five species, which was possible since we had bird orders where 2 or 3 species were sequenced (**Fig. 1**). Thereafter, aberrant sequences were identified and removed from the segments using the same approach applied to the introns, and individual remaining segments of the MULTIZ alignment were realigned with MAFFT (version v6.860b). We were not as confident that a SATé+ MAFFT alignment would give more accurate alignments and calculating SATé alignments on all segments was not feasible due to computational challenges (required too much I/O). We used the most accurate version of MAFFT available (L-INS-I) with the following command: mafft --maxiterate 1000 –localpair. The combined filtering steps resulted in about 70 Mb removed from the initial alignment. All individual segments were concatenated (using custom Perl scripts) to get a final whole genome alignment containing 322,150,876 sites.

Results: filtered out and missing data in the alignment
Figure S20 shows the relative amounts of data filtered out in our manual analyses of the 200 protein coding genes, and in all exons, introns, and UCEs in the alignment across species. Overaligned sequences (false positives) occurred at a higher percentage than single species sequence alignments. Not surprisingly, more sequences were filtered out from the introns and

UCEs (with their flanking divergent sequences) as they are more divergent than exons. The outgroups had the highest filtered out values, which is consistent with them being more divergent to all birds than birds among birds. Within birds, the woodpecker had the most sequences filtered out (10-12% of the intron and UCE alignments; 1.4% of the exon alignment), consistent with the finding in our companion study that the woodpecker has an extremely higher amount of unique repeat elements found in no other bird species sequenced, at levels closer to those found in mammals (*44*). Bird species that had the next highest level of filtering (between 5-10%) across data sets included the paleognaths (tinamou and ostrich), turkey, and Anna's hummingbird. The turkey had many miss-assembly artifacts relative to all the other bird genomes, and the tinamou, ostrich, and hummingbird had greater amounts of divergent sequences relative to chicken than other species (*44*). The Acciptrimorphae birds of prey (the two eagles and turkey vulture), ibis, and some others had the least amount of sequence removed, consistent with some of these species showing low genome diversity due to near extinction events as shown in a companion study (*50*). Overall, these findings suggest that in addition to validating the manually analyzed 200 genes, our filtering approaches appear to have correctly removed mostly divergent non-homologous sequences unique to each species in the alignment.

Figure S21 characterizes the missing data in our intron alignment, as an example of the relative amount of missing data across species. For each ortholog, we measured the sequence length of each species relative to the average sequence length for that ortholog. The histogram shows the distribution of this relative length statistic across all the intron orthologs. The four non-avian outgroups clearly have more missing data, characterized by histograms centered around values far below 1. Among birds, the tinamou, turkey, woodpecker, and mousebird have the highest levels of missing data, consistent with the filtering results. On the other hand, most bird species' values are heavily centered around 1, meaning that their orthologous sequence length is typically very close to the average length across all bird species. Thus, the filtering approach seems to have removed appropriate alignment errors and unique sequence in taxa with greater divergence.

SM4: Species tree and gene tree inferences using maximum likelihood
Andre Aberer, Alexandros Stamatakis, Siavash Mirarab, Tandy Warnow, Brant C. Faircloth

Maximum likelihood species tree inferences and advances in inference software
The computational requirements of the datasets examined in this study inspired major improvements of our phylogenetic inference software. To infer a species tree, we used maximum likelihood (ML) approaches on concatenated datasets to obtain a ML species tree with bootstrap support and a greedily refined majority-rule consensus tree (reviewed in (*124*)). We began with our standard RAxML (Randomized Axelerated Maximum Likelihood) method (*125*) (versions 7.3.2 to 7.4.2) to compute bootstrap alignment replicates and randomized step-wise addition order parsimony starting trees, but found that it was not sufficient to generate stable trees in reasonable computational time on our large genome-scale concatenated sequence alignments. Thus we developed and tested RAxML-Light (*55*) version 1.1.1, and found that it worked well for unpartitioned datasets, but still had limitations for partitioned datasets. Thus, we developed and used a new RAxML variant called ExaML (Exascale Maximum Likelihood) (*57*) (pre-release versions up to version 1.0.9) that can handle many partitions under the more memory

14

intensive Γ (gamma) model of rate heterogeneity.

While the core routines of ExaML (such as the implementation of the likelihood functions and search algorithms) are the same as in other RAxML variants, ExaML uses a new parallelization approach that significantly reduces the communication overhead and hence the parallel efficiency on large concatenated datasets with many partitions. RAxML-Light employed a master-worker scheme for parallel inference. This means that a single master process steers the tree search and triggers parallel regions in which worker processes compute the likelihood of all sites assigned to them in parallel and finally report the result back to the master process. Thus, two communication steps are required for executing each parallel region. With the introduction of ExaML, we shifted from this parallelization scheme to a decentralized scheme (*57*). Here we do not employ a single master process. Instead, each process executes a constant and synchronized copy of the tree search algorithm. This eliminates the need for initiating parallel regions. Given the high number of parallel regions in RAxML-Light and ExaML (e.g. optimization of each branch requires several parallel regions), we found that this new implementation in conjunction with the modification of the data distribution scheme described below increases runtime efficiency by a factor of more than 3.

We developed a second improvement to deal with another major challenge that became evident by the avian datasets using the GTR [General Time Reversible] model on large alignments that are highly partitioned. On the one hand, for each partition, a GTR model and thus a large overall number of parameters must be optimized which in turn makes tree inference more expensive. On the other hand, while computation of the log-likelihood can be efficiently parallelized over alignment characters, sequential computations (e.g., the exponentiation of the matrix containing the instantaneous substitution rates for each partition based on its Eigenvector/Eigenvalue decomposition) are necessary, prior to computing the likelihood. In the standard data distribution scheme, characters of a partition are assigned in a cyclic manner to processes. Thus, in the worst case, a process will only compute a few characters for each partition, but still have to execute the aforementioned sequential operations for each partition and each branch. We addressed this problem by assigning entire partitions to processes (*56*). Thus, the initial sequential computations that were necessary for computing the conditional likelihood the conditional likelihood array of a partition at each node of the tree are now distributed across processors as well. We found that applying this scheme sped up computations by one further order of magnitude.

Using RAxML, RAxML-Light, and ExaML, we inferred a varying number of bootstrap trees and ML trees for each dataset (**Table S3**). While GTR model parameters and parameters for rate heterogeneity are optimized for each partition, we used a joint branch length optimization across all partitions for the partitioned datasets. We modeled among-site rate heterogeneity using either the Γ model (*126*) or the PSR (Per Site Rate) approximation (*127*). For inferences under the PSR model, we calculated the likelihood of all final trees under the Γ model of rate heterogeneity using standard RAxML to identify the best-known ML tree for each dataset. Scoring final trees under Γ was not feasible for the whole-genome trees inferred under PSR because of excessive memory requirements (described below).

We tested if we had computed enough bootstrap replicates using the bootstrap convergence criterion (-I autoMRE in RAxML) as implemented in RAxML (*128*). Because of the substantial computational effort associated with bootstrapping and the limited computational resources, we did, however, not continue the bootstrapping procedure if support values had not

converged after 200 bootstrap replicates (**Table S4**). In many instances, a small set of poorly supported branches (<30%) accounts for a large part of support value instability. Since these relationships are not considered indicative, it is not essential to infer the exact degree of instability induced by a weak support value.

Partitioning and gene clustering by parameter similarity

For some analyses, we partitioned regions of the alignment with different evolutionary rates to determine if such a partitioning would impact the tree results. Each partition in an alignment has its own set of parameters (substitution rates and base frequencies of a GTR model (*129*) and parameters modeling among-site rate heterogeneity), which are optimized separately by the maximum likelihood (ML) inference software for each partition. Partitioned alignments have a larger number of distinct site patterns because identical sites that form part of different partitions (and hence evolve according to a different model) cannot be compressed into a single site pattern (**Table S3**, **Σ(#pattern)**).

For comparatively smaller datasets (e.g., the amino acid supermatrix) running the analysis with the maximum number of partitions was computationally still feasible. However, analyzing a huge alignment with a large number of partitions (e.g., $3x8^{-295}$ for the c123 dataset) would result in prohibitive runtimes because model parameters need to be optimized separately for each partition and because of parallel load imbalance. Although we managed to improve the efficiency of parallel tree inferences with ExaML on datasets with a high number of partitions (*56, 57*), it was still not sufficient for complete partitioning. Applying advanced tools such as PartitionFinder (*130*) to cluster partitions was also not feasible due to the sheer size of the datasets. Thus, to address computational limitations, we reduced the number of partitions per inference either by simply partitioning on gene marker type (e.g. exon, intron, UCE in the TENT) or clusters within gene type (i.e. within exons and introns) for sequences of similar parameters. We then compared trees generated with clustered partitioning to unpartitioned trees to determine the effect of partitioning.

To cluster the genes, for each per-gene sequence alignment, we inferred a maximum likelihood tree to obtain model parameter estimates for the respective gene trees (α shape parameter of the Γ model of rate heterogeneity (*126*) and the 5 free parameters of the GTR model of nucleotide substitution matrices). We used the k-means algorithm to cluster genes of the 8,295 exon and 2,516 intron datasets into k = 500 genes in each cluster (i.e. partition) as a trade-off between model accuracy (demanding a higher number of partitions) and efficient utilization of available computational resources. For the exons, we created 2-3 additional partitions (i) either excluding the 3rd codon position and treating the 1st and 2nd codon positions of each cluster as separate partitions or (ii) by treating the 1st, 2nd, and 3rd codon positions as separate partitions each.

We assembled the distance matrix for the clustering procedure by using the α parameters and substitution rates (yielding a distance matrix with a total of 6 columns). For the exonic per-gene alignments, we modeled codon positions as separate partitions. Thus, matrices with 12 columns (2 x 6 for 1st and 2nd codon positions) served as input for k-means clustering. We re-scaled columns, such that the weight of the α parameter corresponded to the combined weight of the 5 substitution rates. The rationale of this re-scaling was to ensure that the rate heterogeneity parameter (i.e., the α parameter) has the same impact on the clustering of genes as all individual substitution rates put together. For each parameter (α and substitution rates), we defined outliers

as values that were more than 3 standard deviations above or below the mean and set those values to the maximum value within the 3 standard deviation range around the mean. This treatment of outliers ensured that a single (outlier) parameter cannot dominate the Euclidian distance that is calculated by the k-means algorithm between gene pairs.

For the amino acid dataset, we were able to treat each gene as a separate partition in reasonable computational time (> between 124,000-164000, cpu hours; **Table S5**). We employed the following model selection technique to identify adequate fixed-rate substitution matrices. For each partition, we created a non-random tree topology (via parsimony) and computed the log-likelihood (lnl) for each available protein substitution matrix implemented in ExaML either by employing the state frequencies provided by the substitution model or empirical base frequencies. We then selected the highest-scoring model as setting for the inference on the concatenated alignment. In other words, for each partition, we chose the amino acid substitution matrix that maximizes the likelihood for the given, fixed tree topology. On per-partition alignments including outgroups, the JTT matrix (*131*) with empirical (per-partition) amino acid frequencies was the most frequent best-fit model and was found to be optimal for 4,988 out of the 8,295 gene partitions. The standard JTT matrix (with pre-defined frequencies) was optimal for 2,559 out of 8,295 partitions. Thus, we also used the JTT matrix with empirical frequencies (drawn from the data) for the analyses of the unpartitioned amino acid dataset. This procedure was repeated for partitioned alignments excluding the outgroups with a similar (JTT-dominated) result.

RY-recoding

For the non-outgroup exon-only dataset, the 3rd codon position was recoded to RY with a custom-made replacement shell-script (A or G = R; T or C = Y). Thereafter, the recoded alignment was applied to ExaML with the sites split into 3 partitions: c1,c2,c3-RY.

Resources and computational effort

We carried out tree inferences at seven computing centers: the Heidelberg Institute for Theoretical Studies (HITS), the San Diego Supercomputer Center (SDSC), and the Leibniz Rechenzentrum Munich (LRZ), the Texas Advanced Computing Center (TACC), the Georgia Advanced Computing Resource Center (GACRC, for UCE trees), Amazon Web Services (AWS, for UCE trees), and the Nautilus supercomputer at the National Institute for Computational Sciences of the University of Tennessee and Smithsonian. Computations at HITS were conducted on clusternodes consisting of 4 AMD Magny-Cours processors (12 cores each) with either 128 GB or 256 GB RAM. Most inferences on the whole genome dataset under PSR were conducted on computing nodes at HITS consisting of 3 Intel Sandy Bridge CPUs (4 cores each) with 32 GB RAM per node. The cluster at SDSC has nodes with 2 Intel Sandy Bridge CPUs (8 cores each) and 64 GB RAM. For inferences at the LRZ, we used the SuperMuc supercomputer that currently is on rank 10 among the 500 fastest supercomputers in the world [top 500 supercomputer sites, 2013]. The SuperMuc computer comprises 9,216 Intel Sandy Bridge nodes with 16 cores each and 32 GB RAM per node.

For the UCE species tree, it was not necessary to use ExaML. We inferred the best fitting ML tree using the PThreads version of RAxML (v7.3.5 12-Oct-2012, available at https://github.com/stamatak/standard-RAxML) with 16 cores, the GTR+Γ model, and 20 maximum likelihood (ML) searches on distinct starting trees, on a 16-core Intel server with 244

GB RAM. We estimated support values for the best ML topology using the MPI version of RAxML, on 12 compute cores, the standard RAxML bootstrapping procedure, and 100 bootstrap replicates. Following estimation of the best ML tree and bootstrap support replicates, we reconciled both into a concatenated species tree using standard RAxML.

Table S5 shows the amount of CPU hours spent for most ML tree inferences described in this study. These runtimes solely refer to the time invested in ML tree inference, excluding pre- and post-processing steps or repeated runs because of software and dataset adaptations. Initially, we inferred whole genome trees under the PSR model on the HITS cluster. The substantial memory requirements of this dataset under PSR (242 GB RAM) impeded efficient execution at HITS. Because of an additional constant per-MPI process memory overhead, it was not possible to start one MPI process per core on any cluster system used. In addition, some phases of the inference process temporarily required up to twice as much main memory (approximately 500GB). Thus, the number of MPI processes per node had to be limited to 24 instead of using all 48 for the whole genome inferences on the AMD Magny-Cours nodes and to 4 (later 6 after a swap space increase) for inferences on the HITS Sandy Bridge nodes. These idle CPU times are included in **Table S5**.

Memory requirements did not pose as much of a problem for whole-genome inferences under Γ, since the parallel memory overhead under Γ is lower (despite of higher overall memory consumption). Thus, the immense amount of main memory needed (1 terabyte) to conduct these inferences could be distributed among 4,096 cores per run.

We used the number of unique site patterns for calculating the size of the conditional likelihood arrays that dominate the memory requirements of ML inference. The Γ model of among-site rate heterogeneity (*126*) took more than 4 times the amount of memory than the position specific rates (PSR) model (*127*) (**Table S5, (Γ) [GB]**). For instance, for the inference of a single tree on the whole genome alignment comprising more than 161,000,000 unique site patterns, we require more than 1 terabyte of main memory when using Γ versus 256 gigabytes when using PSR.

In summary, ML tree analyses conducted for this study in **Table S5** alone consumed a total of 2,340,888.89 CPU hours (cpu-h) or 267.3 CPU years, and this does not include over 100 CPU hours taken for generating alignments or coalescent tree inference. The most expensive analysis was the whole genome inference under Γ (363,464 cpu-h). This is followed by the partitioned (500 partitions) analysis on the intron supermatrix (excluding outgroup) under Γ with 238,343.8 cpu-h. The high number of partitions (500) coupled with a comparatively high number of alignment characters and the fact that twice as many trees as for the whole genome analysis were computed leads to runtime requirements in the same order of magnitude as the whole-genome inference under Γ.

Additional ML inference species tree results

We computed all pairwise Robinson-Foulds (RF) distances (*132*) between all result trees (best-known ML tree and consensus tree). The resulting RF-distance matrix was used to cluster the topologies by means of hierarchical clustering (average linkage). We computed RF-distances based solely on the ingroup part of the tree (i.e., we pruned down all trees to the 48 ingroup taxa). Figure S22 shows the dendrogram and underlying plain RF distances for each dataset.

Although the PSR approximation generally requires less runtime and reduces the memory requirements of a dataset by a factor of 4, we found that tree searches under PSR yielded similar

18

(in terms of RF-distance) but more diverse topologies compared to Γ (**Fig. S22**). The reason for this difference is that we found for most datasets analyzed under PSR, bootstrap support was substantially lower compared to support observed under Γ. The consensus trees inferred from PSR on the TENT and other datasets with large sequenced amounts was more often different than the best tree, whereas the consensus tree from Γ replicates was identical to the best ML tree, thus yielding a substantially clearer phylogenetic signal. This suggests that bootstrap inferences under Γ yielded trees that are consistently more likely than the corresponding PSR trees. Although the log likelihood differences are small (**Fig. S23**), this led us to the conclusion that PSR fails to model rate heterogeneity as accurately for small numbers of taxa with large sequence alignments as our datasets.

Generating gene trees
Unless otherwise specified, gene trees were estimated using RAxML version 7.3.5 with 200 replicates of bootstrapping.

Exon datasets: To estimate exon gene trees, we removed the 3rd codon position because these positions in the alignments showed evidence of greater base composition heterogeneity, and hence do not conform to the assumptions of the GTR model (**Fig. S15A,B**). The alignment used for the gene tree estimation was the AA alignment translated back to DNA. For exon analyses, RAxML version 7.7.7 was used.

> RAxML maximum likelihood inference: 10 RAxML searches, each starting from a different parsimony tree, were run. For each gene, the resulting tree with the highest GTRGAMMA likelihood score was selected as the best tree. The following RAxML command was used:

```
raxmlHPC-AVX -m GTRGAMMA -n [a name] -s [SATé alignment with 3rd
   position removed] -N 10 -p [random number] -q [the partition file
   separating 1st and 2nd positions]
```

> Partitioning: We partitioned 1st and 2nd codon positions separately, so that rate matrices and empirical frequencies were estimated per partition, but branch lengths were estimated jointly.
> RAxML Bootstrapping: Bootstrapping with 200 replicates was performed using RaxML under the GTRGAMMA model, with the following RAxML command for bootstrapping:

```
raxmlHPC-AVX -m GTRGAMMA -n [a name] -s [SATé with 3rd position
   removed] -N 200 -b [random number] -p [random number] -q [the
   partition file separating 1st and 2nd positions]
```

Estimating exon gene trees took roughly 96 days of serial computation time.

Intron dataset: We estimated two sets of gene trees for introns, one based on alignments that included outgroups and another that excluded outgroups. The RAxML parameters for the intron gene tree estimation were identical to exon gene trees, except that no partitioning was involved.

> RAxML maximum likelihood inference: 20 RAxML searches, each starting from a different parsimony tree, were run. All searches were performed under the GTRGAMMA model. For each gene, the resulting tree with the highest GTRGAMMA likelihood score was selected as the best tree. We used the following command:

19

```
raxmlHPC-SSE3 -m GTRGAMMA -n [a name] -s [SATé alignment] -N 20 -p
    [random number]
```
Partitioning: data were not partitioned in these analyses.

RAxML Bootstrapping: Standard bootstrapping with 200 replicates was performed using
    RaxML under the GTRGAMMA model, with the following RAxML command for
    bootstrapping:
```
raxmlHPC-SSE3-PTHREADS -m GTRGAMMA -n [a name] -s [SATé alignment] -
    N 200 -b [random number] -p [random number] -T2
```

Estimating intron gene trees took roughly 1,100 days of serial computation for the alignments
without outgroups (gene trees with outgroups were not used in subsequent analysis for reasons
described under the MP-EST section). These computations were performed at supercomputers of
Texas Advanced Computing Center (TACC).

UCE dataset: The process used for UCEs was similar to the process used for introns. However,
we performed the UCE calculation on the GACRC and AWS computer clusters. We inferred
UCE gene trees in parallel by scheduling 3,679 RAXML-PTHREADS ML tree searches on a
2,600-node cluster using the GTRGAMMA model, 20 ML search replicates per locus, and 2
compute cores per locus/gene. We parallelized estimation of support for each gene tree in a
similar fashion, by using RAXML-PTHREADS and the standard RAXML bootstrapping
procedure to generate support values from 200 bootstrap replicates. We used commands identical
to those used to generate the intron gene trees. Estimating UCE gene trees took roughly 470 days
of serial computational time.

Gene tree statistics
Many of our estimated gene trees had low to moderate bootstrap support (BS) (**Fig. S24**). Exon
gene trees had the lowest average BS, with typical values around 25%, followed by UCEs at
around 40% and introns around 50%. This low support was mostly explained by a combination
of short alignments (**Fig. S25**) and low rates of evolution (**Fig. S26**). Lack of strong support in
UCE gene trees was not very surprising, given that UCE markers are not very long (2000-
3000bp), and the core part of the UCE sequence is highly conserved. However, it is interesting
that UCEs produce better support values than exons. The higher bootstrap support of intron gene
trees is likely due to the fact that introns are longer and also have higher rates of evolution than
exons (**Fig. S26**) and UCEs. These extremely low support trees were not suitable for coalescent-
based inference of species trees using methods such as MP-EST that combine estimated gene
trees, as shown in a companion paper (*58*).

SM5 Species tree inference using multispecies coalescence
Siavash Mirarab, Tandy Warnow, Md Shamsuzzoha Bayzid, Bastien Boussau, Liang Liu, Scott
Edwards

Standard concatenation approaches do not model discordance among gene trees beyond
differences in sequence evolution rates; instead they assume that "hidden support" for correct
clades will overcome the noise of ILS (*133*). Simulation studies have also shown that ILS has the

potential to lead to incorrect clades with high support, possibly due to estimation bias in a concatenated analysis where the mixture of gene trees represents a model violation (*134*). These possible limitations can theoretically be overcome with multispecies coalescence methods, such as MP-EST. We used MP-EST version 1.0.3 on both unbinned (i.e. original) and binned gene trees from the TENT and intron only data sets. Most MP-EST binned versus ubinned analyses were conducted at the Texas Advanced Computing Center (TACC) at The University of Texas at Austin (http://www.tacc.utexas.edu)

Gene binning
The statistical binning approach is discussed in detail in a companion paper (*58*) and described briefly here. Coalescent-based methods that combine gene trees to estimate the species tree are called "summary methods". Summary methods can have reduced accuracy or resolution when input gene trees have low support (*33, 66*). The statistical binning method addresses this issue.

Statistical binning creates "supergene alignments" by grouping together sets of genes, and uses gene trees estimated on these supergene alignments as input to the summary method. Supergenes are formed based on the notion of "combinability". Initial gene trees are estimated and bootstrapping is used to estimate branch support. Two gene trees are considered combinable if they have no pairs of incompatible edges that have support above a given threshold. The statistical binning approach uses a graph algorithm to partition the input set of genes into roughly equally sized subsets (called "bins") so that each subset contains genes that are all pairwise compatible. The alignments from genes in the same bin are combined to form a "supergene", and partitioned maximum likelihood analysis on each supergene alignment is used to produce a supergene tree. As shown in the companion paper (*58*), this procedure dramatically increases the accuracy of gene trees, the accuracy of triplet gene tree distributions, and as a result the accuracy of estimated species trees. As an example, Mirarab et al. (*58*) created a simulated dataset of 14,350 genes that closely resembled the TENT dataset in terms of gene tree count and bootstrap support. On this dataset, MP-EST applied to binned gene trees had 7% error (or 3 incorrect branches), but MP-EST applied to unbinned gene trees had 11% error (**Fig. S27**).

In this study, we used statistical binning to estimate supergene trees on two datasets: all 14,446 markers (8251 exons, 2516 introns, and 3679 UCEs) in the total evidence data set, and all 2,516 introns only. We used a threshold of 50% for determining combinability. Thus two genes were combined into the same supergene only if all their conflicting edges had support below 50%. On the TENT 14,446 marker dataset, binning created 1,730 bins containing 7 individual genes each, and 293 bins with 8 genes each. On the intron only dataset, binning created 542 bins containing 2 genes, 472 bins with 3 genes, and 4 bins with 4 genes each.

Supergene trees were constructed by a procedure similar to the gene tree estimation for unbinned intron gene trees. The main difference was that we also used partitioning in supergene tree estimation, such that each gene has its own partition. The exact commands used were as follows:

RAxML maximum likelihood inference: 20 RAxML searches, each starting from a different parsimony tree, were run, under the GTRGAMMA model. For each gene, the resulting tree with the highest GTRGAMMA likelihood score was selected as the best tree. Command:

```
raxmlHPC-SSE3 -m GTRGAMMA -n [a name] -s [SATé supergene alignment] -N 20 -
   p [random number] -q [gene partition file]
```

Partitioning: each marker that was put into a bin was defined as one partition.

RAxML Bootstrapping: Normal bootstrapping with a fixed number of 200 replicates was performed using RaxML, using the following command:

```
raxmlHPC-SSE3 -m GTRCAT -n [a name] -s [SATé alignment] -N 200 -b [random
    number] -p [random number] -q [gene partition file]
```

Estimating supergene trees took roughly 1,800 days of serial computational time.

MP-EST runs

We used a site-only multi-locus bootstrapping procedure (*135*) for all MP-EST analyses. From the 200 bootstrap replicates of each gene, 200 different inputs to the summary method were built by choosing one replicate of each gene for each input. MP-EST was run on each of the 200 inputs, and hence 200 "bootstrapped" species tree replicates were obtained. A greedy (extended majority) consensus of these 200 bootstrap species tree replicates was built, and support values were drawn on this greedy consensus by counting occurrences of each bipartition in the 200 replicates.

After initial experimentation, we realized that running MP-EST multiple times with varying random seed numbers did not always yield the same tree. We therefore ran MP-EST multiple times and took the result from the run with the best likelihood score. We used 50 runs of MP-EST for the binned MP-EST* trees and 10 runs for unbinned MP-EST trees (10 runs and 50 runs produced similar results).

MP-EST requires rooted gene trees. We rooted each gene tree with ostrich, and if ostrich was not present, then with tinamou. The MP-EST allows only one outgroup, because it is difficult to root gene trees by multiple outgroups when they do not form a monophyletic group. Thus, while the correct rooting is at the parent node of ostrich and tinamou, we always used one taxon as the outgroup. There were 58 genes in the exon dataset and 30 genes in the intron dataset that did not include either of these two outgroup taxa (UCEs were selected for only those present in all avian taxa). These particular genes were left unrooted, and were excluded from MP-EST analyses.

The intron dataset that included non-avian outgroups suffered from too much missing data among the non-avian outgroups. A non-avian outgroup typically included 10-30% of the alignment; much of the missing portions of non-avian sequence were removed in the alignment filtering step because they did not have sufficient homology to the avian taxa (see **SM3**, **Fig. S21**). These levels of missing data caused the outgroups to be placed in incorrect places in many of the gene trees reconstructed (e.g., they were placed inside the aves). These incorrect placements in turn resulted in incorrect rooting of the gene trees, which negatively affected the MP-EST analyses. Thus we decided to include MP-EST analyses on intron gene trees only without the non-avian outgroups.

SM6. Justifications of names for higher taxa

Joel Cracraft, Edward L. Braun, Peter Houde, Jon Fjeldså, David Mindell, Frank Rheindt, Scott Edwards, Gary Graves, Warren Johnson, M. Thomas P. Gilbert, Erich D. Jarvis

To name clades, we avoided as much as possible adding new names, where possible used previously published names or new names that followed a clearly defined protocol, and adhered

to the Internal Code of Zoological Nomenclature (http://iczn.org/code) for the order and next several supraordinal levels. Thus, all superorder names used the subordinate taxon as the taxonomic prefix, followed by a standard suffix, such as imorphae. Whether previously published or not, we only used names in the tree figures for groups that had 100% support in the ExAML TENT and multiple other analyses and that did not differ between phylogenetic reconstruction methods with the total evidence data set; one exception was Cursorimorphae with 96% in the ExAML TENT, but still 100% in several other analyses.

Given these criteria, our primary source of names for ordinal classification and one higher-level supraordinal level was the recent Howard and Moore (H&M) checklist edition 4 (*36, 37*). This classification was chosen because all of the named orders are monophyletic based upon the previous evidence (e.g., Hackett et al. 2008) (*17*) and most, although not all, were consistent with the results of this study. The H&M 2013 checklist, however, was generated without full use of the tree of the current study, and adopted the philosophy of reducing redundancy among names. Thus, the previously defined Apodiformes and Caprimulgiformes were placed into one group based upon interpretations of the prior literature. Given that we find their divergence occurred before 50 MYA along with the other orders, should future investigation with more taxa support this divergence timing, then the ordinal status for these two lineages could be justified. A similar proposal can be made for families within the H&M named Accipitriformes and Pelecaniformes in our dated tree (**Figs. 1, S1**). Other higher order level names include Aequornithia from Howard and Moore (*36*), adapted from Aequornithes from Mayr (*16*), Australaves and Afroaves from Ericson et al (*60*) with the former modified from Australavis by Yuri et al (*59*), and Telluraves from Yuri et al (*59*). The clade names for Australaves and Afroaves is based on a biogeographic hypothesis of where these lineages diverged (*60*), but our adaption of the names is not necessarily an endorsement of the biogeographic hypothesis upon which they are based. We used the names given the currently published evidence and precedence. The result is that of the 18 names higher than the order level, three are new: Cursorimorphae described above, Columbea and Passerea. The Columbea-Passerea node is robust because it received 100% bootstrap support in both our likelihood (ExAML) and coalescent (MP-EST*) total evidence trees, as well as in nearly all genome-scale trees from diverse non-overlapping data partitions, except for the protein coding trees that instead show convergent relationships between these two groups (**Fig. 2, S2**).

Traditional classifications of avian higher taxa were constructed based on morphological and other features prior to the use of molecular sequence data and the composition of these taxa often differs significantly from those based on molecular data ((*17*) and this study). Thus, for example, although we use the many of the same names as used traditionally (including Falconiformes, Cuculiformes, Ciconiiformes, Coraciiformes, Columbiformes, Gruiformes and Pelecaniformes), among the major conclusions of this study are that these orders are non-monophyletic (**Figs. 1**, **2**) as they were traditionally conceived (**Fig. S3A-B**).

The taxon sampling for the present study is insufficient to test whether monophyly of few named orders will be corroborated by analyses of much larger number of taxa, but it is ideal for the delineation of higher-level groups. However, it is difficult to envision how increased taxon sampling could affect our result of the Columbea and Passerea split, as it was found at 100% BS in multiple analyses with TENT, WGT, and intron data sets. We did not use the protein coding trees and other smaller data sets alone to support named clades, as we demonstrate these are

23

either not sufficient for generating a highly resolved phylogeny or show massive sequence convergence.

The Internal Code of Zoological Nomenclature (http://iczn.org/code) we used has the following rank-endings for superordinal ranks:

Infraclass -ae
  Parvclass -es
    Cohort -ia
      Superorder   -imorphae
        Order –iformes
          Family -idae

Ranked clades above the level of cohort have been widely used prior to this study and we retain them because they were corroborated by our data. The Passerea and Columbea are unranked clades. Using H&M for the supraordinal names meant the following: We use Phoenicopterimorphae rather than Mirandornithes to refer to flamingoes and grebes; Caprimulgiformes rather than Cypselomorphae to refer to traditional Caprimulgiformes and Apodiformes combined; Passerimorphae instead of Psittacopasserae in Suh et al (*29*) to refer to Psittaciformes and Passeriformes combined. We grouped Eurypygiformes (Sunbittern) and Phaethontiformes (tropicbirds) into the superorder Phaethontimorphae, instead of each being in separate superorders; Gruiformes (cranes) and Charadriformes (plovers) into one superorder Cursorimorphae; and Otidiformes (bustards), Musophagiformes (turacos), and Cuculiformes (cuckoos) into one superorder Otidimorphae.

For consideration of future classifications, we noted that nearly all (24 of 26 = 92%) ordinal Neognathae divergences recognized across various studies of the past literature represented by our species, including orders differently defined across studies, occurred between 69 MYA and 50 MYA in our dated timetrees (**Figs. 1, S1**). The two exceptions were the split between Coraciiformes (represented by bee-eaters in our study) and Piciformes (represented by woodpeckers in our study), which was dated to ~43 MYA, and the split between the Trochili (hummingbirds) and Apodi (swifts), which used to be considered separate orders (Trochiliformes and Apodiformes) also dated to ~44 MYA (in the TENT). This suggests that future investigations with increased taxon sampling may show that divergence time could be integrated meaningfully with phylogeny as a criterion for classification. For this reason, in **Figure S1** we also list the family names of those species for which their divergence occurred before 50 MYA where the H&M list considered them as part one order.

SM7 Metatable analyses of species tree and gene trees

Siavash Mirarab, Tandy Warnow, Peter Houde, Edward L. Braun, Joel Cracraft, David Mindell, Erich D. Jarvis

The meta-analysis summarizes similarities and differences between alternative species trees or sets of gene trees, based on support, for specific sets of clades. Clades are included either if they receive strong support from one or more of our analyses or are representative of other literature, i.e., traditional composition of orders and representative "literature trees" assembled from DNA-

DNA hybridization, mitochondrial, and morphological data. All analyses were performed using a custom script written in python and based on the Dendropy (*136*) package; results were visualized using custom R code (*122*).

Species tree metatable
We first determined monophyly of each selected clade. If a clade was monophyletic, its support was determined by examining the branch corresponding to the most recent common ancestor (MRCA) of all taxa in that clade. For clades that were not monophyletic, we used the concept of "compatibility" to distinguish between weak and strong rejection. In a tree that has multifurcations, a group of taxa are said to be compatible with monophyly if there exists a resolution of multifurcations that makes those that group of taxa monophyletic. We contracted edges with support lower than 95% in all species trees (we used 95% instead of the standard 75%, as we noted with genome scale data, support values were much higher compared to typical single gene alignments). If a clade was incompatible with monophyly even after contracting edges with support below 95%, it was labeled as strongly rejected; otherwise, it was labeled as weakly rejected (i.e. compatible with monophyly).

Once we determined the monophyly and support of each potential clade in each potential species tree, we used a custom R code (using the ggplot2 package) to build a block diagram with trees as columns and potential clades as rows. For each clade that is monophyletic in a certain tree, the corresponding block is in green, with darker shades of green showing increased support for that clade. Clades that are incompatible with monophly are shown as red, and those that are strongly or weakly rejected are distinguished using two different shades of red colors; dark red, for strong rejection and light red for weaker rejection.

We had to substitute representatives of some families or orders to compare our results with trees from the past literature (**Table S6; Fig. S3**). The substituted taxa in different families, but within the same order are: 1) Antrostomus (Caprimulgiformes: Caprimulgidae) was substituted with Nyctibius (Caprimulgiformes: Nyctibiidae) (*14*); 2) Charadrius (Charadriiformes: Charadriidae) was substituted with Haematopus (Charadriiformes: Haematopodidae) (*14, 24*); 3) Merops (Coraciiformes: Meropidae) was substituted with Eurystomus (Coraciiformes: Coraciidae) (*14*); and 4) Manacus was substituted with Cnemotriccus and Pitangus ("Tyrannides" or "New World suboscines": Tyrannidae) (*14, 15*). Phylogeny used for selecting nearest relatives and their familial names followed Barker et al 2001 (*137*), Barker et al 2004 (*138*), Barker et al 2013 (*139*), Pitra et al 2002 (*140*), Fain and Houde 2007 (*141*), Hackett et al 2008 (*17*), and Cracraft 2013 (*36*). Some trees from the literature were missing some of our taxa altogether. In these cases, monophyly of a clade was not rejected if taxon sampling was incomplete, as long as it was represented by at least two families. Blank cells in the table indicate insufficient sampling to test monophyly. Conversely, some genera in literature studies did not match ours closely enough to capture the same terminal branches and where thus not included. The Hackett et al (*17*) study did not report support values with BS below 50%. For these branches, we show results in the metatable with the color corresponding to 25% support (average between 0-50%).

Gene Tree metatable
Determining the monophyly for gene trees was similar to the species tree, but we needed to take into account the complicating fact that gene trees could miss some taxa since we allowed a

minimum of 42 of 48 avian species to be represented. For monophyletic clades, we chose to distinguish between cases where all taxa from a potential clade were present in the tree, cases where at least two of the taxa were present in the tree, and cases where at most one taxon was present. When two or more taxa belonging to a clade were present but some were missing, we categorize the monophyly as "partially missing". If less than two taxa (i.e. zero or one taxa) from a clade are present in a tree, it is not meaningful to talk about monophyly, and so we labeled that scenario as "missing". Putting all this together, we obtained seven different possibilities, as summarized in **Table S7**. We refer to these seven possibilities as monophyly categories. Note that for gene trees, unlike the species trees, we used the standard threshold of 75% to distinguish between high and low support.

　　　To visualize the monophyly status of gene trees, we used a custom R code to create stacked bar graphs, showing for each potential clade the number of trees where the potential clade falls into each of the categories.

　　　Note that these analyses reveal the number of gene trees that support or reject a potential clade. Besides showing these results as bar graphs, we have annotated each branch of the ExaML TENT and MP-EST* TENT trees with the percentage of genes that either strongly support or strongly reject the monophyly of the clade defined by that branch. In calculating these percentages, we excluded those genes that were categorized as "missing" as they were irrelevant for those clades. For calculating the percentage of genes that support a clade, we counted all genes that supported the clade, whether they were complete, or missing some species. Since each branch also has a length, these percent support and percent reject values could be easily compared to branch lengths.

Species tree incompatibility analyses
We compared various species trees in terms of their compatibility (node-by-node congruence) with the reference TENT tree at various support thresholds. A branch is compatible if it is the same in two trees; incompatible if it is not. For various bootstrap thresholds (0%, 25%, 50%, 75%, 95%, and 100%), we created a version of each species tree where branches with support below that threshold were contracted. We then compared all these contracted versions of the species trees against a reference species tree (ExaML TENT) contracted at the same level and counted the number of incompatible branches between the two trees. For example, this analysis showed that the ExaML TENT tree restricted to edges with 50% support or more has four incompatible branches with the intron ExaML tree restricted to edges with 50% support or more. These numbers were simply shown in a line graph where each line corresponded to one support threshold.

SM8 Phylome-based analyses of gene trees relative to the species tree
Salvador Capella-Gutiérrez, Jaime Huerta-Cepas, Toni Gabaldón.

Phylome reconstruction pipeline
Proteins encoded in 48 avian genomes plus 4 non-avian ones were used to reconstruct 5 phylomes, using five avian species as seeds (**Table S8**) that were distributed across the avian phylogeny: chicken, bald eagle, hoatzin, cuckoo-roller, and white-tailed tropicbird (**Fig. S1**). The phylome pipeline used is described in reference (*142*). In brief, for each protein encoded in the

seed genome, a Smith-Waterman (*143*) search was used to retrieve homologs in the rest of the species listed in Table S8, using an e-value cut-off of 1e-5, and considering only sequences that aligned with a continuous region representing more than 50% of the query sequence. Thus, the resulting homologous set contained the seed protein as well as its homologs in the 52 species. If more than 250 homologs were retrieved, the set was limited to the 250 closest ones. Then, the selected homologous sequences were aligned using three different programs: MUSCLE v3.8 (*118*), MAFFT v6.712b (*144*), and KAlign v2.04 (*145*). Alignments were performed in forward and reverse directions (i.e. using the Head or Tail approach (*146*)), and the six resulting alignments were combined in a consensus alignment using M-Coffee (*147*). The resulting consensus alignment was subsequently trimmed with trimAl v1.4 (*148*), using a consistency score cutoff of 0.1667 and a gap score cutoff of 0.1, to remove poorly aligned regions.

Gene trees were reconstructed using a Maximum Likelihood (ML) approach. For the chicken phylome, single gene trees were reconstructed directly from the protein alignments using amino acid evolution models. For the remaining four species, single gene trees were reconstructed from protein alignments back-translated into their corresponding codons with codon-based models. The reason for using amino acid as opposed to nucleotide sequences for the chicken phylome reconstruction was that the chicken is more distantly related to most of the other species and amino acid sequences are less divergent than the nucleotide sequences, allowing for a more comparable reconstruction.

For protein-based trees used with chicken as the seed, the selection of the evolutionary model that best fit each protein family was performed as follows: 1) A phylogenetic tree was reconstructed using a Neighbour Joining (NJ) approach as implemented in BioNJ (*149*); 2) The likelihood of this topology was computed, allowing branch-length optimization, using eight different models (JTT, LG, WAG, Blosum62, MtREV, VT, DCMut and Dayhoff), as implemented in PhyML v3 (*150*); and 3) The two evolutionary models that best fit the data were determined by comparing the likelihood of the used models according to the AIC criterion (*151*). Then, these two models were used to derive ML trees, with the default tree topology search method NNI (Nearest Neighbor Interchange); the one with the best likelihood was used for further analyses. A similar approach based on NJ topologies to select the best-fitting model for a subsequent ML analysis has been shown previously to be highly accurate (*142*). Branch support was computed using an aLRT (approximate likelihood ratio test) parametric test based on a chi-square distribution, as implemented in PhyML. A discrete gamma-distribution with four rate categories plus invariant positions was used, estimating the gamma parameter and the fraction of invariant positions from the data.

For codon-based trees, trimmed alignments were back-translated from protein sequences to their corresponding codons prior to phylogenetic tree reconstruction. Then, ML phylogenetic trees were inferred from these DNA alignments using codon-based models. ML trees were reconstructed using codonPhyML v1.0 (*152*) with GY as the specific substitution model for codon data and F3X4 as the model for defining the codon frequency in the individual alignments. Similar to trees based on protein data, branch support was computed using an aLRT parametric test based on a chi-square distribution. In all cases, a discrete gamma-distribution with three rate categories was used, estimating the gamma parameter from the data.

For subsequent analyses, the five phylomes were combined into a set of 75,853 ML trees that span the evolution of genes across the 48 bird species, and cover 94.58% of all predicted genes. This set contains a high redundancy from different phylomes and seeds, and thus

27

computed values in the analyses are normalized (see below). The results were highly similar when each phylome was used independently. All gene trees, alignments and orthology and paralogy calls for the five phylomes are available through phylomeDB (htp://phylomedb.org; (*68*)).

Phylogeny based orthology predictions
The species overlap algorithm described in (*153*) was used to detect speciation events in all phylome trees as implemented in the ETE toolkit (*154*). A comprehensive list of ortholog pairs was generated using the MetaPhOrs pipeline (*155*), which combines predictions from different trees and phylomes and allows to filter lowly supported pairs based on consistency (consistency score <0.5).

Gene tree support and species tree congruence
The five phylomes described above were used to measure the congruence of individual gene family trees with several species tree alternatives. The 75,853 gene trees were scanned using TreeKO (*156*), a duplication-aware algorithm that generates all the species topologies observed in a single gene family tree so that all treeKO subtrees contain only one orthologous sequence per species. To avoid signal redundancy among overlapping gene family trees, species tree topologies not containing the seed sequence – the one used to start the homology search- were discarded from the analysis. Next, the gene tree support was calculated for every node in the reference species tree. Each node in the species tree defines two daughter clades, each containing a set of species. The gene tree support for that node is computed as the number of gene trees in the phylome that are congruent for that split, divided by the total of trees that are informative for that node (i.e. contain at least some species in both of the daughter partitions). To determine congruence between the species tree and a treeKO-derived subtree tree, for each node in the reference species tree, a match was counted if the two sets of species defined by the two daughter clades were monophyletic also in the gene tree. The gene tree support consisted of the average of all its TreeKO subtrees.

Gene losses were inferred based on the duplication events detected for each gene family and taken into account when computing gene tree supports. That is, a match was also considered if all the missing species in a given clade were associated to one or more gene loss events (species are missing in one side of the duplication but not in the other). Gene duplication detection, the inference of lost branches and all tree scanning operations were performed using the ETE toolkit (*154*).

Normalized RF and incompatibility
A normalized RF distance was calculated for the 75,853 gene trees using the two main reference tree topologies (ExaML TENT and MP-EST* TENT). Given that most of the gene trees contained duplications and a different set of species, we used the TreeKO tree decomposition method and the speciation distance described in the same paper (*156*) to calculate a normalized and weighted distance from all possible species tree topologies contained in a single gene tree and the reference. As in the case of the species congruence calculation, only the branches leading to the seed sequences within a given gene tree were used to compute the normalized RF distance of that gene tree. Normalized compatibility is measured among high support branches (aLRT>0.95). Edges with lower support are collapsed and the number of edges that remain

incompatible is counted. The values were computed on treeKO subtrees and then normalized per gene tree as explained above.

SM9 Indel analyses and ILS

Peter Houde, Nitish Narula, Andre Aberer

Indels were scored in the alignments of the exons, introns, and UCEs from the total evidence data (SM3), using the principle of simple gap coding (*69*) as implemented in 2Xread (*157*). Gap coding was verified using GapCoder (*158*) and by visual inspection of alignments for a small subset of data. Intron indels were scored on alignments with and without non-avian outgroups (48 and 52 taxa, respectively), UCEs indels were scored on alignments that included alligator (49 taxa), whereas exons were scored on alignments that included all non-avian outgroups (52 taxa). Individual introns of the same gene were scored independently to avoid creating artifactual indels between concatenated introns, whereas exons were concatenated as complete unigenes before scoring. Intron and UCE indels were partitioned into size classes of $\geq$1bp, $\geq$10bp, $\geq$50bp, and $\geq$100bp for separate analyses. For exons, indels >30bp were excluded to avoid scoring missing exons as indels. The result was 0.15 to 4.2 million indels per data set, with 7.5-25% being parsimony informative (**Table S9**).

We next performed phylogenetic analyses and character state mapping of exon, intron, and UCE indels on the TENT trees, both separately and combined. Parsimony analyses were performed using the mult (1000 multiple random additions, 10 trees held per replicate, TBR branch swapping) and resample (10,000 bootstrap replicates, parsimony uninformative sites excluded) options in TNT software (*159*).

TNT outputs a list of character state changes (apomorphies) per node. In addition, it computes the Retention Index (RI) for every indel character, which is a measure of its consistency or "fit" to the tree, based on the principles of character state mapping optimized by the parsimony criterion. Binary indel characters with a RI=1.0 correspond to those that were transformed between the binary states only once uniquely on the tree and therefore fit the tree perfectly ("consistently"). Homoplasious indels (RI<1.0) are binary characters that are inferred to have transformed twice or more in order to explain their distribution in taxa as they are arranged on the tree. For every internal branch in the tree, we determined the number of indels with RI = 1.0 that change on that branch, and divided that number by the total number of indels that changed on the branch. We refer to that value as %RI=1.0, and express it as a percentage.

%RI=1.0 was regressed against measures of internal branch length, since the rate-dependent process of lineage sorting predicts that these should be correlated. Branch lengths of the ExaML TENT were measured in likelihood units for this regression, but recalculated as time intervals from the dating analysis (SM12) for both the ExaML TENT and MP-EST* TENT so the regressions of the two trees could be compared using the same units of branch length. Regressions were also performed on raw numbers of indels against branch lengths. The high correlations among all of these variables document that similar %RI=1.0 was not achieved by significantly different numbers of indel characters.

To produce the total evidence indel tree (TEIT; **Fig. S12**), we performed likelihood analyses using the BINGAMMA model in RaxML 7.2.8 (*125*)

To compare indel and nucleotide homoplasy, we used the same data partitions to construct the tree as the characters that were mapped to the tree. Thus, indels were mapped to an indel-optimized tree in the same manner nucleotides were mapped to a nucleotide-optimized tree. We confirmed as expected that indels were less homoplasious than nucleotides in a random sample of 400 introns (**Table S10**). Nevertheless, a much larger percentage of indels than nucleotides were parsimony uninformative (**Table S11**). To measure the effect of indel length on indel homoplasy, we mapped indels of progressively restrictive size classes onto parsimony and maximum likelihood indel trees as well as the reference ExaML TENT (**Table S12**). Longer indels were less homoplasious than short ones (**Tables S12** and **S13**). In spite of the difference in homoplasy of short and long indels, we included all scored indels in our ILS analyses because there were relatively few if any parsimony informative long indels in some clades.

Character-mapping revealed homoplasy at all nodes, regardless of whether indels were mapped to the reference EaxML TENT (range RI=0.49-0.91), the alternative MP-EST* TENT (range RI=0.50-0.91), or to parsimony trees optimized for the indel data themselves (evaluated by Consistency Index instead using PAUP* (*160*) or visually using MacClade 4 (*161*)). Homoplasy was markedly highest at short internodes at the base of Neoaves that were otherwise characterized by lower bootstrap support. We regressed the percentage of indels scored as RI=1.0 (perfectly consistent, no homoplasy) against two measures of internode length, log maximum likelihood distance and log time as measured on our timetree for the EaxML and MP-EST* TENTs. In all regressions, % indels RI=1.0 was highly correlated with branch length (**Fig. 3E,F**).

SM10 TE analyses and ILS

Alexander Suh, Linnéa Smeds, and Hans Ellegren

Retrophylogenomics of owl affinities and ILS/hemiplasy at the base of the core landbirds
Despite genome-scale phylogenomic analyses of nucleotides and indels in this study, the position of the Barn Owl remained the most ambiguous among the core landbird taxa. To examine this problem from an independent perspective, we made use of retroposon insertions as phylogenetic markers. Retroposons are transposable elements (TEs) whose master genes 'copy and paste' via a RNA intermediate, leaving behind daughter copies that are scattered across the genome. These daughter copies are usually unable to reproduce copies (i.e., "dead on arrival") and germline genomic integrations remain, once fixed in a population, as non-coding DNA that is vertically inherited within each orthologous insertion locus.

Many studies, especially in mammalian phylogenetics, have shown that retroposon presence/absence patterns are powerful phylogenetic markers capable of resolving long-standing controversies (e.g. refs. (*162, 163*)) and of detecting non-homoplastic incongruences caused by incomplete lineage sorting (ILS) of ancient polymorphisms (*164, 165*) – a phenomenon that has been termed hemiplasy (*70*). This is due to the assumption that retroposon markers constitute nearly homoplasy-free, neutrally evolving witnesses of evolution, as homoplasious events are expected to be very rare and certainly rarer than single nucleotide substitutions (*72, 166*). A homoplasious indel event is either the independent acquisition of the same TE in the same

30

orthologous locus and target site, or the precise excision of a TE insertion and one copy of the duplicated target site.

In avian phylogenetics, previous retroposon studies (*29, 167-169*) based on limited genomic sequences showed that the different retroposon subfamilies remained active during certain time periods in avian evolution, allowing the focused targeting of retroposons relevant for specific phylogenetic questions and providing evidence for controversial relationships (e.g., the passerines+parrots clade (*29*) and the flamingo+grebe clade (*167*)). Based on prior evidence (*29, 168*) on the activity of *hitchcock*-related long terminal repeat element (LTR) retroposons during early avian evolution, we selected the most numerous subfamily for our owl TE analyses, namely TguLTR5d.

Taxon Sampling

Our core taxon sampling comprised, in addition to the retroposon reference genome of the Barn Owl (*Tyto alba*), the following 9 core landbirds: *Melopsittacus undulatus*, *Falco peregrinus*, *Cariama cristata*, *Colius striatus*, *Haliaeetus albicilla*, *Cathartes aura*, *Merops nubicus*, *Apaloderma vittatum*, and *Leptosomus discolor*. Furthermore, to ensure specificity to core landbirds, our taxon sampling comprised the following 16 non-core landbird taxa within Neoaves: *Charadrius vociferous*, *Opisthocomus hoazin*, *Phaethon lepturus*, *Eurypyga helias*, *Pelecanus crispus*, *Gavia stellata*, *Cuculus canorus*, *Chlamydotis undulata*, *Tauraco erythrolophus*, *Mesitornis unicolor*, *Pterocles gutturalis*, *Phoenicopterus ruber*, *Columba livia*, *Chaetura pelagica*, *Antrostomus carolinensis*, and *Balearica regulorum*. This reduced taxon sampling (26 of 48 bird genomes) was chosen for computational reasons and facilitated manual inspection of alignments of hundreds of marker candidates. After manual inspection and selection of TE informative marker candidates, we sampled them from all the remaining bird genomes for compilation of final alignments of all 48 species.

Computational Procedures

We identified 3,641 insertions of the retroposon subfamily TguLTR5d in the Barn Owl genome, including 1 kb flanks. These insertion loci were masked using RepeatMasker (http://repeatmasker.org) and BLASTn (*170*) searches of the flanks were conducted against the remaining 25 species of our core taxon sampling. The resultant BLAST hits were extracted and locus-specific alignments were generated using MAFFT (*144*) (E-INS-I, version 6).

We applied several steps of post-filtering to reduce the amount of non-informative marker candidates. This included the omission of alignments with less than 10 species, alignments that covered only one of the two flanks of the retroposon insertions, alignments that featured a plesiomorphic TguLTR5d insertion (i.e., presence in all sampled species), and alignments that featured an autapomorphic TguLTR5d insertion (i.e. presence only in the Barn Owl). Furthermore, we checked our alignment data set for redundancy of loci and potential paralogy of insertion loci. All potentially paralogous loci were excluded from subsequent analysis. This reduced the dataset to 153 TguLTR5d TEs.

Validation of Retroposon Markers

We manually checked alignments of retroposon marker candidates for orthology of TE presence in owl and other core landbirds. Potential markers with a Neoaves-wide, partial Neoaves-wide or core landbirds-wide presence were excluded, as these were not of relevance to the position of the

31

Barn Owl within core landbirds. For the remaining 61 relevant marker candidates, we extended the taxon sampling to include sequence information from all 48 bird genomes.

From this set, we then applied strict criteria for retroposon markers used in other retroposon studies (e.g. ref. (*29*)), if the following situation applied to an orthologous insertion locus:

1. Clear TE presence in all species sharing the specific retroposon insertion (character state "1"), as indicated by an identical insertion point (target site), identical orientation of the TE, identical TE subtype, and identical target site duplication (direct repeats).
2. Clear TE absence in other species (character state "0"), as indicated by the presence of only one copy of the target site, and an alignment gap precisely corresponding to the TE presence/absence region.
3. Only few species (those outside the core landbirds and thus not critical for our specific question) with missing data (character state "?") due to gap in the genome assembly or due to large unspecific deletion of the insertion locus.

Control Comparison

We re-analyzed retroposon data on the position of Passeriformes as a control comparison for ILS levels, using the presence/absence matrix of reference (*29*). This is based on the initial assumption that the lineage leading to the zebra finch within the Neoaves radiation appears to have gone through a lower level of ILS than other parts of the core landbirds tree (**Fig. 3A-F** of this study and **Fig. S2** in reference (*29*)).

SM11 GC content, codon position, and low-variance vs high-variance genes

Claudia C. Weber, Bo Li, Benoit Nabholz, Bastien Boussau, Hans Ellegren, Sankar Subramanian, Cai Li, Edward L. Braun, M. Thomas P. Gilbert, Guojie Zhang, Erich D. Jarvis

GC content calculations

We calculated the GC content across species and genomic partitions using the following formula:

$$\frac{G+C}{A+T+G+C} \times 100$$

For the protein coding positions, we calculated GC content at the 1st, 2nd, and 3rd codon position (GC1 GC2 and GC3) for each species, respectively. For all other data sets, we calculated the average GC content of 48 species for all nucleotide positions in the exons, introns, and UCEs.

Relationship between GC content, tree branch lengths, and body mass of avian species

A number of studies have suggested a significant relationship between life history traits such as body mass, metabolic rate and generation time and the rate of sequence evolution (*171-173*). Here we examined the relationship between body mass, GC content, and the species tree branch lengths.

Nucleotide content for c123, c12, and c3 were determined for exons of 830 orthologs genes (10% of total) with the highest and lowest variance in GC3, as well as the introns associated with these genes. To identify the genes, we calculated the variance in GC content

across species and then sorting the orthologs by the rank of the variance, using code in R. Nucleotide counts were tallied for all sites in a given class before computing the proportion of GC nucleotides for each species. From this ranking, we selecting the top and bottom 10% for analyses.

RAxML analyses on low variance vs. high variance introns were conducted with version 7.2.8 on UPPMAX (see Supplementary Acknowledgements) using the GTRGAMMA model and 100 bootstrap replicates. From these trees, we used the root-to-tip branch lengths, since the lengths of time between the root of the avian lineage of the most recent common ancestor (MRCA) and the tips of each avian species are the same. Theoretically the root-to-tip branch lengths of all avian species are expected to be similar (under a molecular clock assumption). Therefore variations in the root-to-tip lengths of avian species manifest the difference in the rate of evolution between them. Furthermore using root-to-tip branch lengths is advantageous particularly when comparing two different tree topologies (as is the case here).

Using the branch length estimates of the exon trees shown in figures 6A and 6B we calculated (by summing up) the root-to-tip branch length of each avian species for the homogeneous and heterogeneous genes respectively. We then performed correlation analysis between these branch lengths and the respective body masses. Body mass data was extracted from the CRC Handbook of Avian Body Masses (*174*), and from data available of persons of this collaboration that work with those species. Where multiple entries for a given species were present, the mean was calculated.

As described in the main text, we observed a significant positive correlation between branch length and GC content (**Fig. 6C**) and a negative correlation between branch length and body mass (**Fig. 6D**) for both low-variance and high-variance exons (also see **Fig. S17A,B**). In addition, we determined here if there was any effect of phylogenetic bias. To remove possible phylogenetic bias, we performed independent contrast analysis (*175*) using the ExaML TENT topology. The module *CONTRAST* of the software *PHYLIP* (*176*) was applied to the log-transformed values of body mass and branch lengths and the respective tree files. We found that the correlations were still highly significant for both low-variance and high-variance exons (**Table S14**). The most important finding was that the magnitude of the relationship between body mass and branch length was still much higher (four times) for high-variance exons than low-variance exons (slope of the regression is -0.12 vs -0.03 respectively; **Fig. 6D**). This suggests that reconstructing phylogenetic trees using high-variance exons could be severely affected by heterotachy caused by the variation in the body masses between avian species. This effect is much reduced for low-variance exons.

Bowker statistics

Bowker tests were computed on the 1st, 2nd and 3rd positions of the data set containing 1185 1:1 orthologs (genes without paralogs) across all avian species, using an approach described in (*177*) and modified in (*178*). Bowker tests are pairwise tests that compare the composition of two sequencest. In our analyses, they are significant if the two sequences cannot have evolved according to the homogenous GTR model. The metric we used is the number of significant Bowker tests (at the 5% level) for a given alignment.

Chromosome position

To plot the relative position of genes on chromosomes, we normalized the chromosome position

of each gene according to the chicken or zebra finch coordinates into a ratio, by dividing the original chromosome position (start bp site of the gene) by its chromosome size (total bp size). The ratio positions of all genes of a set (high variance or low variance genes) were then split into 100 bins, with bin size being the relative position values and the heights of the bins representing gene counts. To determine statistical differences, instead of using the bar plot directly, we transformed the position values into relative distances to the closest end of each chromosome, to get position values ranging from 0~0.5. The smaller values mean closer to the ends of the chromosomes. With the transformed position values, we performed a Wilcoxon rank sum test for the two sets of numbers (high variance and low variance), to determine if one set was closer to the ends of the chromosomes than the other set.

SM12 Fossil dating analyses

Simon Ho, Peter Houde, Joel Cracraft, Bent Lindow, Erich D. Jarvis, Jon Fjeldså, M. Thomas P. Gilbert, David P. Mindell, Scott V. Edwards, Edward L. Braun

Methods
To estimate the timescale of avian evolution and diversification, we first identified a subset of the 8,295 orthologs that has undergone clocklike evolution (constant evolutionary rate among lineages). This was done by analyzing the 1st and 2nd codon positions of each alignment using an uncorrelated lognormal relaxed clock (*179*) in the Bayesian phylogenetic software BEAST v1.7.2 (*180, 181*). This relaxed-clock model produces a coefficient of variation (CoV) of rates, which measures the degree of rate heterogeneity among lineages. A value of 0 reflects rate homogeneity among lineages (a strict molecular clock), whereas values >1 indicate a large degree of rate heterogeneity among lineages. Orthologs were selected for the dating analyses when the mean estimate of the CoV was less than 0.5 and the lower and upper limits of the 95% credibility interval of the CoV were less than 0.1 and 1.0, respectively. These criteria were satisfied by 1156 orthologs (722,202 nucleotides).

Bayesian dating analysis was conducted using a concatenated alignment comprising the 1st and 2nd codon positions of the 1156 orthologs selected in the previous step. The tree topology was fixed to each of different species trees that were estimated in this study, with a focus on the ExaML TENT tree (**Fig. S1**). Divergence times were estimated using the autocorrelated and uncorrelated relaxed clocks in MCMCTREE in PAML 4.6 (*77*). Both types of relaxed clock methods produced similar date estimates; results from the autocorrelated method are reported in this study. We used the HKY85+GAMMA model of nucleotide substitution, with four rate categories for gamma-distributed rates across sites. Due to the very large size of the dataset, we used the approximate-likelihood method with branch lengths estimated using maximum-likelihood in the PAML program baseml. We also examined the effects of varying the gamma prior for the overall rates for genes (rgene_gamma) and found that our date estimates were robust to changes in this prior.

Posterior distributions of divergence times were estimated by Markov chain Monte Carlo sampling, with samples drawn every 2000 steps over a total of 10^8 steps after a discarded burn-in of 2×10^7 steps. To check for convergence to the stationary distribution, each analysis (including the baseml step) was run in duplicate and the results were compared between runs.

Fossil calibrations
To estimate evolutionary timescales, it is necessary to include temporal information from an independent source. Our dating analysis was calibrated using between 17 and 20 minimum age constraints for nodes within Neornithes, with the exact number of calibrations dependent on the presence or absence of specific nodes in the tree (**Table S15**). For the ExaML TENT and MP-EST* TENT trees, respectively, we used 18 and 19 age constraints within Neornithes, represented by a set of non-redundant calibrations, selected from 39 candidate calibrations that are described in detail below. In all analyses, we placed a minimum age constraint of 66 Myr at the base of Neornithes (divergence between Neognathae and Palaeognathae). A maximum age constraint was placed on the divergence between Neognathae and Palaeognathae, corresponding to the lower boundary of the Upper Cretaceous (99.6 Myr). This value far exceeds the age of paleontological evidence for the existence of Neornithes, and it is 30 million years older than the divergence our dating analyses revealed for Neoaves.

Since an individual fossil represents a single lineage, it cannot be used reliably or consistently to date the divergence of two lineages. An individual fossil can either under- or overestimate the timing of a divergence event (**Fig. S28**). Ambiguity in taxonomic assignment can result not only from differences in opinion about similarity, but also from lack of knowledge of character state polarity. Because some avian "clades" are known to be paraphyletic, "characteristics" of clades may not be phylogenetically informative in documenting monophyly. Simply stated, symplesiomorphic characters may be mistaken for synapomorphies. The exception to this is when it is deemed "impossible", on the basis of specialization (e.g., flightlessness), that one group could not be ancestral to another. Fortunately, consensus can be reached for the placement of any fossil by assigning it to the taxonomic group that is inclusive of all alternative interpretations of placement. For example, if a fossil were identified by some as a penguin and by others as an owl, it can be used to place a minimum age constraint on the stem lineage leading to penguin+owl (plus all other taxa included in such a grouping). On the other hand, it must be acknowledged that requiring fossil representation from both of two lineages to document divergence will tend to systematically underestimate divergence times because it will have taken some unknown amount of time for the two lineages to become phenotypically distinct.

Using these criteria, we chose 39 candidate fossils as calibrations for our dating analysis. Depending on the tree topology, many of these candidate calibrations were redundant. As a consequence, our dating analyses only used between 17 and 20 of the 39 calibrations described below. **Figure S29** shows a graphic tree view of the calibration nodes used on the ExaML TENT.

Additional fossil tree dating results and discussion
Although introns can infer a tree closer to the species, we used clocklike exons, because our analysis of the 2516 conserved orthologous introns revealed widespread and substantial departures from clocklike evolution. Non-clock like rate heterogeneity among lineages can cause considerable difficulty for molecular dating, especially when the patterns of variation differ among loci (*182*). Using clocklike exons allows us to avoid the problem we found with tree inference using high variance exons. Further, since we only included the first and second codon positions of the clocklike exons, we use data that give a topology closer to the total evidence

data. The third codon positions of the high variance genes were the main source of the problems in using exon sequences for estimating the tree topology. Despite the differences in the tree topologies with different data sets, when we performed dating analyses on them, all, including the c123 tree with the biased high variance exons, yielded very similar results with regard to the timing of the Neoaves radiation as well as other nodes of interest in the tree. Thus, we do not believe that the reliance on the clock-like exons caused an error in the dating.

The Neoaves divergence dates were shifted slightly forward (about +2.6 million years) or backwards (about -4.1 million years) in time depending on whether the minimum age for Neornithes was moved ahead or if the non-avian outgroup fossils were removed, respectively, but the radiation was still dated to occur around the K-Pg event (**Table S16**). We also compared dating analyses using two outgroup calibrations: 247.0 and 250.4 Myr for the alligator-bird divergence and 255.9 and 299.8 for the lizard-bird divergence (*183*), and obtained similar results (**Table S16**).

Our findings (*8, 138*) are consistent with the hypothesis that the neoavian radiation was associated with the Chicxulub asteroid or other environmental impact and mass extinction event about 66 MYA (*4, 5*), but with several basal lineages of Neoaves likely diverging before and surviving through the event. This is in contrast to the much older molecular based estimates of neoavian divergences in several prior studies (*8, 138*) placing them 10-40 million years before the K-Pg boundary, which we believe may been biased by incorrect hypotheses of Cretaceous-age vicariance biogeography and a high substitution rate of the genes used for the Passeriformes. Our analysis was unconstrained by Cretaceous-age biogeographic priors (*8, 138*) and lacked the genes with increased substitution rates in passeriforms.

A recent morphology-based study (*12*) also had a similar much earlier Cretaceous date for the neoavian divergences. However, morphological characters are not clock-like, presumably not independent of one another, and are not described by any substitution model. Morphological characters also produce a dramatically different tree than molecular data as shown in this study, although tree topology did not have a dramatic effect on our results. Their upper bound was about 50 million years older than ours and contraindicated by the fossil record. The fossils they used did not meet our criteria for unambiguous temporal calibration. Finally, they used only 6 neoavian species, whereas we used 43. One or a combination of these differences could explain the differences with our study.

Documentation of fossil calibration evidence
Our numbering for fossil calibrations (**Table S15** and below) increases as consecutively as possible up the avian tree from its root, from oldest to youngest. Each calibration includes a heading to define its position on the TENT tree and its age. This is followed by designation of a higher taxon to which the reference fossil has been assigned or can be confidently assigned. This in turn is followed in each case by: a) in boldface italics the reference fossil species used for the calibration and the citation in ( ) of its taxonomic description; b) if warranted, citation of additional relevant papers describing reinterpretation of the reference fossil or additional fossil material; c) the stratigraphic range of the taxon with citation if warranted; and d) the parts of the skeleton from which the fossil is known. Under the same numbered calibration heading, some have additional fossil evidence that tentatively suggest temporal range extensions or provide additional support for the calibration.

1) Internal branch "*Struthio+Tinamus*" = MRCA "Palaeognathae+Neognathae" 60.6-61.57 MY
stem-Palaeognathae, †Lithornithidae
Lithornis celetius (*184*)
Late Paleocene (earliest Tiffanian; 60.6-61.57 MY) (*185*)
complete skeletons Lithornithidae
Latest Cretaceous to **Earliest Paleocene** (latest Maastrichian to earliest Danian), Hornerstown Formation, Monmouth County, New Jersey (*186*)
tentatively referred scapula

2) Terminal Branch "*Struthio*" 20 MY
Struthionidae
Struthio coppensi (*187*)
Early Miocene (East African Faunal Set PI, 20 MY) Elisabethfield, Namibia
hindlimb

3) Terminal Branch "*Tinamus*" = MRCA "*Struthio+Tinamus*" 16.5-17.5 MY
Tinamidae – gen indet, sp indet (*188*)
Early Miocene, Pinturas Formation Santa Cruz, Canadon de las Vacas, Santa Cruz, Argentina
MACN-SC-1399: distal tibiotarsus
Middle Miocene, Santa Cruz Formation, Argentina
referred coracoids and humeri

4) Internal branch "Neognathae" (i.e., 46 bird genomes excluding Struthio+Tinamus) 66-70 MY
stem-Anseriformes
Vegavis iaai (*80, 81, 189*)
Late Cretaceous (Middle? to Late Maastrichtian; 66–68 MY) unit K3, Cape Lamb, Vega Island, Antarctica
most of postcranial skeleton except furcula, sternum, and carpometacarpus

5) Terminal Branch "*Anas*" = MRCA "*Anas*+Galliformes" 51-54 MY
Anseriformes, ?Anseranatidae
Anatalavis oxfordi (*190*)
Early Eocene (Ypresian; 54-51 MY) London Clay Formation, Walton-on-the-Naze, Essex, England
skeleton lacking hindlimb

6) Internal Branch "*Gallus+Meleagris*" = MRCA "*Anas*+Galliformes" 50.3 MY
stem-Galliformes
Gallinuloides wyomingensis (*191-193*)
Early Eocene, Upper Fossil Butte Member, Green River Formation, near Kemerer, Wyoming
complete skeletons

7) Terminal Branch "*Pterocles*" 24.7 MY
stem-Pterocliformes

Leptoganga ("Pterocles") sepultus (*194, 195*)
Late Oligocene (MP28; 24.7 MY)
tarsometatarsi
Archaeoganga pinguis, A. larvatus, A. validis (*196*)
Quercy fissure fillings, no stratigraphic data
coracoid, humerus, tarsometatarsus

8) Terminal Branch "*Columba*" = MRCA "*Pterocles+Columba*+any others in between" 18 MY
Columbidae
Columbina prattae (*197*)
distal tarsometatarsus; >350 referred specimens represent nearly complete postcranial skeleton
Early Miocene (18-19 MY), Thomas Farm local Fauna, Early Hemingfordian, Gilchrist County,
Florida
Rupephaps taketake (*198*)
Early Miocene (Altonian; 16-19 MY) Bed HH1a, Bannockburn Formation, Manuherikia Group,
St Bathans Fauna, New Zealand
coracoid

9) Internal Branch "*Phoenicopterus+Podiceps*" 32 MY
Grebe-Flamingo stem group
Adelalopus hoogbutseliensis (*199*)
Lower Early Oligocene (Rupelian; MP21 32 MY) Belgium
coracoid
Palaelodus ambiguus (*200*)
Early Miocene (Agenian) Saint-Gerand-le-Puy, Allier, France
complete skeletons represented by many thousands of referred bones from hundreds of
individuals from this and congeneric species, *P. gracilipes* and *P. crassipes*

10) Terminal Branch "*Podiceps*" = MRCA "*Phoenicopterus+Podiceps*" 20.43-23.03 MY
Podicipedidae
Miobaptus walteri (*201*)
Early Miocene (Aquitanian; 20.43-23.03 MY) Dolnice, Cheb Basin, Czechoslovakia
proximal humerus, coracoid, tarsometatarsus

11) Terminal Branch "*Phoenicopterus*" 20.43-23.03 MY
Phoenicopteridae
Phoenicopterus croizeti (*202, 203*)
Late Oligocene to **Early Miocene** (Aquitanian; 20.43-23.03 MY), France
complete skeleton

12) Terminal Branch "*Balearica*" 32 MY
Gruiformes sensu Howard and Moore (*36*), Gruidae
Belgirallus oligocaenus and *B. minutus* (*204*)
Earliest Oligocene (MP 21; 32 MY) Boutersem, Belgium
distal humerus, coracoid, distal tarsometatarsus

Parvigrus pohli (*205*)
Early Oligocene (MP 24; 28.4-33.9 MY), Luberon, Vacheres, France
complete skeleton
Balearica exigua (*206*)
Lower Late Miocene (Late Clarendonian) Cap Rock Member, Ash Hollow Formation, Antelope
County, Nebraska
complete skeleton

13) Terminal Branch "*Opisthocomus*" 22-24 MY
Opisthocomidae
Hoazinavis lacustris (*207*)
Late Oligocene to **Early Miocene** (Late Deseadan; 22–24 MY**)** Tremembé Formation, Taubaté
Basin, São Paulo, Brazil
humerus, partial coracoid and scapula

14) Terminal Branch "*Turaco*" ~32 MY
Musophagidae – gen indet, sp indet (*208*)
Early Oligocene, Quarry M, Jebel Qatrani Formation, Fayum, Egypt
CGM 42836: distal tarsometatarsus; CGM 42837: distal humerus

15) Internal Branch "*Phaethon*+sister" 55.8 MY
stem-Phaethontiformes
Prophaethon shrubsolei (*209, 210*)
Early Eocene (Ypresian) London Clay Formation, Isle of Sheppey, England
skull, partial sternum, coracoid, scapula, femur, proximal tibiotarsus, vertebrae, synsacrum (*211*)
Lithoptila abdounensis (*212*)
Late Paleocene (Thanetian), Ouled Abdoun Basin, Morocco
cranium (*213*)
Late Paleocene and **Early Eocene** (Thanetian, Earliest Ypresian, Early Ypresian)
51 referred specimens including all major appendicular elements except scapula and tibiotarsus

16) Terminal Branch "*Gavia*" = MRCA "*Gavia*+sister" 32 MY
Gaviidae
Colymboides minitus (*194*)
Early Miocene Saint-Gerand-le-Puy, France (*201, 214-216*)
referred specimens comprise nearly complete postcranial skeleton
Colymboides metzleri (*217*)
Early Oligocene (Rupelian; MP21; 32 MY) clay pit of the Bott-Eder GmbH (Grube Unterfeld),
Frauenweiler, Baden- Württemberg, Germany
two dimensional rostral vertebrae, limb, sternum, pelvis, tarsometatarsus

17) Terminal Branch "*Fulmarus*" = MRCA "*Fulmarus*+sister" 32 MY
Procellariiformes
Diomedeoides brodkorbi (genus Fischer 1985; species Cheneval 1995) (*218*)

Early Oligocene (Rupelian; MP21; 32 MY) clay pit of the Bott-Eder GmbH (Grube Unterfeld), Frauenweiler, Baden- Württemberg, Germany
femur (*219*)
referred two dimensional complete skeleton

18) Internal Branch "*Phalacrocorax+Pelecanus+Egretta+Plegadis*" 50.2 $\pm$1.9 MY
Pelecaniformes sensu Howard and Moore (Cracraft 2013) (*36*)
Limnofregata azygosternon (*220*)
two dimensional complete skeleton and feathers
Upper Early Eocene (Ypresian or Lostcabinian) to **Lower Middle Eocene** (Lutetian or Bridgerian; 50.2 $\pm$ 1.9; (*221*)
Masillastega rectirostris (*222*)
Lower Middle Eocene (MP11; 47 MY), Grube Messel, Hessen, Germany
two dimensional skull

19) Terminal Branch "*Phalacrocorax*" 24.7 MY
Phalacrocoracidae
Borvocarbo stoeffelensis (*223*)
Late Oligocene (MP28; 24.7 MY) Enspel near Bad Marienberg, Reinland-Pfalz, Mainz, Germany
two dimensional complete skeleton

20) Internal Branch "*Charadrius*+sister" 32 MY
Charadriiformes
Boutersemia belgica and ***B. parvula*** (*204*)
Earliest Oligocene (MP 21; 32 MY) Boutersem, Belgium
Nupharanassa tolutaria and several others (*208*)
Early Oligocene, Quarry M, Jebel Qatrani Formation, Fayum, Egypt
distal tarsometatarsus

21) Internal Branch "*Pygoscelis+Aptenodytes*" 60.5–61.6 MY
Sphenisciformes
Waimanu manneringi and ***W. tuatahi*** (*224*)
W.manneringi:
Late Early Paleocene (60.5–61.6 MY), Basal Waipara Greensand, Waipara River, New Zealand
tibiotarsus, proximal fibula, tarsometatarsus, pelvis, synsacrum
W. tuatahi:
Lower Late Paleocene (58–60 MY) Upper Waipara Greensand, Waipara River, New Zealand
skull fragments, incomplete mandible, cervical vertebrae, synsacrum, furcula, coracoids, partial scapula, humerus, ulna, radius, proximal femur

22) Internal Branch "*Egretta+sister*" 25.3-26.39 MY
Pelecaniformes sensu Howard and Moore (Cracraft 2013) (*36*), stem-Ardeidae
Proardea amissa (*225*)
distal tarsometatarsus

"undescribed specimens"
Late Oligocene (MP 28; 25.3-26.39 MY) Quercy fissure fillings, Pech Desse, France (*96*)
Proardeola (=*Proardea*) *walkeri* (*226*)
Late Oligocene to Early Miocene, Chavroches, Allier, France
tarsometatarsus
Calcardea junnei (*227*)
Early Eocene (Wasatchian), Willwood Formation, Bighorn Basin, Wyoming
partial coracoid

23) Terminal Branch "*Plegadis*+sister" 47 MY
Pelecaniformes sensu Howard and Moore (Cracraft 2013) (*36*), stem-Threskiornithidae
Rhynchaeites messelensis (*228-230*)
Lower Middle Eocene (MP11; 47 MY), Grube Messel, Hessen, Germany
several referred complete two-dimensional skeletons

24) Terminal Branch "*Tyto*" = MRCA "*Tyto*+sister" 56.8-61.7 MY
stem-Strigiformes
Ogygoptynx wetmorei (*231*)
Late Paleocene (Tiffanian), Mason Pocket, Colorado
tarsometatarsus
Berruornis orbisantiqui (*232*)
Late Paleocene (Thanetian; MP 6), Reims area (Cernay and Monte Berru), Marne Département,
France
distal tibiotarsus and tarsometatarsus
Berruornis – sp indet (*233*)
Late Paleocene, Walbeck fissure filling, Germany
incomplete tarsometatarsus, premaxilla
Eostrix (Protostrix) mimica (*234*)
Early Eocene, Wasatch Fm, South side of Ten Mile Creek, near Worland, Wyoming
distal tibiotarsus, referred distal tarsometatarsus

25) Internal Branch "*Haliaeetus*+*Haliaetus*+*Cathartes*" 37.7-38.9 MY
stem-Accipitriformes
Horusornis vianeyliaudae (*235*)
Late Eocene (MP17), Gisement de La Bouffie, Phosphorites du Quercy
tarsometatarsus; referred material includes all major postcranial bones and phalanges

26) Internal Branch "*Colius*+*Picoides*+all others in between" 56.0-56.5 MY
Coraciimorphae, †Sandcoleidae
Sandcoleus copiosus (*97*)
Earliest Eocene (Middle Clarkforkian, *Plesiadipis cooki* zone; 56-56.5 MY), Sand Coulee Beds,
Willwood Formation, Clark's Fork Basin, Wyoming
complete skeleton, referred partial skeletons
Chascacocolius oscitans (*97*)

Early Eocene (Early Wasatchian; max. 55.1 MY) Grey Bull Beds, Willwood Formation, Clark's Fork Basin, Wyoming
mandible and appendicular skeleton except tarsometatarsus

27) Internal Branch "*Colius*+sister" 37.7 MY
Coliiformes
Primocolius minor and ***P. sigei*** (*236*)
Late Eocene, Perriere (MP 17), Escamps (MP 19; 35.5 MY), Phosphorites du Quercy, France (*237, 238*)
P. minor:
humerus, proximal carpometacarpus
P. sigei:
tarsometatarsus, distal humerus
Palaeospiza bella (*239, 240*)
Upper Late Eocene (Chadronian; 34.07-36.73 MY), Florissant Formation, Colorado
Oligocolius brevitarsus (*241*)
Early Oligocene (Rupelian; MP21; 32 MY) clay pit of the Bott-Eder GmbH (Grube Unterfeld), Frauenweiler, Germany
postcranial skeleton lacking one wing and foot

28) Internal Branch "?*Leptosomus*+sister" – 53 MY
Coraciimorphae, †Plesiocathartidae
Plesiocathartes kelleri (*242, 243*)
Lower Middle Eocene (MP11; 47 MY), Grube Messel, Hessen, Germany
complete two dimensional skeletons with feathering
Plesiocathartes wyomingensis and ***P. major*** (*244*)
Early Eocene, Green River Formation, Wyoming
Plesiocathartes wyomingensis: complete two-dimension skeleton
Plesiocathartes major: two dimensional postcranial skeleton lacking wings

29) Terminal Branch "*Apaloderma*" = MRCA "*Apaloderma*+sister" – 55.5 MY
Trogoniformes
Septentrogon madseni (*245*)
 Latest Paleocene-Earliest Eocene, Fur Formation, Ejerslev Industrial Pit, Island of Mors, Jutland, Denmark
neurocranium
 "Primotrogon?" pumilio (*246*)
Lower Middle Eocene (MP11; 47 MY; cited as 49 MY in above reference), Grube Messel, Hessen, Germany
two dimensional skeleton

30) Terminal Branch "*Picoides*" = MRCA of "Piciformes+Passeriformes+any others in between" 32 MY
Piciformes (suborder Pici)
Rupelramphastoides knopfi (*247*)

Early Oligocene (Rupelian; MP21; 32 MY) clay pit of Bott-Eder GmbH (Grube Unterfeld) Baden- Württemberg, Germany
two dimensional appendicular skeleton
Capitonides europeus (*248*) *as cited by* (*249*)
Middle Miocene (early Burdigalian fissure deposit) Bavaria: Wintershof (West), Germany
carpometacarpus (*250*)
referred humerus, ulna, tibiotarsus, tarsometatarsus

31) Terminal Branch: *Buceros* 47 MY
Bucerotes, stem-"Upupiformes" or "Bucerotiformes"
Messelirrisor grandis (*251, 252*)
Lower Middle Eocene (MP11; 47 MY), Grube Messel, Hessen, Germany
pectoral girdle and limb; referred complete skeleton and pigmented feathers

32) Internal Branch "Steatornithidae+sister" 50.2 +1.9 MY
Caprimulgiformes sensu Howard and Moore (Cracraft 2013) (*36*), stem-Steatornithidae
Prefica nivea (*253, 254*)
Late Early Eocene (Lostcabininan substage of Wasatchian or Ypresian) to **Early Middle Eocene** (Bridgerian or Lutetian; 50.2 + 1.9 MY), Fossil Lake locality F-2, Fossil Butte Member, Green River Formation, Lincoln County, Wyoming (*221*)
mandible and two dimensional postcranial skeleton

33) Terminal Branch "*Antrostomus*" = MRCA "*Antrostomus*+(*Chordeiles*,*Calypte*)" 47 MY
Caprimulgiformes sensu Howard and Moore (Cracraft 2013) (*36*), Nyctibiidae
Paraprefica kelleri (*254, 255*)
Lower Middle Eocene (MP11; 47 MY), Grube Messel, Hessen, Germany
two dimensional caudal half of skeleton and wing; referred two dimensional postcranial skeleton and nearly complete skeleton and feathers

34) Internal Branch "*Chaetura+Calypte*" 55.5 MY
Caprimulgiformes sensu Howard and Moore (Cracraft 2013) (*36*), suborder Apodi
Eocypselis vincenti (*256, 257*)
Earliest Eocene (Ypresian), London Clay Formation, England (*258*)
Earliest Eocene (Ypresian), Fur Formation, Isle of Mors, Jutland, Denmark
pectoral appendage and girdle; referred complete and postcranial skeletons
Scaniacypselus szarskii (*259*)
Middle Eocene, Messel, Germany
complete two dimensional feathered skeleton

35) Terminal Branch "Calypte" 32 MY – MRCA hummingbird and swift
Caprimulgiformes sensu Howard and Moore (Cracraft 2013) (*36*), suborder Trochili
Eurotrochilus inexpectatus (*260, 261*)
Early Oligocene (Rupelian; MP21; 32 MY) clay pit of the Bott-Eder GmbH (Grube Unterfeld), Frauenweiler, Baden- Württemberg, Germany
two dimensional complete skeletons

36) Internal Branch "Cariamidae+sister" 47 MY
Stem-Cariamiformes
Idiornis tuberculata (*262*)
Lower Middle Eocene (MP11; 47 MY), Grube Messel, Hessen, Germany
complete two dimensional skeleton
Elaphrocnemus phasianus (*225, 263, 264*)
Late Eocene, Phosphorites du Quercy, Escamps (MP 19)
skull and all major appendicular elements
Paleopsilopterus itaboraiensis (*265*)
Late Paleocene
distal tibiotarsus, proximal tarsometatarsus

37) Internal Branch "*Acanthisitta+Manacus+Corvus+Taeniopygia+Geospiza+Merops*+any
others in between" 54.6 MY
Coraciopasseres, ?Passeriformes – fam indet, gen indet, sp indet
Early Eocene (Wangerripian; 54.6 MY)**,** Tingamarra local fauna, Murgon, Queensland,
Australia (*80, 96, 266-269*)
QM F20688: proximal carpometacarpus; F24685: distal tibiotarsus
fam indet, gen indet, sp indet (*270*)
Early Oligocene (Rupelian; MP21; 32 MY) clay pit of the Bott-Eder GmbH (Grube Unterfeld),
Frauenweiler, Baden-Württemberg, Germany
SMF Av 497: two dimensional complete skeleton

38) Internal Branch "*Manacus+Corvus+Taeniopygia+Geospiza*" 16.3-13.6 MY – MRCA
suboscine and oscine
Passeriformes, suborder Tyranni (suboscines) ?Eurylaimidae – gen indet, sp indet
Middle Miocene (early Burdigalian) Bavaria: Wintershof (West) (*250*) *as cited by* (*271*)
Early Oligocene (Rupelian; MP21; 32 MY) Baden-Württemberg, Germany
distal humerus, proximal ulna, distal tarsometatarsus
Passeriformes, suborder Passeres (oscines), stem-Corvidae
Miocitta galbreathi (*272*)
Late Miocene (16.3-13.6 MY), Kennesaw local fauna, lower Pawnee Creek Fm, Colorado
distal humerus

39) Terminal Branch "*Corvus*" = MRCA "*Corvus*+(*Taeniopygia,Geospiza*)" 11.6-7.2 MY
Corvidae
Corvus larteri (*194*)
Late Miocene (Tortonian) Sansan, Gers Département, France
nearly complete postcranial skeleton

SM13 Data availability
We deposited data generated for this study in several publically available databases. The
assembled genomes as well as the ability to BLAST/BLAT search and browse them are available

in six databases listed below. The GigaScience source [reported as data notes (*276*, *277*)] is useful for downloading the assembled genomes, and all other data. The ENSEMBL, NCBI, and UCSC databases are useful for browsing the genomes, performing sequence BLAST/BLAT searchers, and analyzing pre-determined comparative analyses performed by those groups. The CoGe database is useful for performing your own comparative analyses. In addition, the phylomeDB generated gene trees are analyzable and downloadable from the phylomeDB site listed below. **Table S17** (excel file) list the accession numbers by species for each of the databases that give accession numbers.

Genome downloads, BLAST searchable and Genome Browsing Databases:
Original genome download data repository (http://phybirds.genomics.org.cn)
GigaScience Downloads (http://gigadb.org/dataset/101000; species URLs in Table S17)
ENSEMBL: (http://ensembl-birds.narf.ac.uk)
NCBI: (species URLs in Table S17)
UCSC: (http://genome.ucsc.edu/cgi-bin/hgGateway; under vertebrate genomes)
CoGe: (https://genomevolution.org/wiki/index.php/Bird_CoGe)

Files below are downloadable in the GigaScience data notes (above) associated with this study:

Filtered loci sequence alignments
- 8295 Exons
- 8295 Amino Acids
- 2516 Introns
- 3769 UCE+1000 flanking bp
- 2022 supergene alignments generated from statistical binning.

Unfiltered loci sequence alignments
- Amino.Acid.unfiltered
- Exon.c123.unfiltered:
- Intron.unfiltered
- UCE.unfiltered
- WGT.unfiltered

FASTA files of concatenated datasets in alignments
We provide FASTA files of concatenated sequence alignments of the above filtered loci datasets.

Concatenated alignments used in ExaML analyses:
- Exon.AminoAcid.ExaML.partitioned
- Exon.c123. ExaML.partitioned
- Exon.c123. ExaML.unpartitioned
- Exon.c1.ExaML.unpartitioned
- Exon.c2.ExaML.unpartitioned
- Exon.c12.ExaML.unpartitioned
- Exon.c123-RY.ExaML.unpartitioned

- Exon.c3.ExaML.unpartitioned
- Intron
- TEIT.RAxML
- TENT+c3.ExaML
- TENT+outgroup.ExaML
- TENT.ExaML.100%
- TENT.ExaML.25%
- TENT.ExaML.50%
- TENT.ExaML.75%
- WGT.ExaML

Concatenated alignments used in RAxML analyses:
- UCE concatenated alignments with and without the alligator

Clocklike exon alignment
Concatenated c12 ($1^{st}+2^{nd}$ codons) DNA sequence alignments from the 1156 clocklike genes were used for the dating analyses. These are alignments of the first and second codon positions of clock-like genes among the 8295 exon orthologs:
- c12.DNA.alignment.1156.clocklike.zip
- c12.DNA.alignment.1156.clocklike.txt

High and low variance exons and their associated introns
- High variance exons:
  - Exon.heterogenous.c123
  - Exon.heterogenous.c12
- Low variance exons:
  - Exon.homogenous.c123.
  - Exon.homogenous.c12
- High variance introns: These are heterogeneous introns
  - concatIntronNooutMSAlow.fasta.gz
- Low variance introns: These are homogenous introns
  - concatIntronNooutMSAhigh.fasta.gz

Indel sequence alignments
This is a concatenated alignment of indels from exons, introns, and UCEs.

Transposable element markers
- owl_TE_marker_Table.txt

Species and gene tree files
Species trees (Newick format) were generated with either RAxML, an improved ExaML version for handling large alignments, or MP-EST*. We deposit both the maximum likelihood and bootstrap replicate trees.

Newick files for 32 species trees using different genomic partitions and methods:

- Exon.AminoAcid.ExaML.partitioned.tre
- Exon.c123.ExaML.partitioned.tre
- Exon.c123.ExaML.unpartititoned.tre
- Exon.c123-RY.ExaML.unpartitioned.tre
- Exon.c12.ExaML.partitioned.tre
- Exon.c12.ExaML.unpartitioned.tre
- Exon.c1.ExaML.unpartitioned.tre
- Exon.c2.ExaML.unpartitioned.tre
- Exon.c3.ExaML.unpartitioned.tre
- Exon.RAxML.heterogenous.c123.tre
- Exon.RAxML.heterogenous.c12.tre
- Exon.RAxML.homogenous.c123.tre
- Exon.RAxML.homogenous.c12.tre
- Intron.RAxML.heterogenous.tre.txt
- Intron.RAxML.homogenous.tre.txt
- Intron.RAxML.partitioned.tre
- Intron.RAxML.unpartitioned.tre
- Intron.MP-EST.binned.tre

- Intron.MP-EST.unbinned.tre

- TEIT.RAxML.tre
- TENT+c3.ExaML.tre
- TENT+outgroup.ExaML.tre
- TENT.ExaML.100%.tre
- TENT.ExaML.25%.tre
- TENT.ExaML.50%.tre
- TENT.ExaML.75%.tre
- UCE.RAxML.unpartitioned.tre
- WGT.ExaML.alternative.tre
- WGT.ExaML.best.tree

Newick files of the 11 timetrees (chronograms):

- Chronogram01.TENT.ExAML.tre
- Chronogram02.TENT.ExAML.max865.tre
- Chronogram03.TENT.ExAML.Allig247.tre
- Chronogram04.TENT.ExAML.no-outgroup.tre
- Chronogram05.TENT.ExAML.no-outgroup.max865.tre
- Chronogram06.TENT.MP-EST.tre
- Chronogram07.WGT.ExAML.alternative.tre
- Chronogram08.WGT.ExAML.best.tre
- Chronogram09.Intron.ExAML.unpartitioned.tre

- Chronogram10.UCE.RAxML.tre
- Chronogram11.Exon.c123.RaXML.partitioned.tre

Newick file downloads of gene trees (species abbreviated with 5-letter names):
- ML (bestML) gene trees
- Bootstrap replicates of ML gene trees
- ML (bestML) supergene trees used in MP-EST analyses
- Bootstrap replicates of supergene trees used in MP-EST analyses
- Partition files showing which loci make up which bins for MP-EST analyses

List of scripts used in avian comparative genome project
We also deposit the key scripts used in this project in GigaDB, which include:
- Script for filtering amino acid alignments
- Script for filtering nucleotide sequence alignments
- Script for mapping names from 5-letter codes to full names
- Scripts related to indel analyses

PhylomeDB data: All gene trees, alignments and orthology and paralogy calls for the five phylomes are available through phylomeDB (http://phylomedb.org).
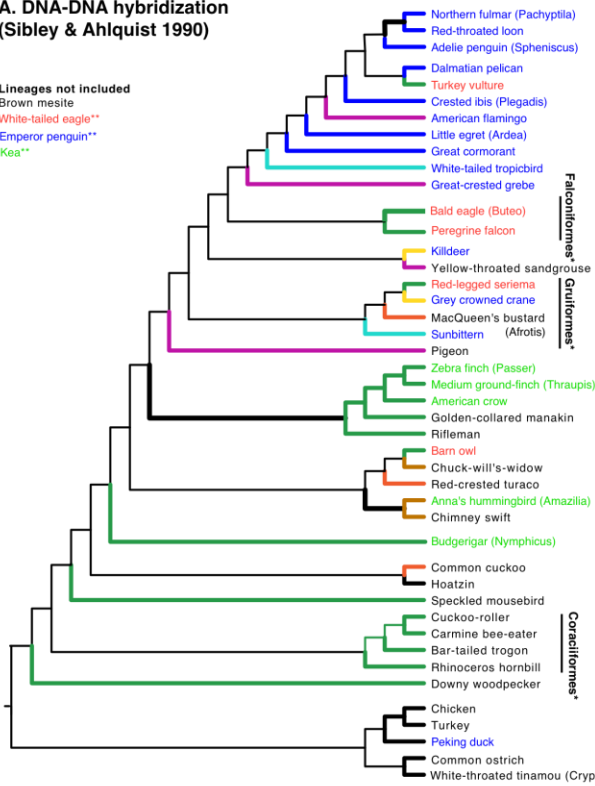
Supplementary figures
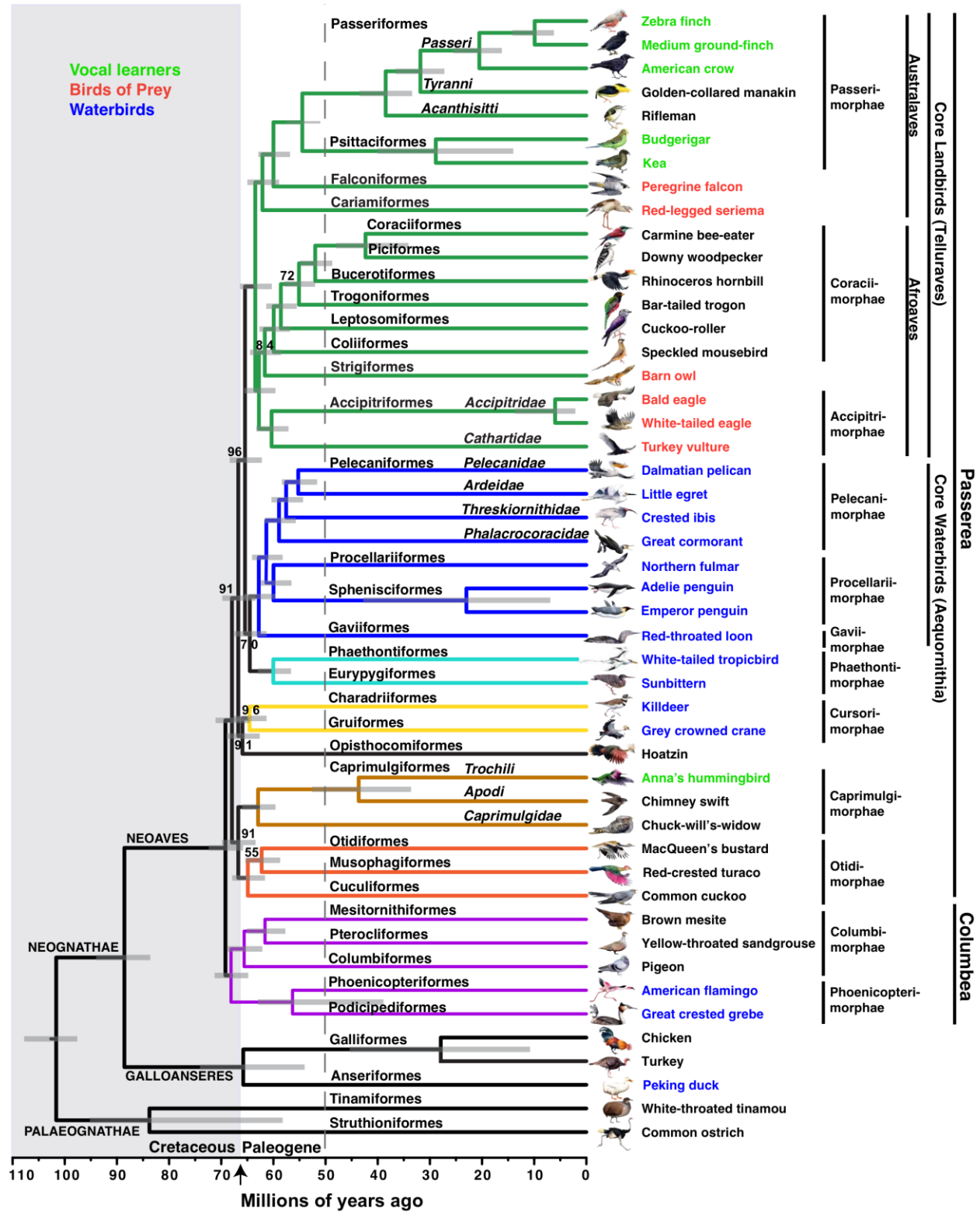
Fig. S1. Genome-scale phylogeny of birds, showing an uncollapsed tree of all species sequenced. Figure explanation is the same as in the legend of Figure 1. In addition, we note the following: The Neoaves radiation appears to exhibit three nested radiations, the initial radiation soon after the Columbea and Passerea split followed by core waterbird and core landbird radiations within the Passerea. Branches with very closely related species within the same order or suborder are not collapsed and thus the tree shows all species sequenced. The 6 branches within Passerea that have less than 100% support included placement of: 1) the superorder Otidimorphae (turacos, bustards, and cuckoos); 2) the Caprimulgimorphae (hummingbirds, swifts, and nightjars); 3) the Cursorimorphae (cranes and killdeer; but 100% in some other analyses); 4) the Phaethontimorphae (sunbittern and tropicbirds; but 100% in other analyses); 5) the hoatzin; and 6) the owl among core landbirds. It is difficult to infer from the tree whether the common ancestor of Neoaves was aquatic or terrestrial, since the number of divergences after the Columbea and Passerea split and thereby also after the Neognathae split to obtain an aquatic or semi-aquatic versus terrestrial species are nearly equal. English species names are listed, as well the names of families (-idae), following the Howard & Moore edition 4 classification (*36*), for orders that we dated to have diverged before 50 MYA. This leaves open the possibility that clades within Accipitriformes (the Accipitridae and Cathartidae families), Pelicaniformes (the Pelecanidae, Ardeidae, Threskiornithidae, and Phalacrocoracidae families), and Caprimulgiformes (the Trochilidae+Apodidae and Caprimulgidae families) could be raised or re-designated ordinal status should future evidence support these findings. This tree was generated using ExaML (SM4) and dated using a Bayesian approach with fossil calibrations (SM12).
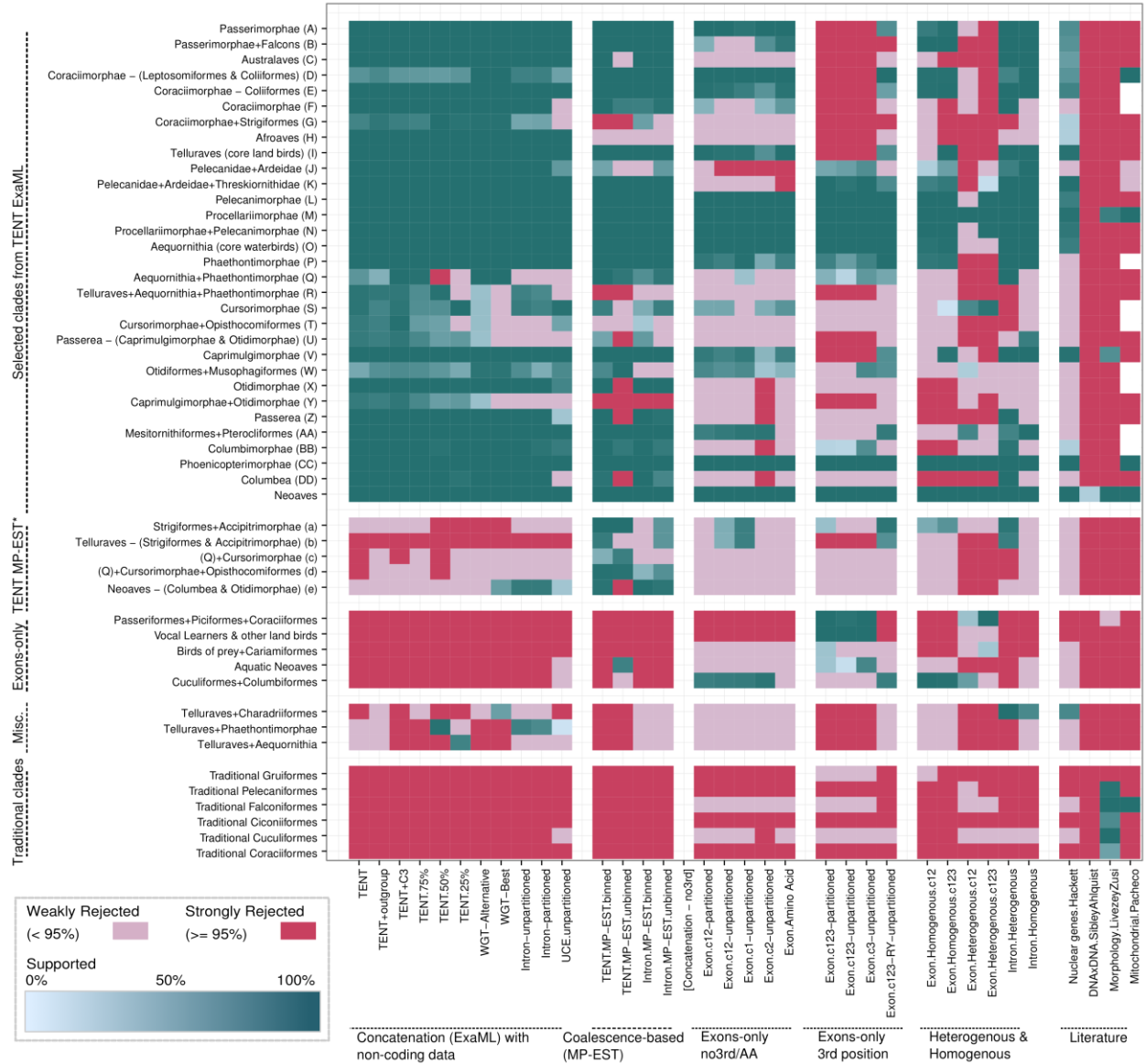
Fig. S2. Metatable analysis of species trees expanded. Figure explanation is the same as in the legend of Figure 2. This table has additional control results from partitioned ExaML, unbinned MP-EST, and Exon codon tree analyses. Letters (A-DD, a-e) denote clade nodes highlighted in Figure 3A,B of the ExaML and MP-EST* TENT trees. Each column represents a species tree; each row represents a potential clade. Blue-green signifies the monophyly of a clade, and shades show the level of its bootstrap support (0-100%); red, rejection of a clade; white, missing data. We used a 95%, instead of a standard 75%, cut-off for strong rejection due to higher support values with genome scale data. The threshold for the mitochondrial study was set to 99% due to Bayesian posterior probabilities yielding higher values than BS. The methods used to generate the metatable analyses is in SM7.
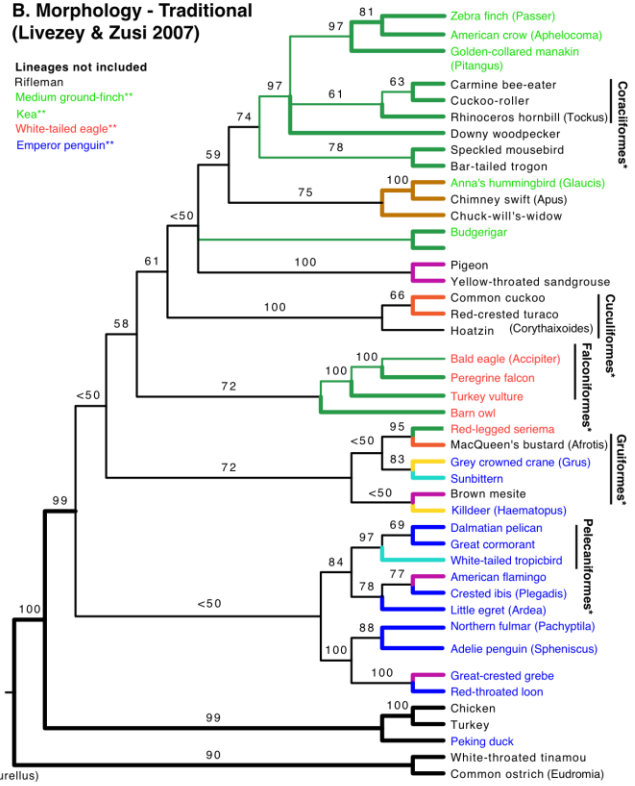
51

A. DNA-DNA hybridization (Sibley & Ahlquist 1990)

Lineages not included
Brown mesite
White-tailed eagle**
Emperor penguin**
Kea**

Northern fulmar (Pachyptila)
Red-throated loon
Adelie penguin (Spheniscus)
Dalmatian pelican
Turkey vulture
Crested ibis (Plegadis)
American flamingo
Little egret (Ardea)
Great cormorant
White-tailed tropicbird
Great-crested grebe
Bald eagle (Buteo)
Peregrine falcon
Killdeer
Yellow-throated sandgrouse
Red-legged seriema
Grey crowned crane
MacQueen's bustard (Afrotis)
Sunbittern
Pigeon
Zebra finch (Passer)
Medium ground-finch (Thraupis)
American crow
Golden-collared manakin
Rifleman
Barn owl
Chuck-will's-widow
Red-crested turaco
Anna's hummingbird (Amazilia)
Chimney swift
Budgerigar (Nymphicus)
Common cuckoo
Hoatzin
Speckled mousebird
Cuckoo-roller
Carmine bee-eater
Bar-tailed trogon
Rhinoceros hornbill
Downy woodpecker
Chicken
Turkey
Peking duck
Common ostrich
White-throated tinamou (Crypturellus)
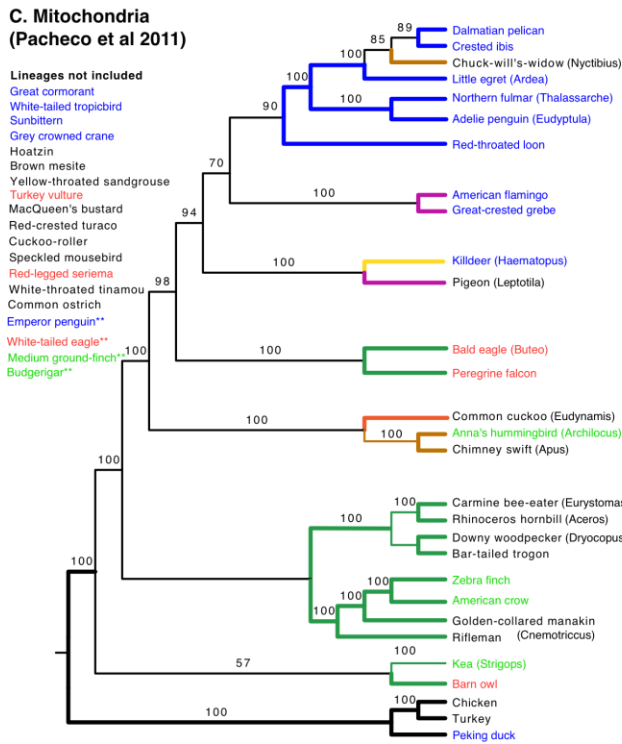
Falconiformes*
Gruiformes* (Afrotis)
Coraciiformes*

B. Morphology - Traditional (Livezey & Zusi 2007)

Lineages not included
Rifleman
Medium ground-finch**
Kea**
White-tailed eagle**
Emperor penguin**

Zebra finch (Passer) — 81
American crow (Aphelocoma) — 97
Golden-collared manakin (Pitangus)
Carmine bee-eater — 63
Cuckoo-roller — 61
Rhinoceros hornbill (Tockus)
Downy woodpecker — 78
Speckled mousebird
Bar-tailed trogon — 97
Anna's hummingbird (Glaucis) — 100
Chimney swift (Apus)
Chuck-will's-widow — 75
Budgerigar
Pigeon — 100
Yellow-throated sandgrouse
Common cuckoo — 66
Red-crested turaco — 100
Hoatzin (Corythaixoides)
Bald eagle (Accipiter) — 100
Peregrine falcon
Turkey vulture
Barn owl
Red-legged seriema — 95
MacQueen's bustard (Afrotis) — 83
Grey crowned crane (Grus)
Sunbittern
Brown mesite
Killdeer (Haematopus)
Dalmatian pelican — 97
Great cormorant — 69
White-tailed tropicbird
American flamingo — 78
Crested ibis (Plegadis) — 77
Little egret (Ardea)
Northern fulmar (Pachyptila) — 88
Adelie penguin (Spheniscus)
Great-crested grebe — 100
Red-throated loon
Chicken — 100
Turkey
Peking duck — 99
White-throated tinamou — 90
Common ostrich (Eudromia)

Coraciiformes*
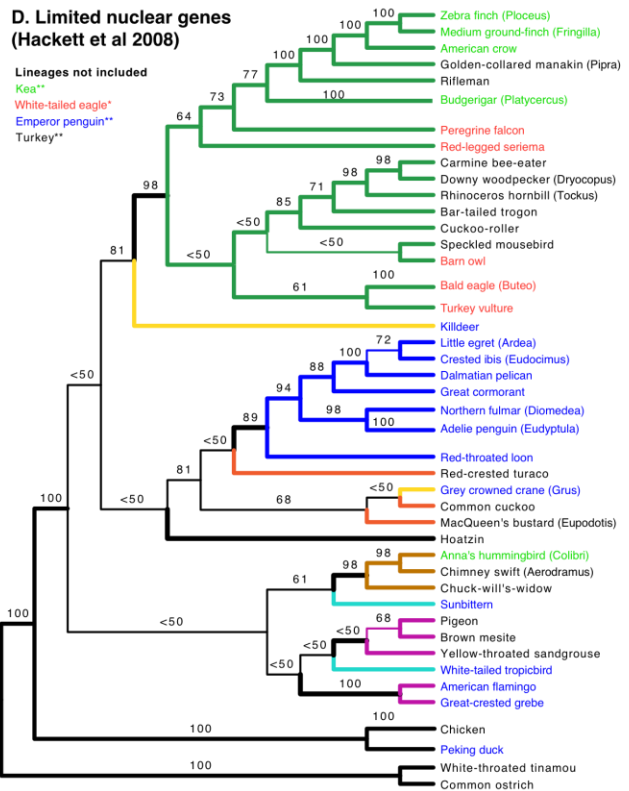Cuculiformes*
Falconiformes*
Gruiformes*
Pelecaniformes*

C. Mitochondria (Pacheco et al 2011)

Lineages not included
Great cormorant
White-tailed tropicbird
Sunbittern
Grey crowned crane
Hoatzin
Brown mesite
Yellow-throated sandgrouse
Turkey vulture
MacQueen's bustard
Red-crested turaco
Cuckoo-roller
Speckled mousebird
Red-legged seriema
White-throated tinamou
Common ostrich
Emperor penguin**
White-tailed eagle**
Medium ground-finch**
Budgerigar**

Dalmatian pelican — 89
Crested ibis — 85
Chuck-will's-widow (Nyctibius) — 100
Little egret (Ardea)
Northern fulmar (Thalassarche) — 100
Adelie penguin (Eudyptula) — 90
Red-throated loon
American flamingo — 100
Great-crested grebe
Killdeer (Haematopus) — 100
Pigeon (Leptotila)
Bald eagle (Buteo) — 100
Peregrine falcon
Common cuckoo (Eudynamis) — 100
Anna's hummingbird (Archilocus) — 100
Chimney swift (Apus)
Carmine bee-eater (Eurystomas) — 100
Rhinoceros hornbill (Aceros)
Downy woodpecker (Dryocopus) — 100
Bar-tailed trogon
Zebra finch — 100
American crow — 100
Golden-collared manakin — 100
Rifleman (Cnemotriccus)
Kea (Strigops) — 100
Barn owl — 57
Chicken — 100
Turkey — 100
Peking duck

(numbers: 70, 94, 98, 100, 100, 100)

D. Limited nuclear genes (Hackett et al 2008)

Lineages not included
Kea**
White-tailed eagle*
Emperor penguin**
Turkey**

Zebra finch (Ploceus) — 100
Medium ground-finch (Fringilla) — 100
American crow — 100
Golden-collared manakin (Pipra) — 77
Rifleman — 73
Budgerigar (Platycercus) — 100
Peregrine falcon — 64
Red-legged seriema
Carmine bee-eater — 98
Downy woodpecker (Dryocopus) — 71
Rhinoceros hornbill (Tockus) — 85
Bar-tailed trogon
Cuckoo-roller — 98
Speckled mousebird — <50
Barn owl — <50
Bald eagle (Buteo) — 100
Turkey vulture — 61
Killdeer
Little egret (Ardea) — 72
Crested ibis (Eudocimus) — 100
Dalmatian pelican — 88
Great cormorant — 94
Northern fulmar (Diomedea) — 98
Adelie penguin (Eudyptula) — 100
Red-throated loon — 89
Red-crested turaco — 81
Grey crowned crane (Grus) — <50
Common cuckoo — 68
MacQueen's bustard (Eupodotis)
Hoatzin
Anna's hummingbird (Colibri) — 98
Chimney swift (Aerodramus) — 61
Chuck-will's-widow
Sunbittern
Pigeon — 68
Brown mesite — <50
Yellow-throated sandgrouse — <50
White-tailed tropicbird — 100
American flamingo — 100
Great-crested grebe
Chicken — 100
Peking duck
White-throated tinamou — 100
Common ostrich

(numbers: 98, 81, 100, <50, <50, 100, 100)

Fig. S3. Example species trees based on the prior literature graphed according to the lineages analyzed in this study. (**A**) Morphology inferred species tree of Livezey and Zusi 2007 (*15*). (**B**) DNA-DNA hybridization species tree of Sibley and Ahlquist 1990 (*24*). (**C**) Mitochondrial species tree of Pacheco et al 2011 (*14*). (**D**) Nuclear DNA species tree of Hackett et al 2008 (*17*). Color-coding of branches and species names are the same as the ExaML TENT tree in Figures 1 and S1. Thin branches are those that are incongruent with our ExaML TENT. To facilitate comparison of our trees with the prior literature trees, we used names of species we studied. If a different genus was studied in the prior literature, then it is identified in parentheses (). The 'lineages not included' list for each panel are species representing ordinal lineages present in our study, but not present in the prior studies of A-C; ** = The few cases where we had two closely related species with the same order (such as the two eagles), where prior studies had only one species (see SM7 for further explanation). Numbers at nodes, percent bootstrap support. The DNA-DNA hybridization tree does not have bootstrap support values associated with it. The mitochondrial DNA tree reports Bayesian Posterior Probabilities, not bootstrap support. Branches labeled "< 50%" were reported as being less than 50% in those studies, but the exact value not specified. * = Traditional clade descriptions of these groups that differ from our findings.

A. TENT

B. TENT + outgroups
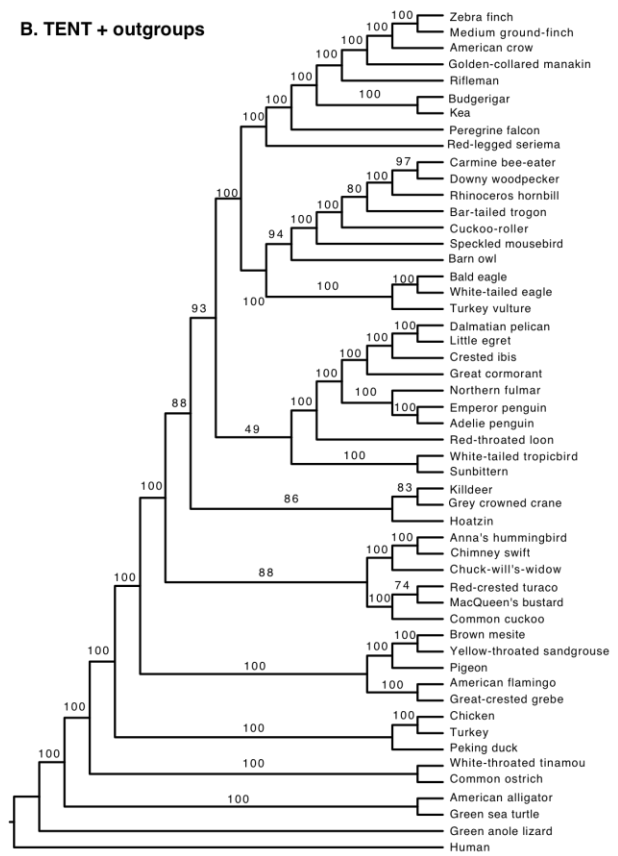
C. Whole Genome Tree - Alternative
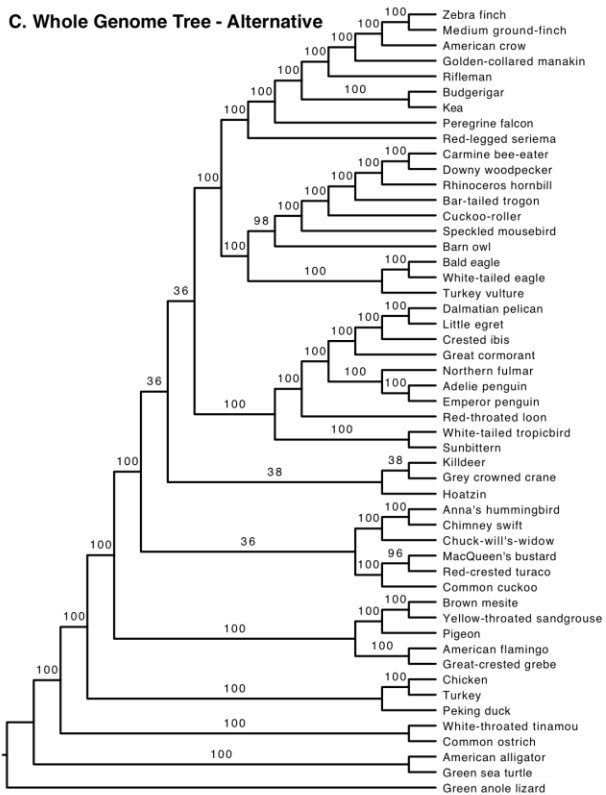
D. Whole Genome Tree - Best

54
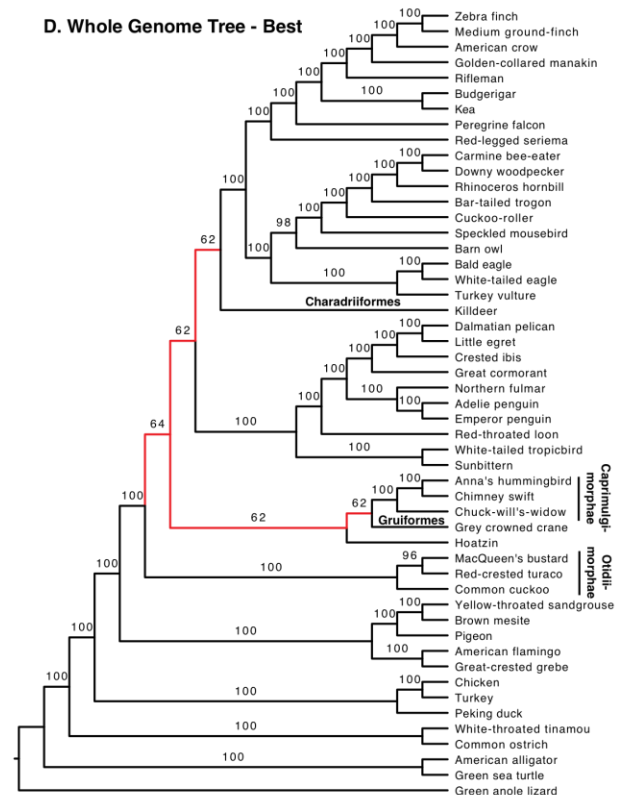
Fig. S4. Outgroup and whole genome species trees. (**A**) TENT from Figure S1 for comparison (not annotated for clade branches or species traits). (**B**) TENT including data from genomes of outgroups (alligator, lizard, turtle, and human); the tree topology is identical to TENT topology without outgroups in A. However, branches that had lower than 100% support in the TENT without outgroups showed a decrease in support when outgroups were included, presumably due to missing outgroup sequence in the alignment. (**C**) Whole genome tree (WGT)-Alternative with reptile outgroups that is identical to TENT topology. (**D**) Whole genome tree (WGT)-Best with reptile outgroups that has local differences (red branches) relative to whole genome tree-A and TENT. The WGT-Best differed from the TENT by local shifts in five closely positioned branches, all clades that had less than 100% BS in the TENT. Specifically, the clade comprising Cursorimorphae (Charadriiformes + Gruiformes) and hoatzin was now split up, with Charadriiformes (killdeer) placed as sister to core landbirds and Gruiformes (crane) and hoatzin as successive sister taxa to Caprimulgimorphae; as a result that also split the superorders Caprimulgimorphae and Otidimorphae from each other. The WGT-Best had a slightly higher log likelihood (-4637815006) than the one identical to the TENT (-4637826564), but it had a lower average BS support than the TENT (**Figs. 5A** and **S4A,D**). The trees were generated using ExaML (SM4) with alignments described in SM3.
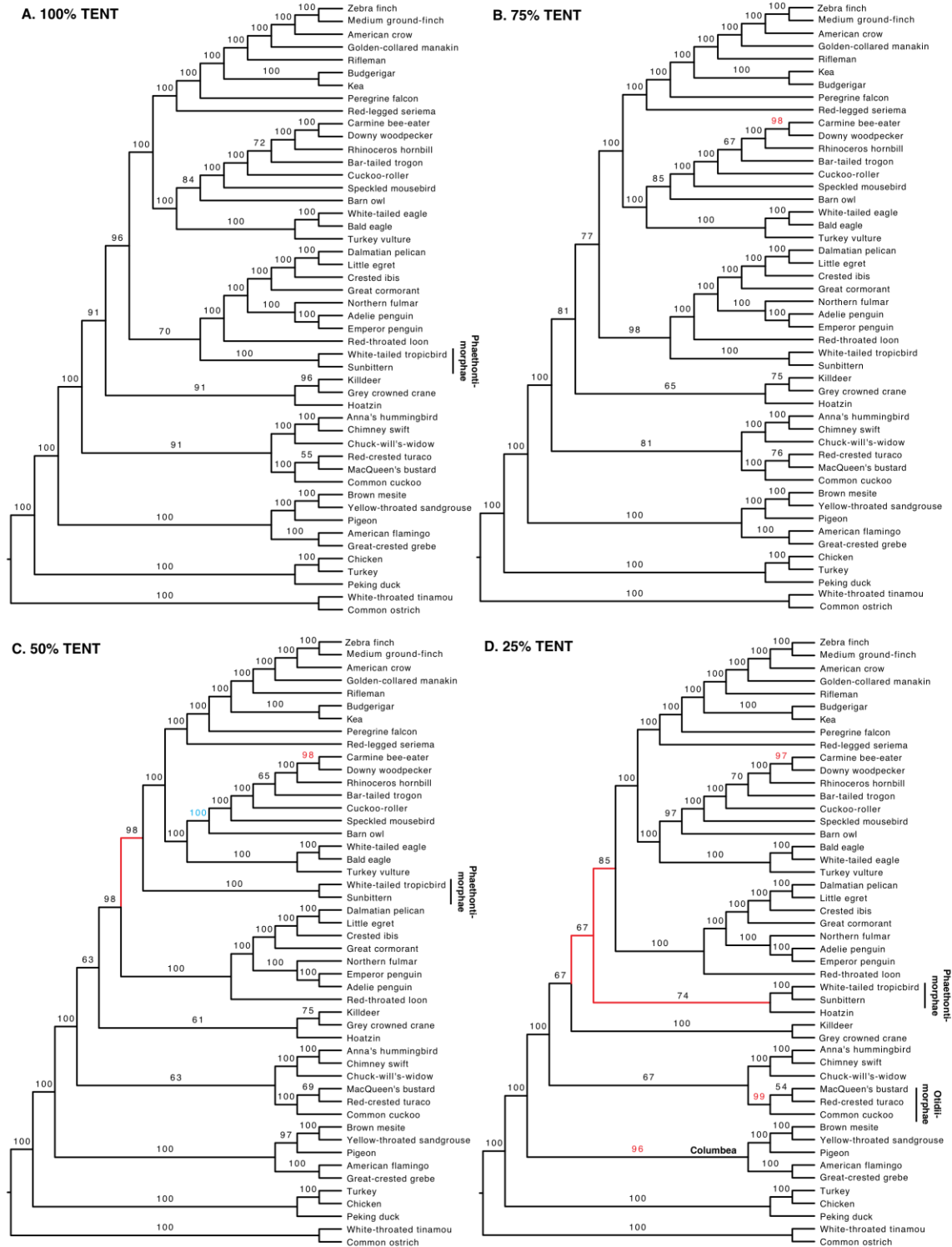
Fig. S5. Influence of genomic data amount on tree support. (**A**) 100% TENT data tree for comparison. (**B**) 75% of TENT data. (**C**) 50% of TENT data. (**D**) 25% of TENT data. Red branches, those that differ from the 100% TENT topology in (A). Red text, branches with 100% support in the 100% TENT that showed decreased support with less TENT data. Blue text, the only branch (with owl) that had less than

100% support (84%) with 100% of the TENT data that showed increased support (to 100%) with 50% of the TENT data. The trees were generated using ExaML (SM4).

A. Average support of species trees

B. Incompatibility with species
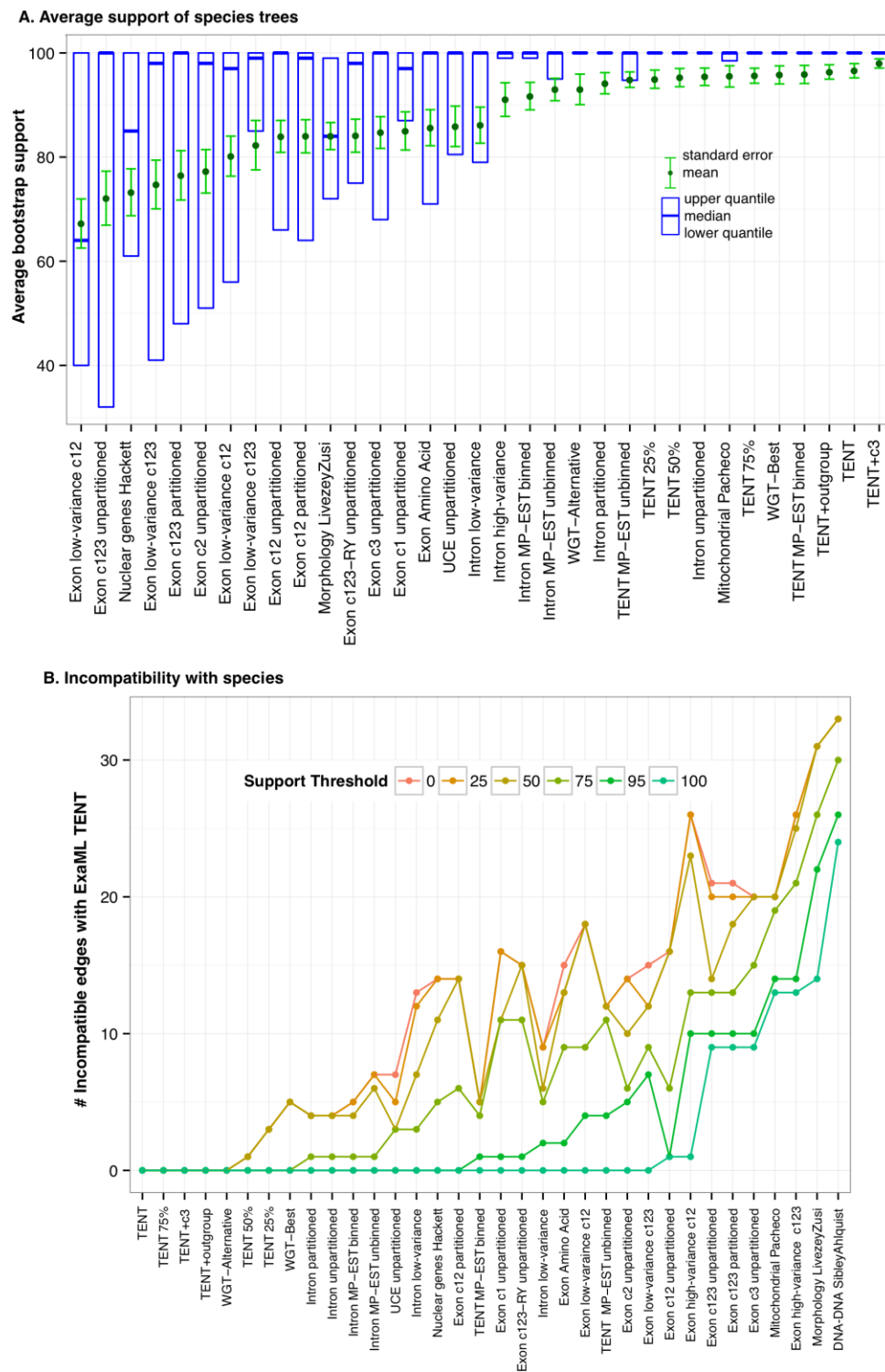
Fig. S6. Comparisons of total support among species trees and gene trees expanded. Figure explanation is the same as that written in the legend of Figure 5. Additional results include partitioned

ExaML, unbinned MP-EST*, and codon trees. (**A**) Average bootstrap support across all branches of species trees from different genomic partitions and methods as in Figure 2, ordered left-to-right from lowest to highest means. (**B**) Proportions of incompatible edges (out of a total of 45) at different support thresholds with the ExaML TENT tree of Figure 1, ordered left-to-right from most to least compatible. Incompatibility method is described in SM7.
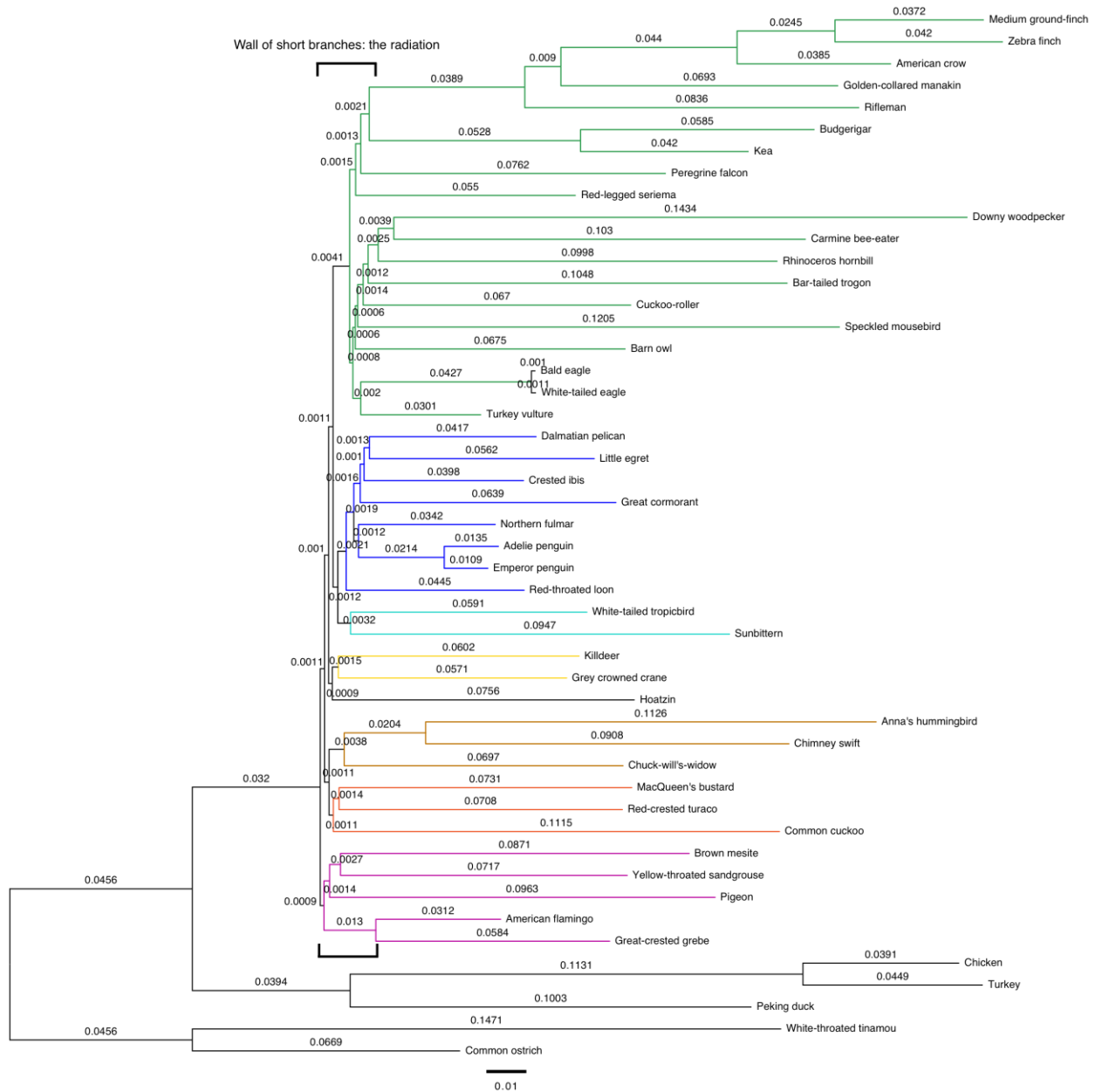
Fig. S7. ExaML TENT tree with branch length values. Note the lowest values of 0.0006-0.0008 around the branches that include the owl, and other short branches at the basal divergences of the Neoaves tree, all forming a wall-like pattern of speciation. Branches are colored according to clades in Figure 1. Branch length calculation is described in SM4 and references therein.

58
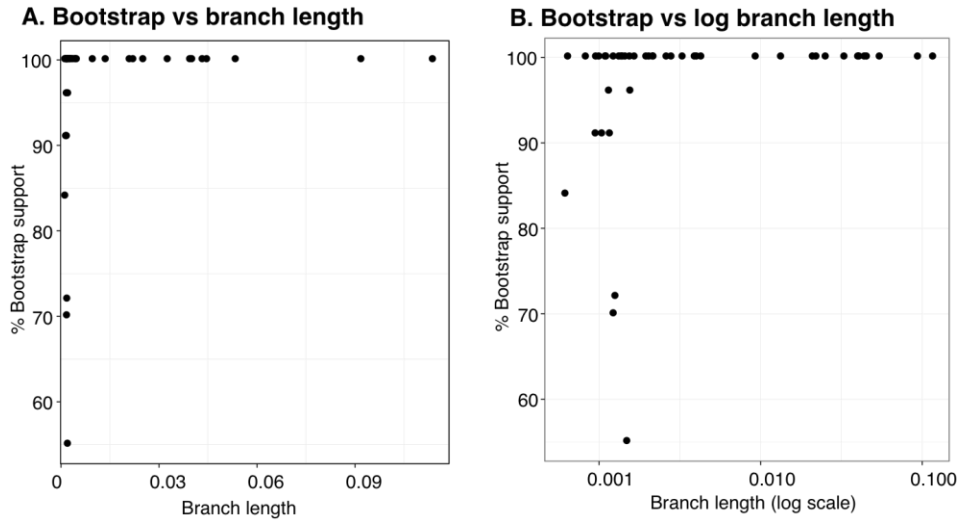
Fig. S8. Percent bootstrap support graphed against branch length of the ExaML TENT. (**A**) Branch length graphed linearly, showing that branches with less than 100% support in the TENT are all grouped at the extreme end of the short branches in the tree. (**B**) The same data as in A, except with branch length graphed on a log scale, showing the relative distribution of the 9 branches with less than 100% support among the short branches.
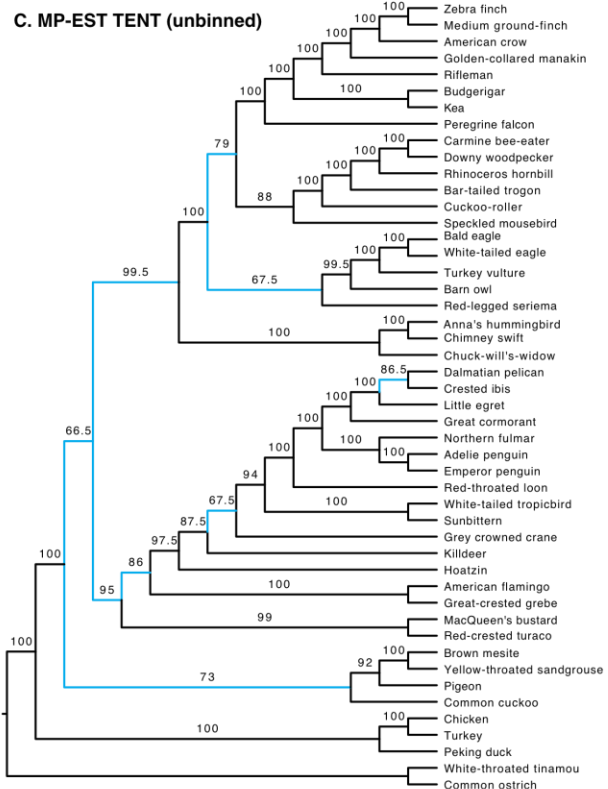
A. MP-EST* TENT (binned)
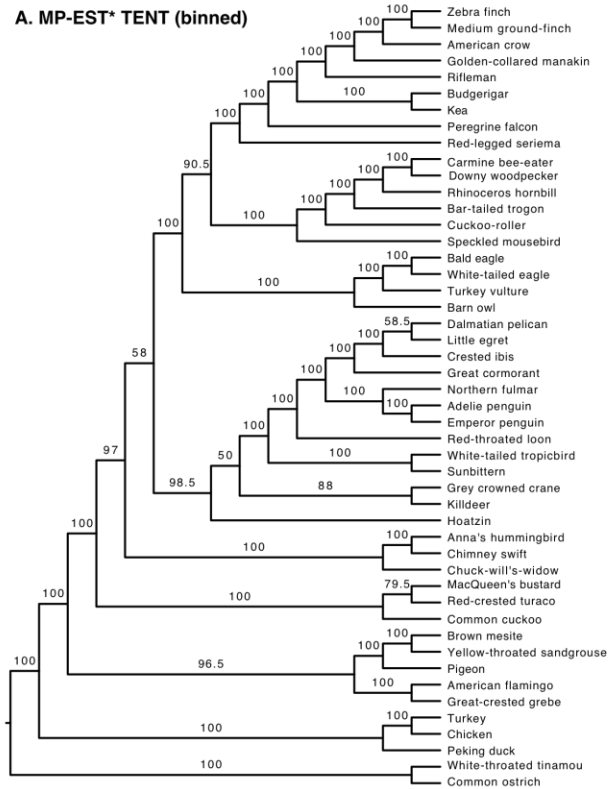
B. MP-EST* Intron (binned)
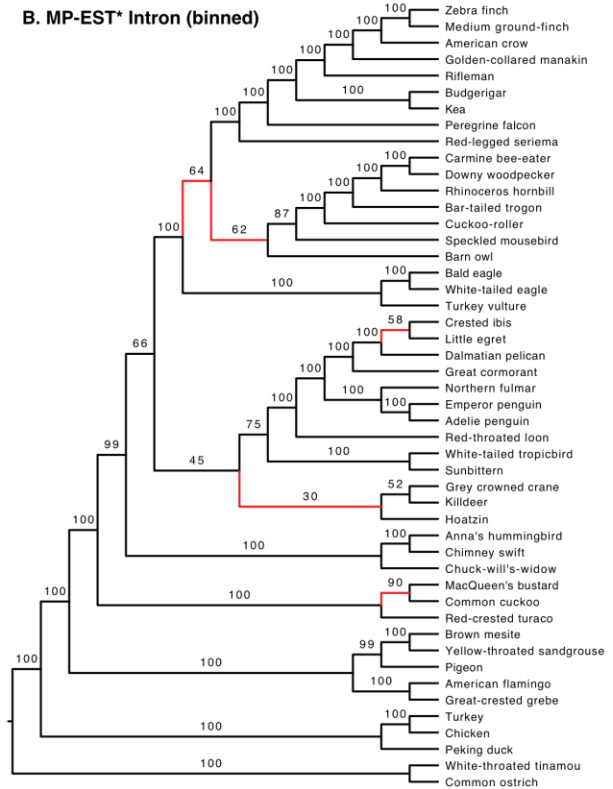
C. MP-EST TENT (unbinned)

D. MP-EST Intron (unbinned)

60

Fig. S9. MP-EST species trees. (**A**) Binned MP-EST* TENT tree from Figure 3B for comparison (not annotated for clade branches or species traits). (**B**) Binned MP-EST* intron tree. (**C**) Unbinned MP-EST TENT tree. (**D**) Unbinned MP-EST intron tree. Red branches, differences between binned MP-EST* intron tree relative to binned MP-EST* TENT. Blue branches, differences in the unbinned trees relative to their respective binned trees. The four branches that had less than 100% BS in the TENT (**Fig. 3A**) that were shifted to nearby positions in the MP-EST* TENT tree (A) included moving owls sister to Accipitrimorphae, Otidimorphae sister to all other Passerea followed by Caprimulgimorphae sister to the remaining Passerea, and Cursorimorphae (killdeer and crane) + hoatzin as successive sister groups to core waterbirds. Like the ExAML intron tree, the binned MP-EST* intron tree had lower support on some nodes, but with a topology more similar to the ExaML TENT than the MP-EST* TENT, specifically for the owl, Cursorimorphae, and hoatzin branches. MP-EST approach is described in SM5 and references therein.
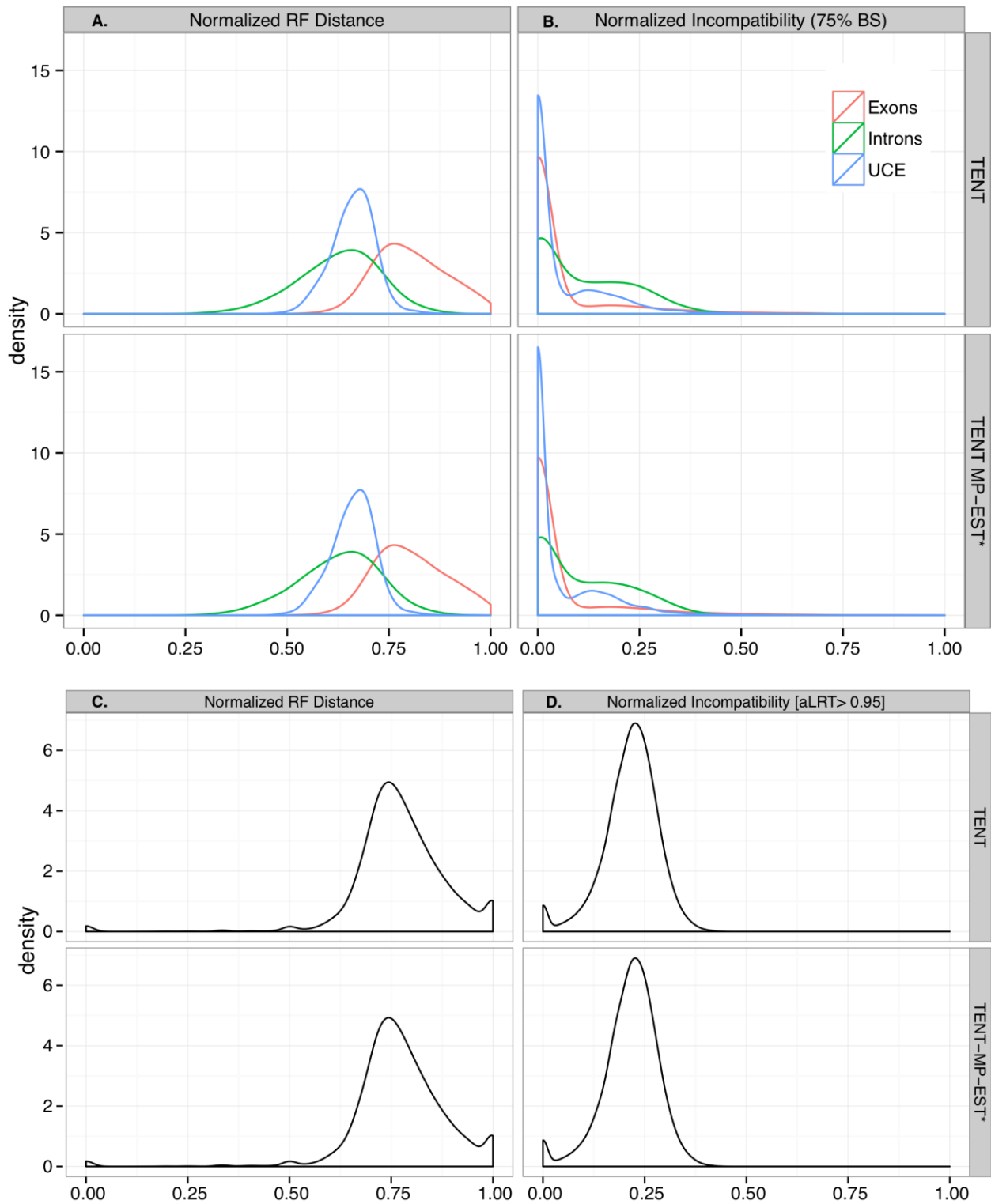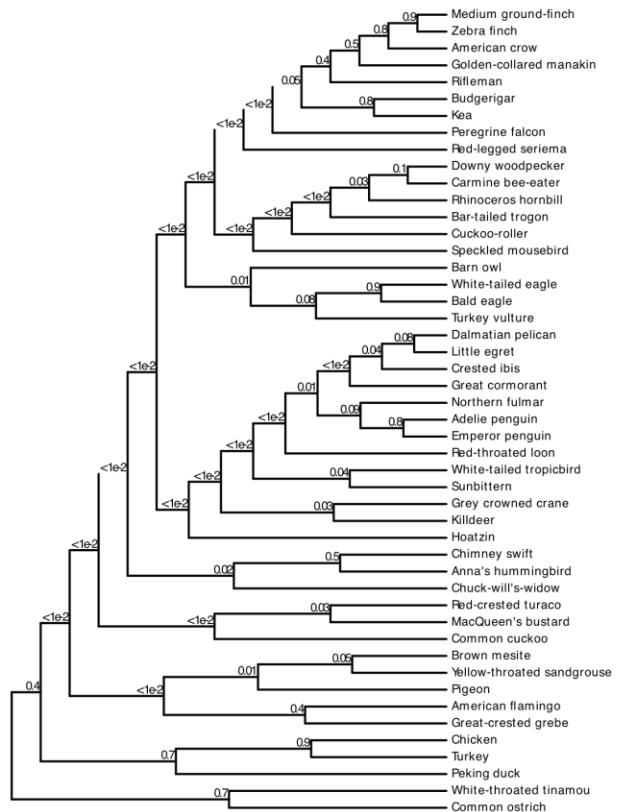
Fig. S10. **Distribution of gene trees topologies distance from the species tree.** (**A**) Density plots of distances between individual gene trees (gene types distinguished by color) and two estimates of the species tree: TENT ExaML (top) and TENT MP-EST* (bottom). Distance is measured as normalized RF distance (left) calculated by counting the number of bipartitions that are present in either the gene tree or

the species tree but are missing from the other tree, and then normalized by the total number of branches (i.e. 96) in both trees. (**B**) Same comparisons made in (A), except the normalized incompatibility distance is restricted to branches with 75% BS. Incompatibility is calculated by first contracting all edges below 75% support in both the species tree and the gene trees, then calculating the total number of remaining branches in the gene tree that are incompatible (*273*); the remaining branches in the species tree that are incompatible with the gene tree is normalized by the total number of branches in the contracted species tree and gene tree. Both distance measures in (A) and (B) are between 0 and 1, with 0 indicating complete lack of incongruence and 1 indicating complete incongruence. The compatibility measure restricts the calculation only to highly supported branches. The distance measures are plotted as kernel density plots, calculated using the default method in R statistical package (*274, 275*), with the adjustment factor set to 2. (**C**) Density plots of distances between 75,853 gene trees reconstructed using phylomeDB and two estimates of the species tree: TENT ExaML (top) and TENT MP-EST (bottom) using normalized RF distance. (**D**) Similar analyses as in (C) using normalized incompatibility distance restricted to branches with 95% branch aLRT support. Both distance measures are between 0 and 1, with 0 indicating complete congruence and 1 indicating complete incongruence. Incompatibility calculation approach is described in SM7, and they phylome DB described in SM8.
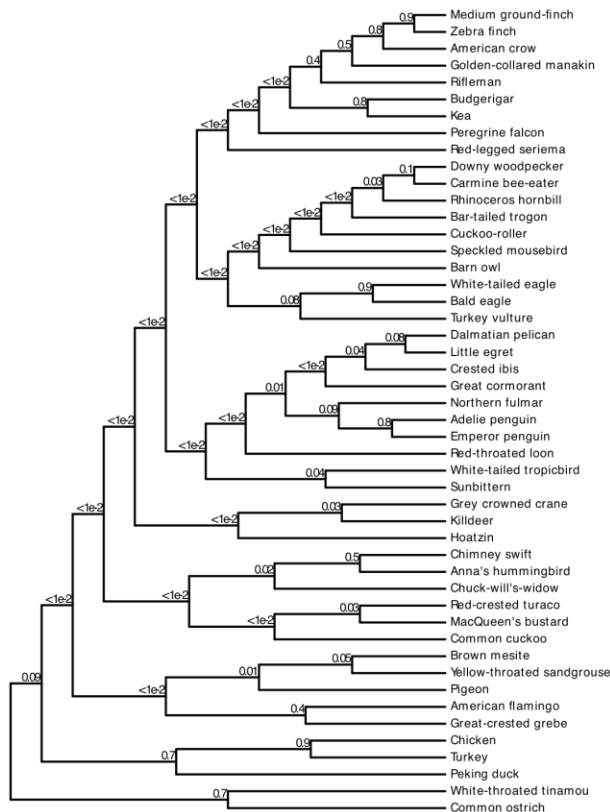

Fig. S11. Genome-wide protein coding gene tree congruence with the ExaML TENT (A) and MP-EST* TENT (B) topologies. The gene tree support for a branch is computed as the number of gene trees in the five reconstructed phylomes that are congruent for that split (see methods), divided by the total number of gene trees that are informative for that node (i.e. contain at least some species in both of the daughter partitions). Since most gene trees contain duplications, they were first decomposed with a duplication-aware algorithm that renders subtrees that only contain orthologous sequences and a weighted

congruence was computed after comparing all subtrees individually to the species tree. ExaML approach described in SM4, MP-EST in SM7, and phylomeDB generated gene trees in SM8.
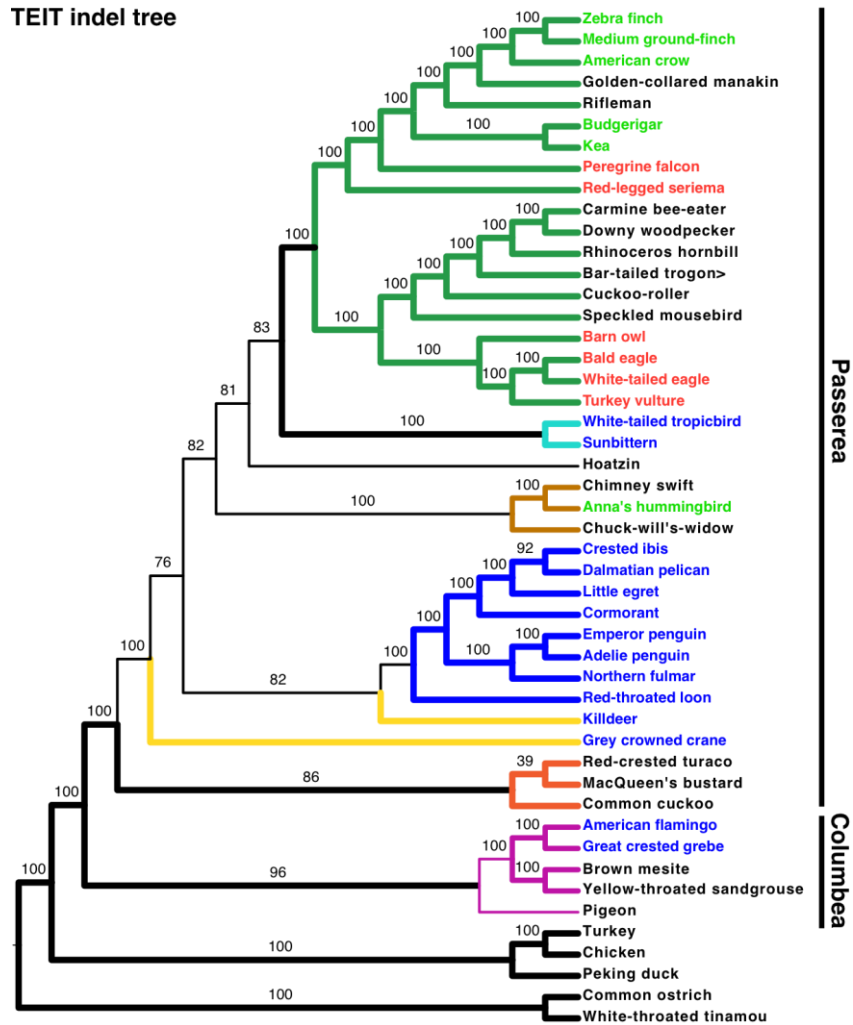

Fig. S12. ExaML total evidence indel tree (TEIT). Color-coding of branches and species' names are the same as in Figures 1 and S1. Branch values = bootstrap support. All branches with 100% support are found in the MP-EST* TENT, except for a local shift in the position of the pigeon within the Columbea clade, going from being sister to brown mesite and sandgrouse, to being sister to the remaining Columbea. The split between Columbea and Passerea is still present at 100% support. Coding of indels is described in SM9.
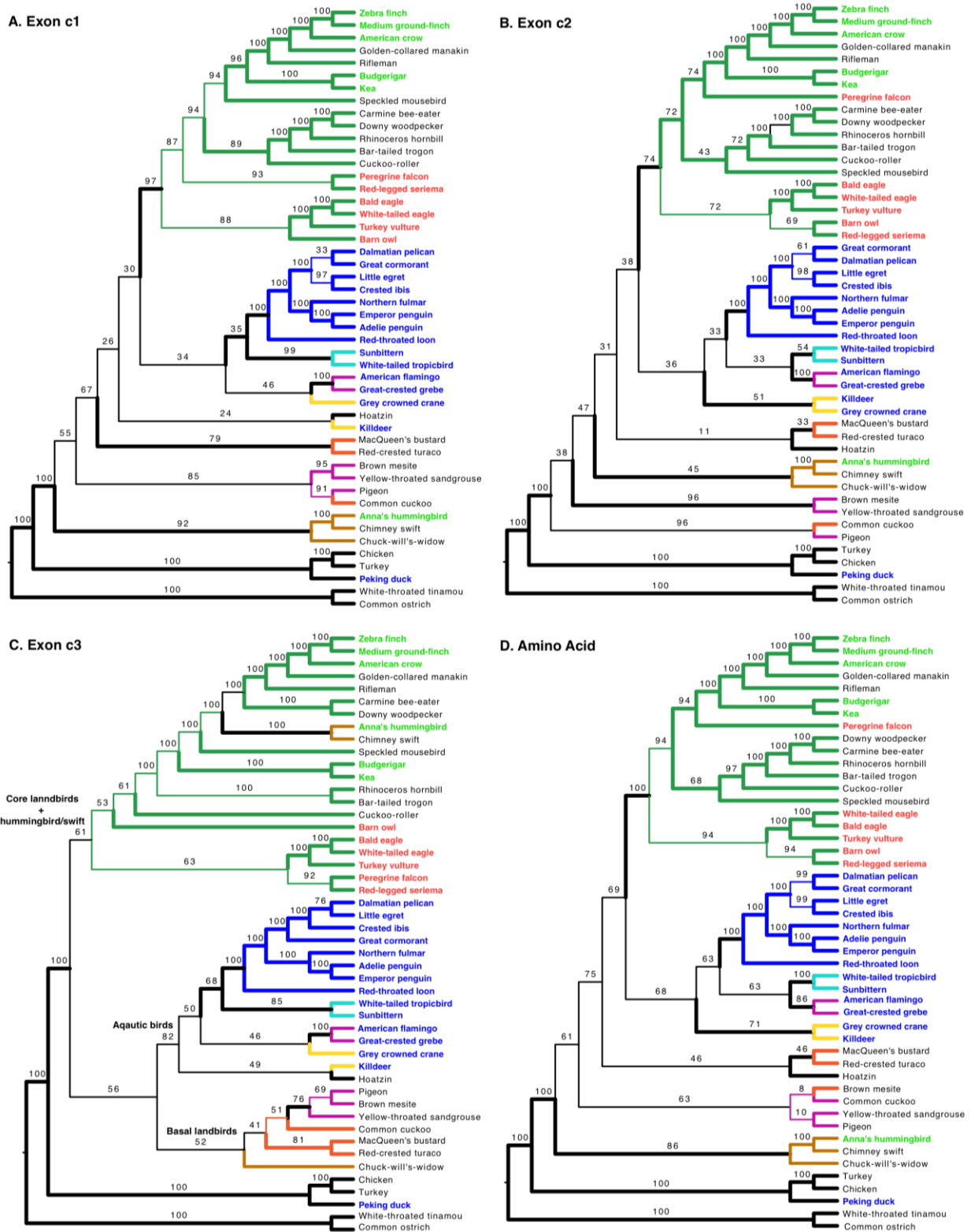
Fig. S13. Protein coding species trees on individual codon positions or amino acid sequence. (**A**) Exon c1 tree. (**B**) Exon c2 tree. (**C**) Exon c3 tree. (**D**) Amino Acid (AA) tree. Color-coding of branches

and species' names are the same as in Figures 1 and S1. Compare these trees with those in Fig. 4. The method used to generate these ExaML-based trees with different genomic partitions is in SM4.
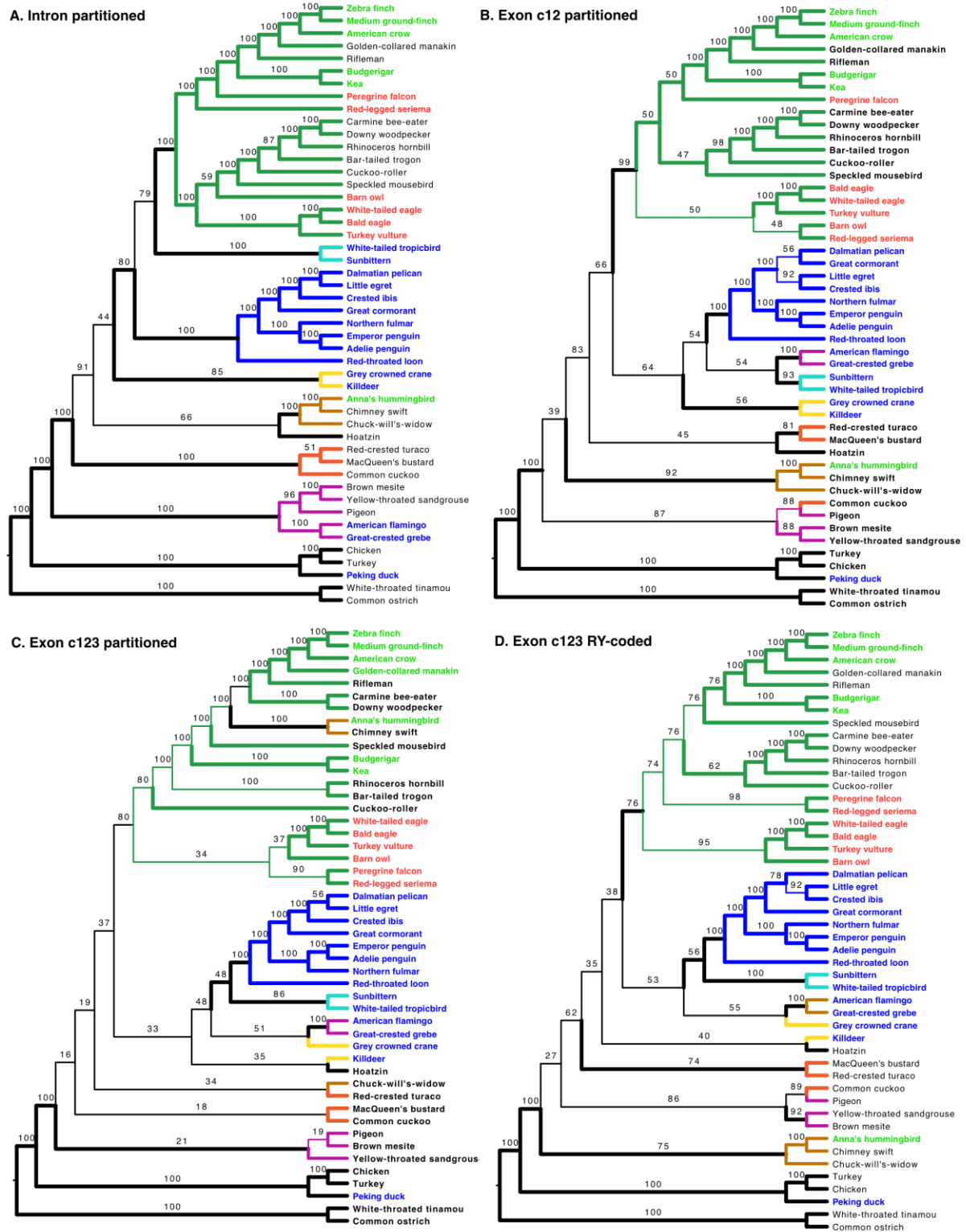
Fig. S14. Partitioned and RY-coded protein coding species trees. (**A**) Intron tree partitioned on gene type. (**B**) Exon c12 tree partitioned on gene type. (**C**) Exon c123 tree partitioned on gene type. (**D**) Exon

c123 tree with the 3rd position RY-coded. Color-coding of branches and species names are the same as in Fig. 1. Compare these trees with unpartitioned and non-RY coded versions in Fig. 4. **Table S4** list number of partitions for each tree. Methods used to generate with different genomic partitions are in SM4.

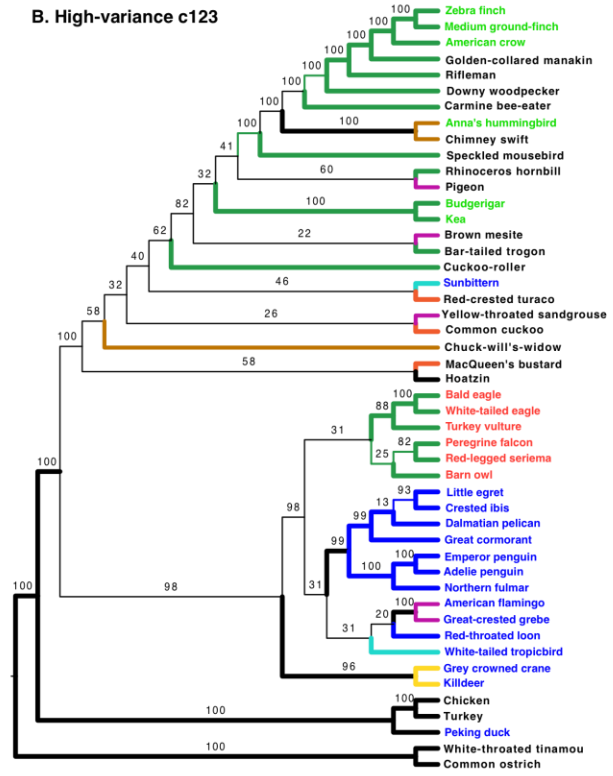**A. Base composition variance**
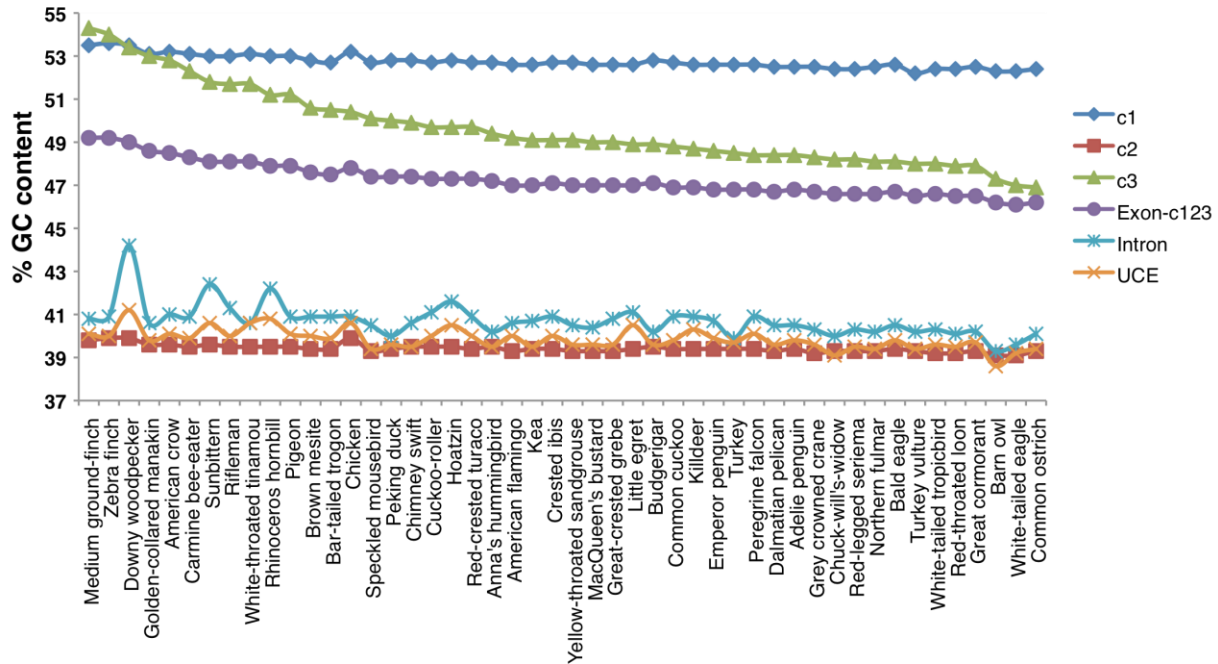
B. GTR model analyses
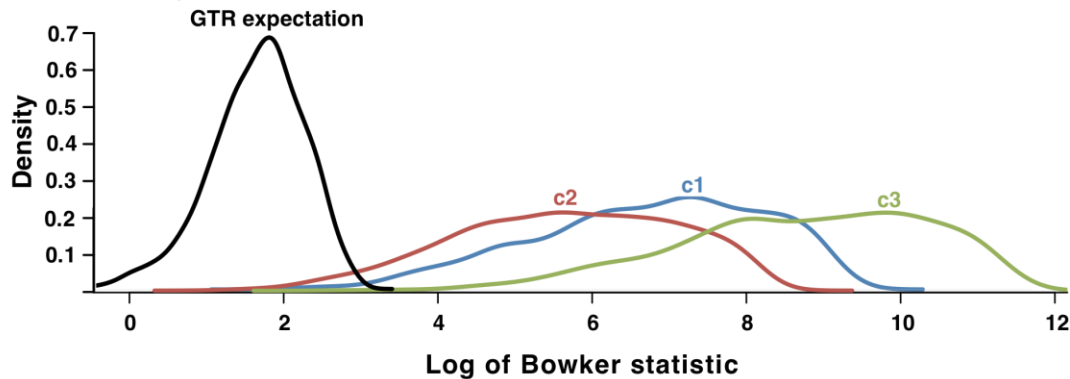
Fig. S15. Base composition analyses. (**A**) GC content in different codon positions and genomic partitions across species, ordered left-to-right from highest to lowest for GC3 (3rd codon). Interestingly, only the 2nd codon position had a GC content similar to that of the non-coding regions we examined (introns and UCEs) and the c2 topology was the most similar to the intron tree topology (**Fig. S2**). (**B**) Bowker statistics for violation of GTR model on different codon positions. The greater the statistic value from the GTR expectation, the greater violation of the GTR model. The Bowker statistic for c3 codons was significantly higher than the c1 and c2 (paired t-test p-value 1.118e-14). GC content methods and Bowker statistics are described in SM11.

Fig. S16. Low-variance versus high-variance exon species trees. (**A**) Low-variance exon c123 tree. (**B**) High-variance exon c123 tree. (**C**) Low-variance exon c12 tree. (**D**) High-variance exon c12 tree. Color-

coding of branches and species' names are the same as in Figures 1 and S1. Compare these trees with those in Fig. 4. Methods used to generate these trees are described in SM11.

A. Low-variance exon GC content vs body mass
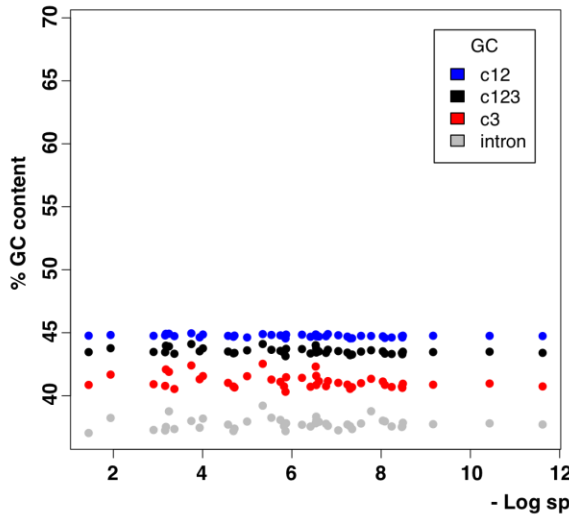
B. High-variance exon GC content vs body mass
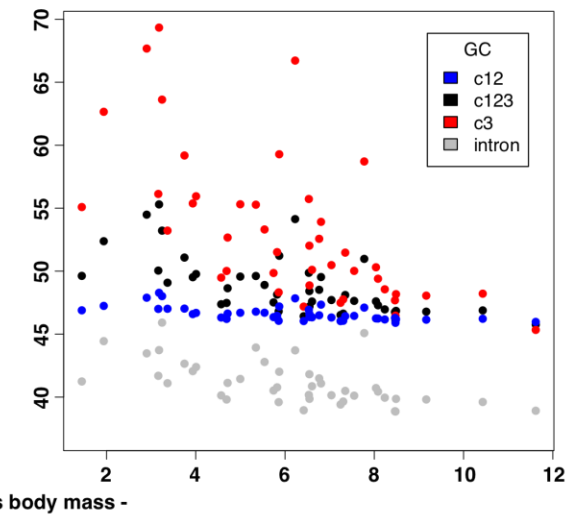
C. Low-variance exon chromosome position (zebra finch)
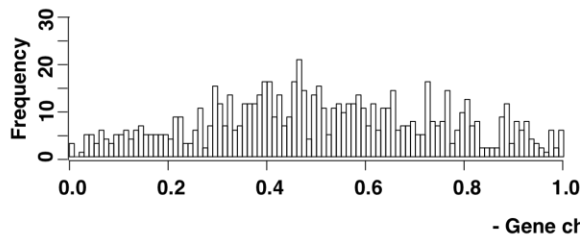
D. High-variance exon chromosome position (zebra finch)
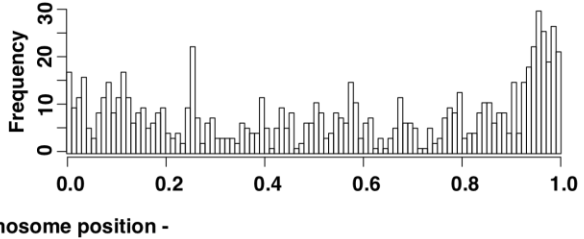
E. Low-variance introns

F. High-variance introns

71
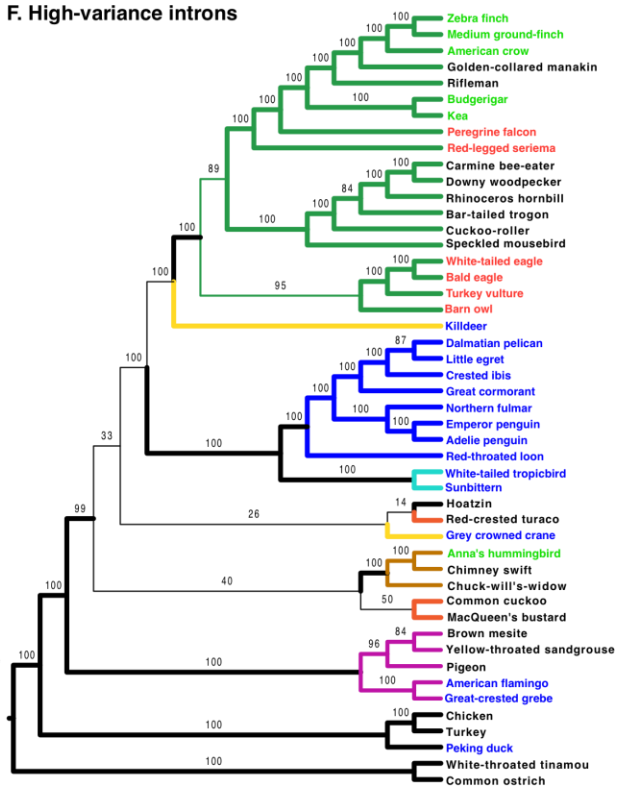
Fig. S17. Low-variance versus high-variance intron species trees. (**A-B**) Correlations of GC content and body mass for low-variance (A) and high-variance (B) exons on different codon positions (c1, c2, or c3) or within introns of these same genes. Note relationship is stronger with the high-variance genes, including on the introns. (**C-D**) Relative chromosome positions of the low variance (C) and high variance (D) exons normalized between 0-1 for all zebra finch chromosomes and separated into 100 bins (bars), showing that the difference is not specific to the chicken chromosome positions. The height of each bar represents the number of genes in that specific relative location. The two distributions in C and D are significantly different (p-value $< 2.2e\text{-}16$; Wilcoxon rank sum test). (**E**) Low-variance intron tree. (**F**) High-variance intron tree. Color-coding of branches and species names are the same as in Figures 1 and S1. Compare these trees with those in Fig. 4. GC content analyses and chromosome position methods are described in SM11.
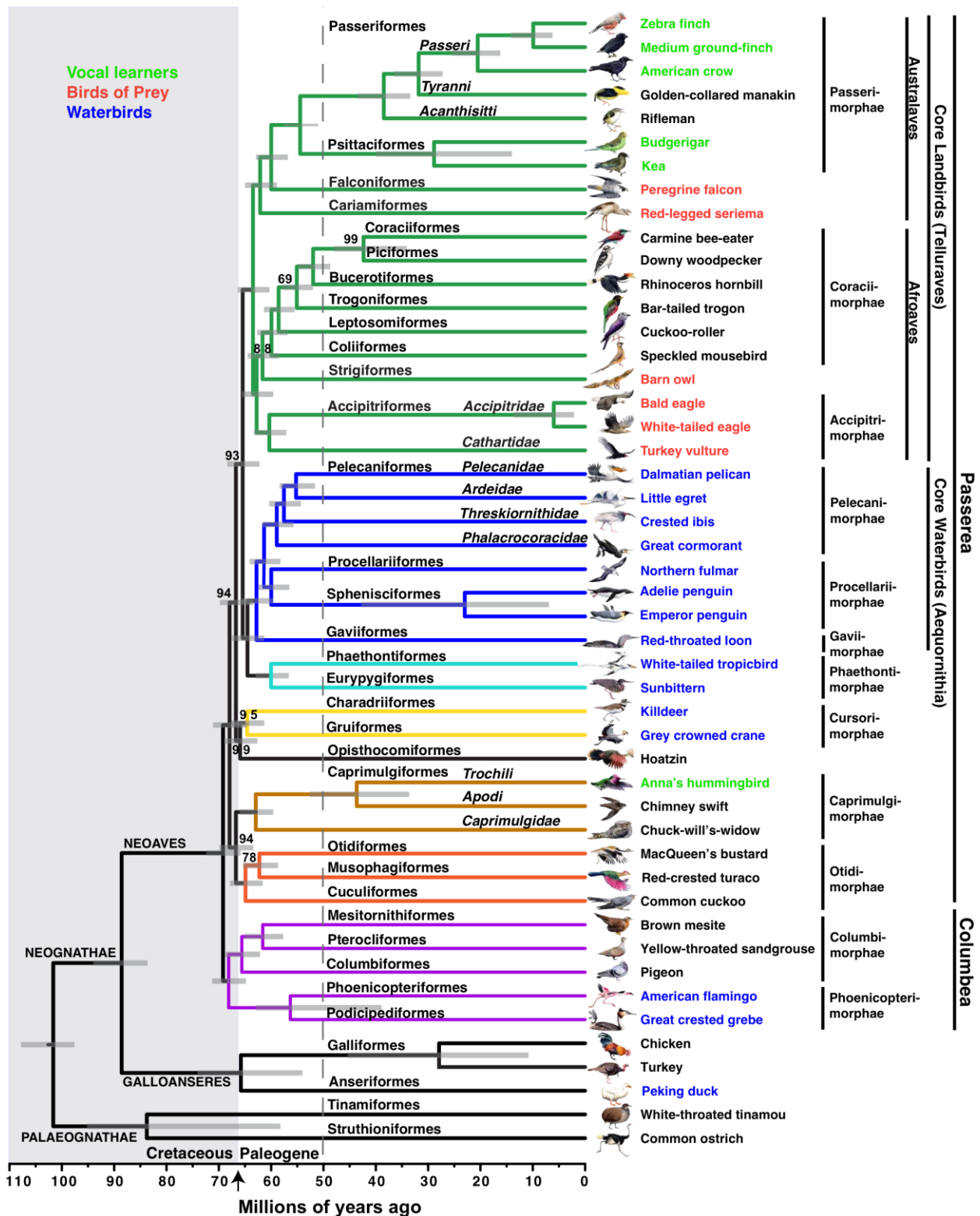
Fig. S18. TENT+3rd codon tree. This tree has the same topology as the TENT without the 3rd codon in Figure S1. The differences are mostly increased supported on some nodes.

73
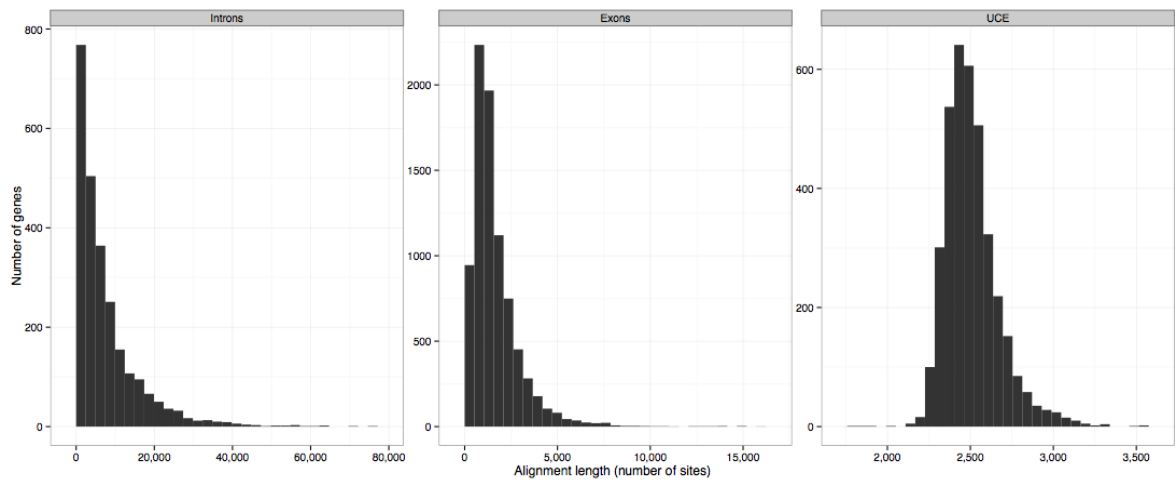
Fig. S19. Alignment length of genes from different genomic partitions. Alignment length is measured as the number of nucleotide sites in each alignment, and histograms are shown for the distribution of alignment length among all genes in each dataset. Axes are on different scales for the three panels. Introns are the longest, followed by exons and UCEs. For further details see SM3.

B. Intron sequences filtered

C. UCE sequences filtered

- % of alignment filtered out -
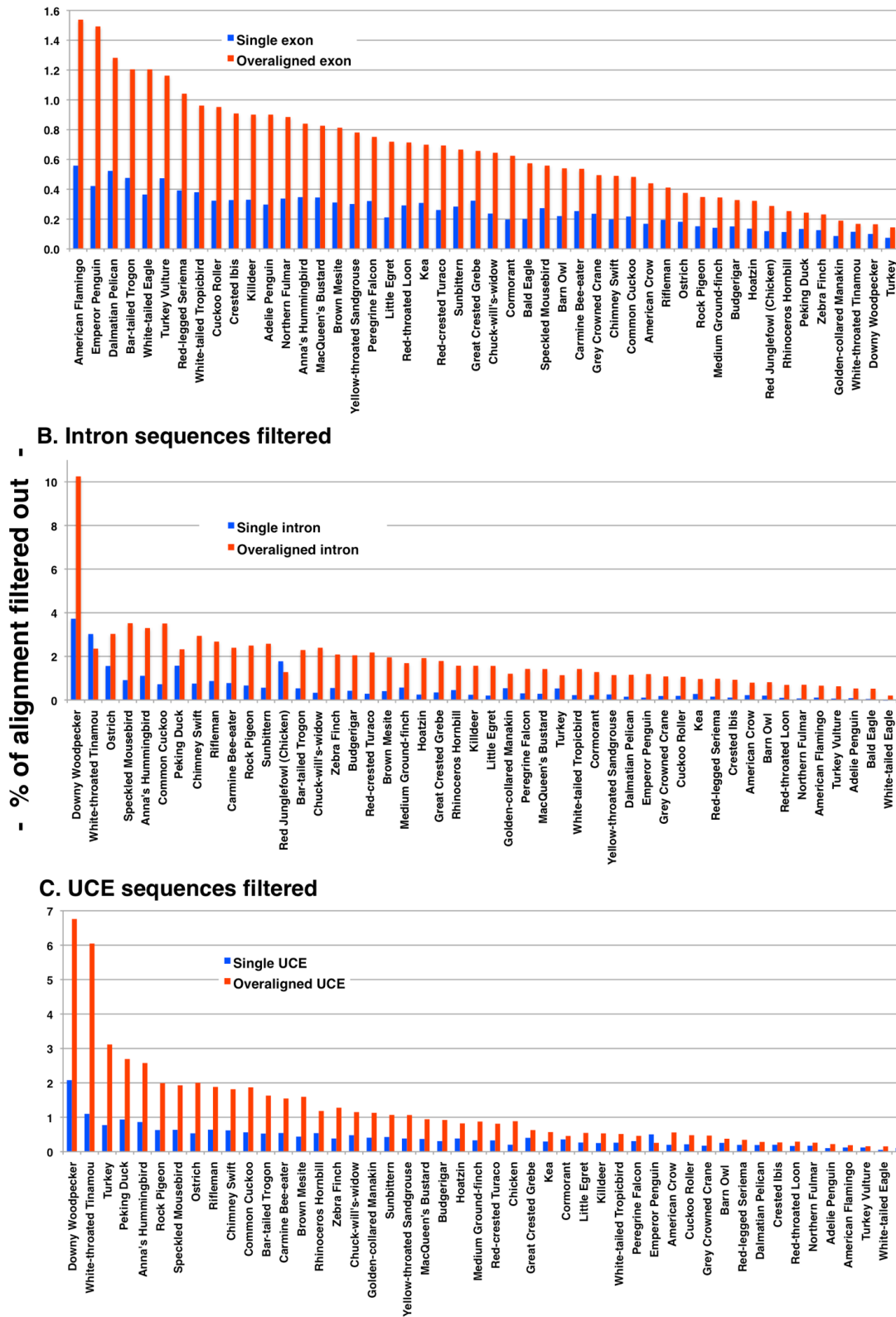
Fig. S20. Percentage of aligned sequences filtered out in the exons (A), introns (B), and UCEs (C) across species. The species are order left to right according to the highest percentage of sequence filtered out. Single, sequence present in only that species. Overaligned, incorrectly aligned sequence due to alignment error. For further details see SM3.
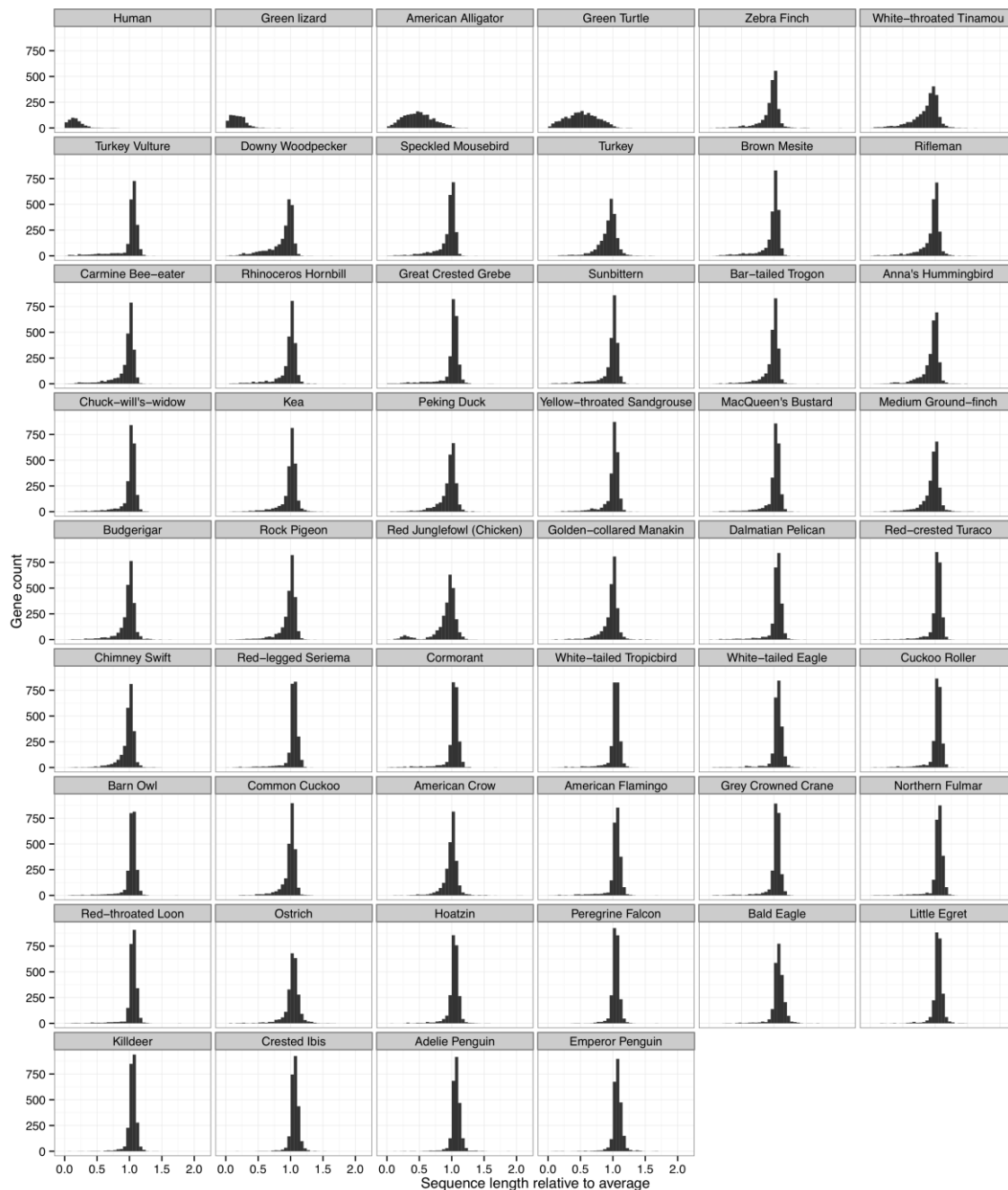
Fig. S21. Characterization of missing data in the intron alignment. Shown are histograms characterizing the missing data across all the intron genes in each of the 52 species. Histograms for each species are only over genes that included some sequence for that species. On the x-axis is the sequence length of each gene in each species divided by the average sequence length of the gene across species. Thus, 1 indicates that that the sequence for a species is the same size as the average sequence, values below 1 indicate more missing data than the average, and values above 1 indicate having more data than average. Most distributions of avian species are tightly centered around 1, meaning that each gene in each species has relatively even coverage with all other species. However, for the four non-avian taxa, namely alligator, turtle, lizard, and more so human, for most genes, large portions of the sequence are not homologous enough to align and are therefore missing. For further details see SM3.

76
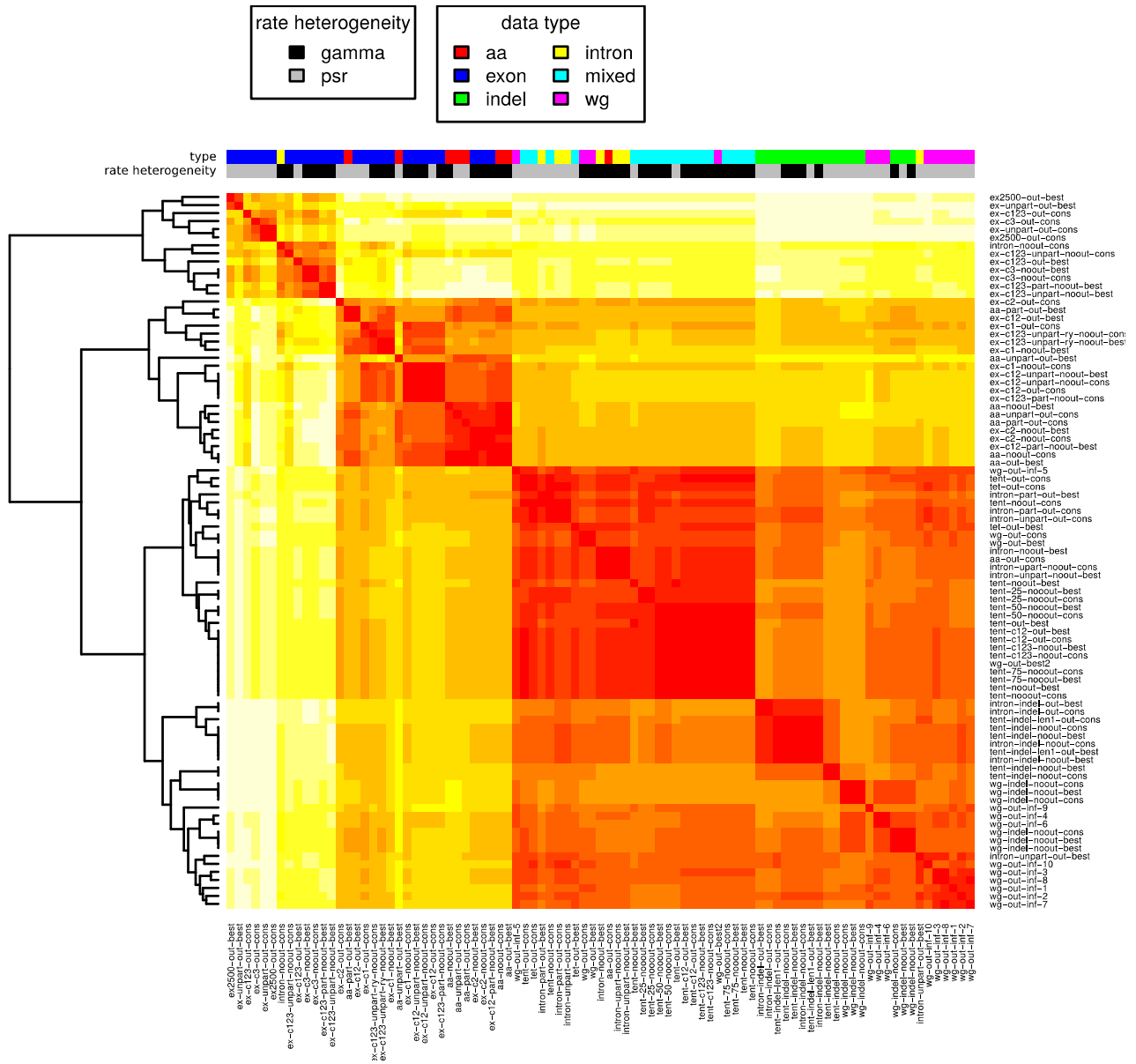
Fig. S22: Clustering of RF-distances of all main result trees (best tree and consensus tree). Low RF distances (dark red blocks) indicate topologically identical or similar trees; high RF distances (white) indicate topologically distant trees. Trees are labeled by model of rate heterogeneity and categorized according to the data set type (where TET/TENT data are labeled as mixed and whole genome data are labeled as WG. For further details see SM4.
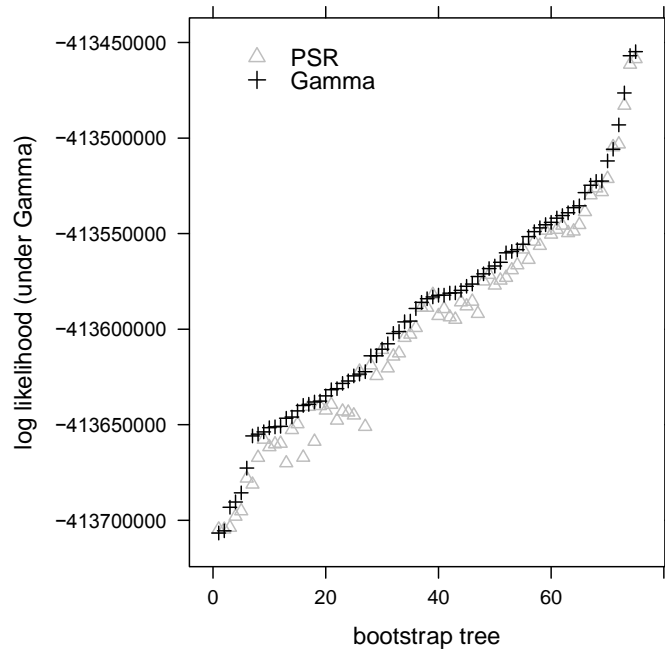
Fig. S23: Log likelihoods. Graphed are comparison of log likelihoods (evaluated under Γ) for bootstrap trees inferred either under the Γ or PSR model for identical alignment replicates and identical parsimony starting trees. For further details see SM4.
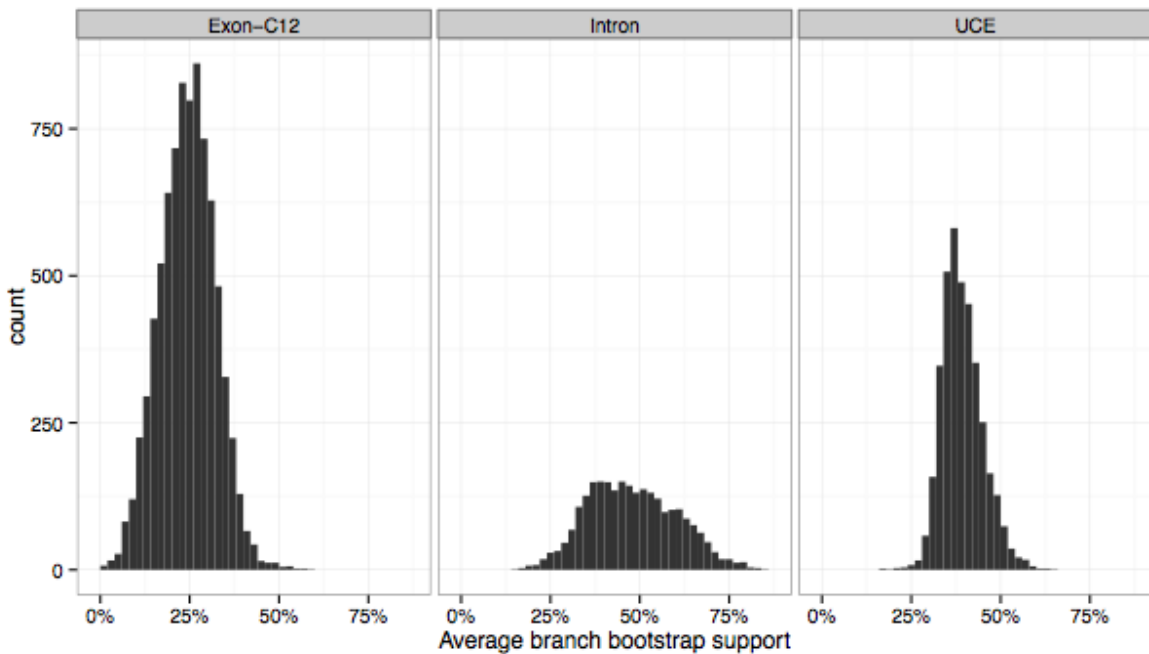
Fig. S24. Distribution of bootstrap support for individual genes/loci. Graphed is the average bootstrap support for locus trees estimated from various data partitions (exon-c12, intron, and UCE) of the avian dataset. For further details see SM4. 78
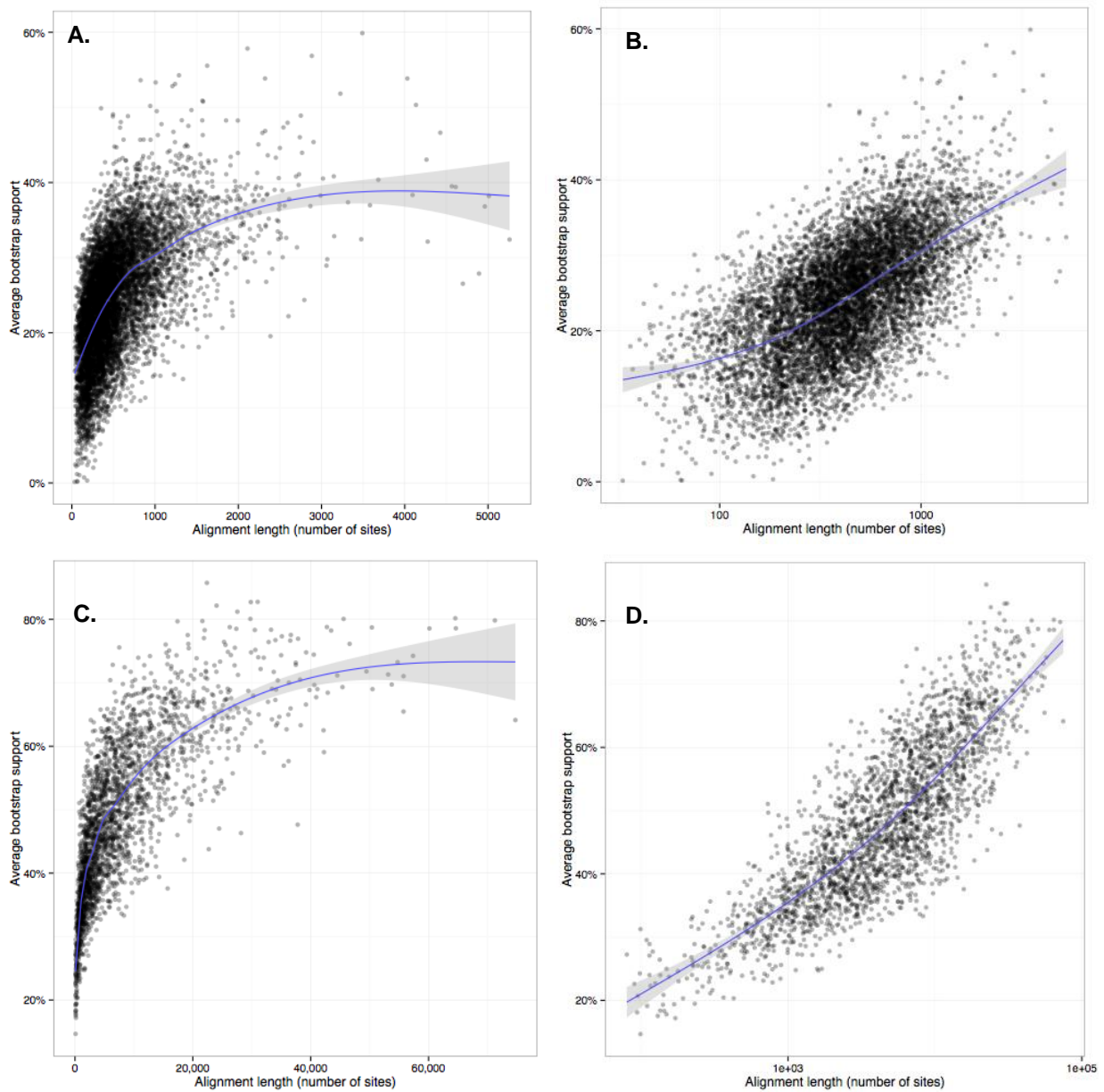
Fig. S25. Correlation between locus tree bootstrap support and alignment length for the exon and intron datasets. (A) Comparison of the exon data set on a normal scale. **(B)** Exon dataset on a log scale. **(C)** Intron dataset on a normal scale. **(D)** Intron dataset on a log scale. Alignment length is measured as the number of sites in the alignment. Average bootstrap support is clearly correlated with the alignment length (Spearman correlation coefficient = 06. for exons and 0.82 for introns, p < 2.2e-16 for both). For further details see SM4.
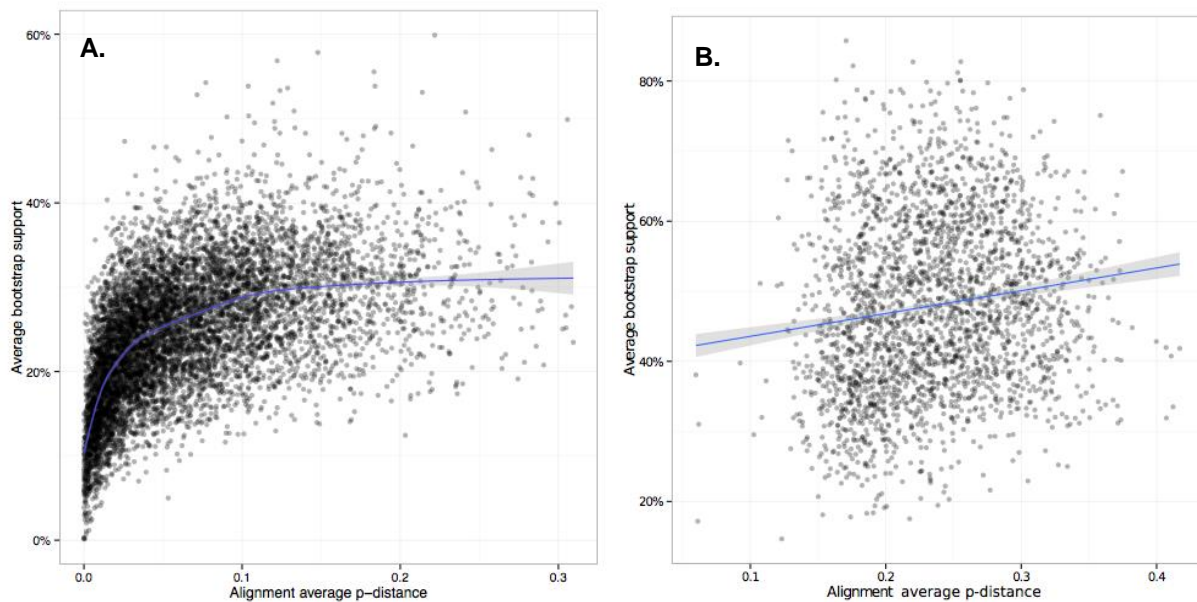
Fig. S26. Correlation between average p-distance and average bootstrap support. (**A**) Correlation between rate of evolution (measured by average p-distance) and average bootstrap support in exon gene trees. (**B**) Correlation in intron gene trees. The p-distance between two sequences is defined as the proportion of non-gap sites where the two sequences are different. Average p-distance (shown on x-axis here) is the average distance between any pairs of sequences, and reflects the rate of evolution. Most exon genes have very low rates of evolution, which result in low bootstrap support. These correlations are similar for the exons (Spearman correlation coefficient = 0.6) but weaker for the introns (0.166), relative to the alignment length correlations in figure S25; both are significant ($p < 2.2e\text{-}16$). For further details see SM4.
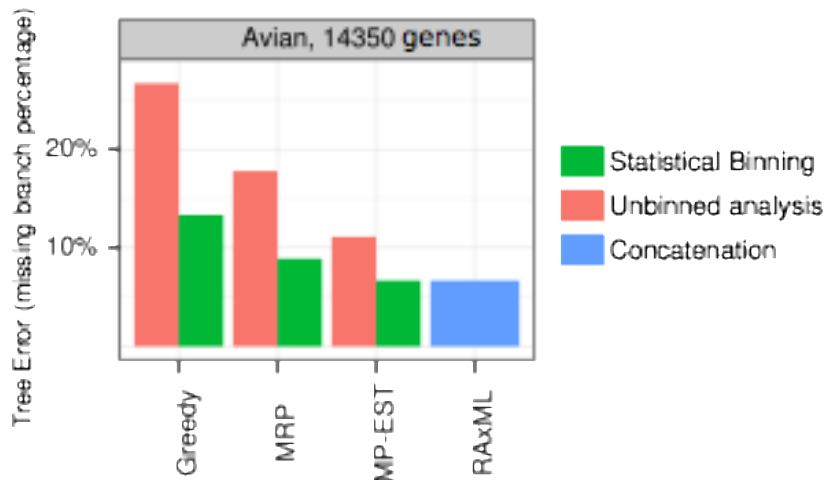
Fig. S27. Binned versus unbinned analyses. Shown are results comparing error rates among three multispecies coalescence methods (Greedy, MRP, and MP-EST) and an ML method (RAxML) using simulated data from 14,350 gene trees that closely resemble our TENT data matrix in terms of bootstrap support and number of genes. Tree error is measured compared to the known true species tree with respect to the percentage of incorrect branches. For further details see SM5 and a companion study by Mirarab et al. *(58)*.
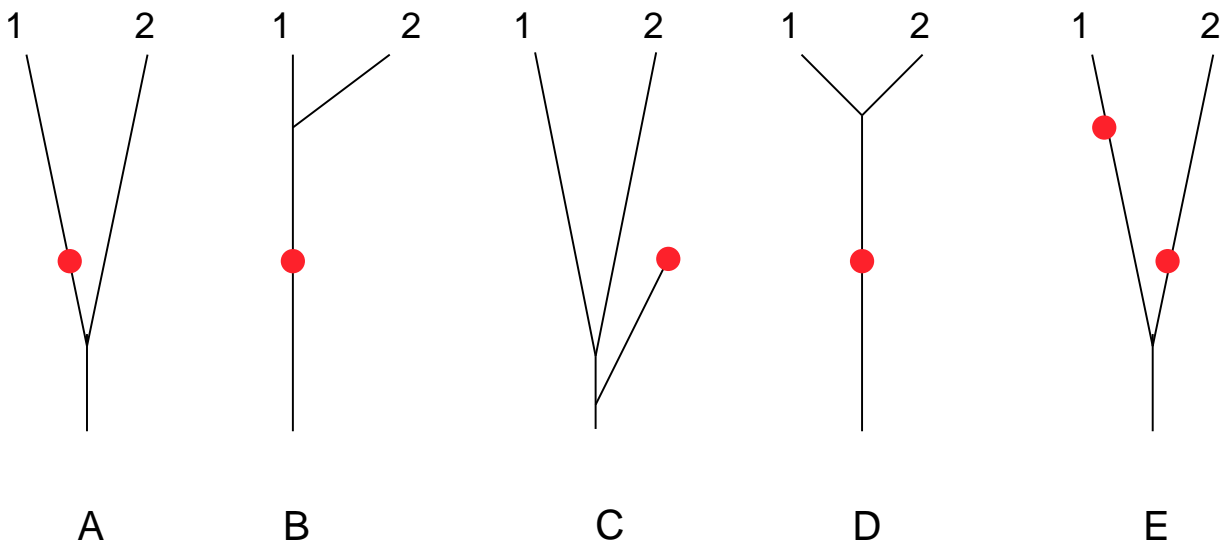
Fig. S28. Reasons why individual fossils cannot be used to calibrate divergences consistently. (**A**) Classic inference that fossil (red) is identifiably crown-1 and therefore can be used to infer divergence of 1 & 2; this is justifiable in rare cases in which the fossil exhibits an unambiguous synapomorphy of crown-1 (e.g., flightlessness). (**B-D**) Alternative possibilities: (**B**) Fossil appears to be crown-1 based on morphology, but pan-1 is paraphyletic to 2 so fossil overestimates MRCA; there are many known examples in birds. (**C**) Fossil is stem-1 & 2 but later than MRCA-1&2; fossil underestimates MRCA. (**D**) Fossil is stem-1&2 and predates MRCA-1&2; fossil overestimates MRCA. (**E**) Two fossils reliably document divergence of crowns-1 and -2 and consistently underestimate age of MRCA, especially since calibration depends on both. For further details see SM12.

81
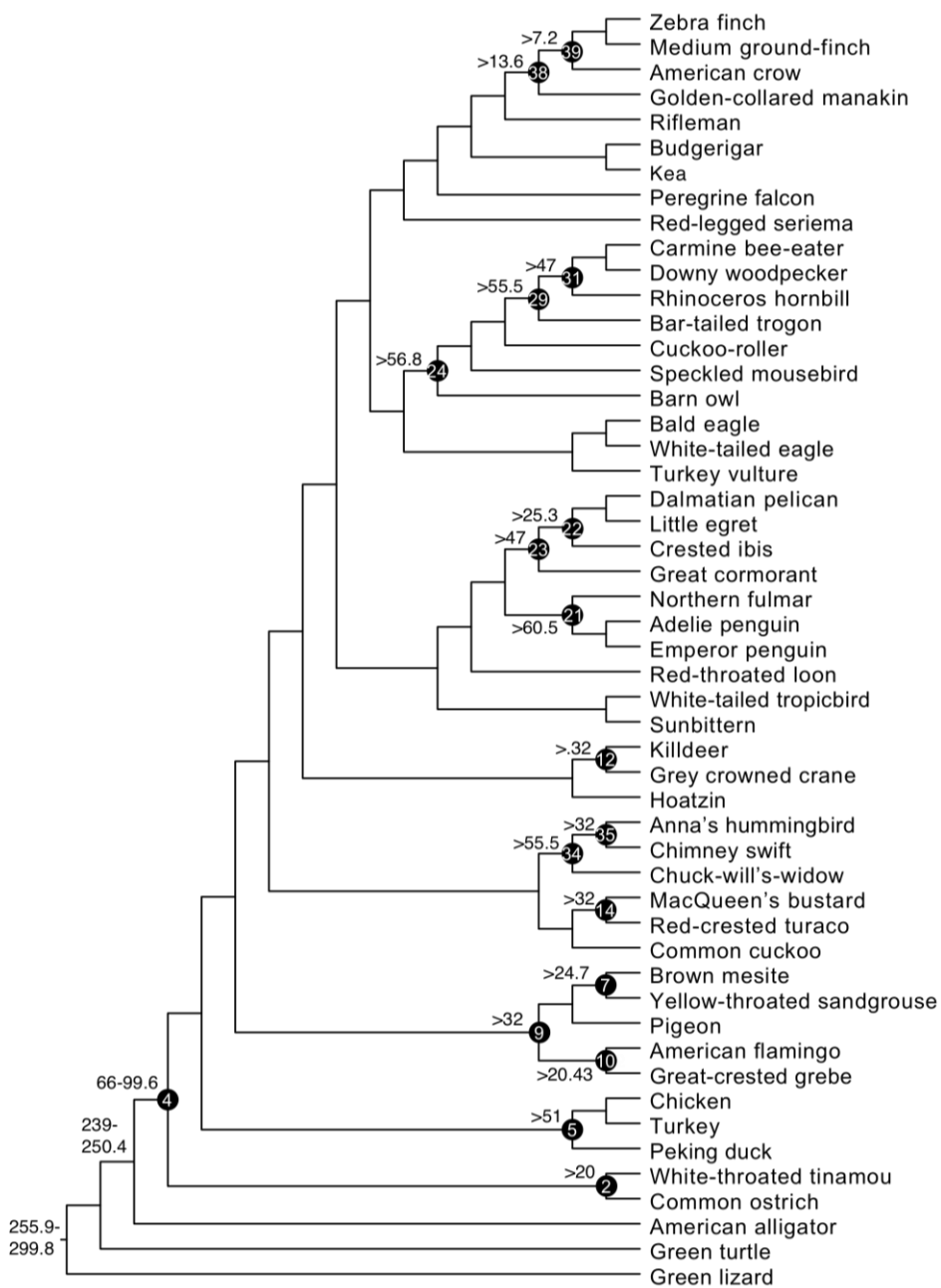
Fig. S29. Calibrations used for the dating analysis of the TENT tree (with outgroups included). The numbers in black circles refer to the calibrations in Table 1 and below. The numbers outside the circles represent minimum age bounds. For further details see SM12.

Supplemental Tables

Table S1. List of the 48 species used for the avian phylogenomics project (only legend provided here, full table in a separate tab-delimited text file). Listed are scientific Latin and common English names in columns A and B, respectively. The group responsible for the sequencing is in column C, with the primary or secondary publication source in column D. Tissue and animal information list the persons and/or institutions responsible for obtaining, processing, and overseeing processing of the tissue and animals. The source ID is from the original source of animal or tissue procurement. Other IDs are internal to the current project. Sex was determined for most species by PCR initially, and then from whole genome sequencing and analyses of the Z and W chromosomes. Barcode validation was done with mitochondrial genes, and a match determined by searches against public databases. Barcode ID is the sample reaction ID used for the mitochondrial gene sequencing. For further details see SM1 and SM6.

Table S2. SATé parameters used in alignment of different datasets. SATé version 2.1.0 was used, decomposition technique used the centroid edge. The initial tree was generated using RAxML on a MAFFT alignment, and the stopping rule was 2 consecutive iterations with no improvements in the maximum likelihood score. For further details see SM3.

	Exons; SATé-Prank	Exons; SATé-MAFFT	Introns; SATé-MAFFT	UCEs; SATé-MAFFT
Data Type	AA	AA	DNA	DNA
Subset Aligner	Prank 100311	Mafft 6.860b	Mafft 6.860b	Mafft 6.860b
Alignment Merger	Muscle 3.7 [5]	Muscle 3.7 [5]	Opal 1.0.3 [4]	Opal 1.0.3 [4]
Tree Estimator - ML Model	RAxML 7.2.6 - JTT	RAxML 7.2.6 - JTT	RAxML 7.2.6 - GTRCAT	RAxML 7.2.6 - GTRCAT
Subset Size	20%	50%	50%	50%

Table S3. Alignments and their partitions. Examined datasets: number of species taxa (**#t**), number of partitions (**#part.**), number of alignment sites (**#sites**), sum of per-partition site patterns (**Σ(#pattern)**), memory requirements in gigabytes (**GB**) under the gamma (**Γ**) model of rate heterogeneity. Aligned sequence data sets are available in URLs listed at the end of the supplemental document. For further details see SM4.

Description	#t	#part	#sites	Σ(#pattern)	(Γ) [GB]
Total nucleotide evidence tree (TENT) alignments					
TENT-c12 (Intron, UCE, Exon-c12) 100%	48	4	37,350,521	22,254,030	131.03
TENT-c12 (Intron, UCE, Exon-c12) 75%	48	4	27,960,265	16,755,511	98.66
TENT-c12 (Intron, UCE, Exon-c12) 50%	48	4	18,875,216	11,413,262	67.20
TENT-c12 (Intron, UCE, Exon-c12) 25%	48	4	9,208,236	5,592,070	32.93
TENT-c12 (Intron, UCE, Exon-c12) + outgroups	52	4	37,817,262	23,494,894	150.37
TENT-c123 (Intron, UCE, Exon-c123)	48	5	41,781,933	25,425,011	149.70
Whole genome alignment					
Whole genome + outgroups	51	1	322,107,240	161,845,821	1,015.10
Intron alignments					
Intron	48	1	19,258,311	14,915,382	87.82
Intron, partitioned	48	500	19,258,311	15,424,402	90.82
Exon alignments					
Exon-c12	48	1	8,862,864	2,262,062	13.32
Exon-c12, partitioned	48	400	8,862,864	2,831,526	16.67

Exon c123	48	1	13,294,276	5,169,194	30.44
Exon-c123, partitioned	48	600	13,298,277	6,274,599	36.94
Exon-c1	48	1	4,431,488	1,399,705	8.24
Exon-c2	48	1	4,431,376	1,105,108	6.51
Exon-c3	48	1	4,431,412	3,170,981	18.67
Amino acid, partitioned	48	8253	4,430,770	2,341,493	68.93
Ultra conserved element (UCE) alignment					
UCE	48	3679	9,229,346	4,833,855	27.1
UCE + outgroup	49	3679	9,251,694	5,012,622	28.8
Test alignments with outgroups					
Total evidence tree + indels + outgroups	52	8	48,037,956	31,582,577	183.00
Intron + outgroups	52	1	19,530,152	15,325,328	98.08
Intron, partitioned + outgroups	52	500	19,530,152	15,864,791	101.53
Exon c12, partitioned + outgroups	52	1000	9,035,416	3,550,961	22.73
Exon c123, partitioned + outgroups	52	1500	13,553,087	7,439,705	47.61
Amino acid + outgroup	52	1	4,517,035	2,417,275	77.35
Amino acid, partitioned + outgroups	52	8295	4,517,035	2,752,032	88.07

Table S4. **Number of ML and bootstrap trees computed for each dataset.** Rate-het, rate heterogeneity model of sequence evolution. ML inferences, number of independent starting trees. # BS replicates, number of bootstrap replicates. Converged, denotes if bootstrap support values converged according to the bootstopping criterion. Numbers in brackets indicate how many permutations (out of 100) of the bootstrap convergence test show a weighted RF-distance $\leq 3\%$, if converged, or it not the total number stopped at. For further details see SM4.

Dataset	Rate-het	ML inferences	# BS replicates	Converged
TENT 100%	Γ	40	150	Yes (after 150)
TENT 75%	Γ	20	100	Yes (after 50)
TENT 50%	Γ	20	100	Yes (after 50)
TENT 25%	Γ	20	102	Yes (after 50)
TENT-c123	Γ	40	99	Yes (after 50)
Whole genome tree	Γ	20	50	Yes (after 50)
Intron	Γ	21	100	Yes (after 50)
Intron-partitioned	Γ	40	100	Yes (after 100)
Exon-c12	Γ	40	200	No (41)
Exon-c12 partitioned	Γ	40	200	No (7)
Exon-c12 + outgroups	Γ	40	103	Yes (after 50)
Exon-c123	Γ	40	200	No (32)
Exon-c123 partitioned	Γ	40	200	No (63)
Exon-c123 RY recoded	Γ	40	200	No (70)
Exon-c1	Γ	40	200	Yes (200)
Exon-c2	Γ	40	200	No (26)
Exon-c3	Γ	40	200	No (70)
Amino acid	Γ	40	102	Yes (after 100)
UCE	Γ	20	108	no (52)
Total evidence tree	PSR	40	100	Yes (after 50)
Whole genome tree	PSR	7	NA	NA
Intron	PSR	40	150	Yes
Intron partitioned	PSR	20	100	Yes

Exon unpartitioned	PSR	41	200	No (72)
Exon-c12	PSR	40	200	No (22)
Exon-c123	PSR	40	200	No (62)
Amino acid	PSR	41	200	No (25)
Amino acid partitioned	PSR	40	200	No (36)
UCE+outgroup	PSR	20	208	Yes (after 150)

Table S5. **Breakdown of CPU time spent on ML searches for each tree inference.** Columns 4-6 indicate at which data center the analyses were conducted. For further details see SM4.

Data set	rate-het	CPU-hours	HITS	SDSC	LRZ	TACC	GACRC & AWS
Species trees							
TENT 100%	Γ	69,973.30	X				
TENT 75%	Γ	75,622.60	X		X		
TENT 50%	Γ	63,751.80	X				
TENT 25%	Γ	17,305.02	X		X		
TENT-c123	Γ	88,865.20			X		
TENT-c12 + outgroups	Γ	128,694.00	X		X		
Whole genome tree	Γ	363,464.00			X		
Intron	Γ	55,529.60	X		X		
Intron partitioned	Γ	238,343.80	X				
Exon-c12	Γ	21,462.68	X				
Exon-c12 partitioned	Γ	69,656.05	X		X		
Exon-c123	Γ	51,924.40	X				
Exon-c123 partitioned	Γ	82,481.80			X		
Exon-c123 RY recoded	Γ	26,856.61	X				
Exon-c1	Γ	16,629.30	X				
Exon-c2	Γ	6,288.89	X				
Exon-c3	Γ	36,962.90	X				
Amino acid	Γ	162,465.60	X				
UCE	Γ	9,684.48					X
TIET, indel tree	Bin Γ	9,883.86	X				
TET	PSR	65,512.18	X	X			
Whole genome tree	PSR	19,382.54	X				
Intron	PSR	94,307.07	X				
Intron partitioned	PSR	24,263.47		X			
Exon	PSR	47,880.56	X	X			
Exon-c12	PSR	127,843.36	X	X			
Exon-c123	PSR	87,271.11		X			
Amino acid	PSR	124,726.53	X				
Amino acid partitioned	PSR	65,526.22		X			
UCE + outgroup	PSR	4,972.20					X
Gene trees							
Exons	Γ	2,304.00	X				
Introns	Γ	26,400.00				X	
UCE	Γ	11,453.76					X
Binned gene trees TENT	Γ	43,200.00				X	
Total		2,340,888.89					

Table S6. Substituted species to allow comparisons with the prior literature. " = same genus or species that we used; X = genus not represented in prior literature study. If the order was the same, but the genus/family was different in the prior study, then the name of that family in the prior study is listed. For further details see SM7.

Family, this study	Latin name, this study	Sibley & Ahlquist DNA-DNA hyb	Livezey & Zusi morphology	Pacheco etal mt DNA	Hackett etal Nuclear DNA
Acanthisittidae	Acanthisitta chloris	"	X	"	"
Anatidae	Anas platyrhynchos	"	"	"	"
Trogonidae	Apaloderma vittatum	"	Trogon	Trogon	Trogon
Spheniscidae	Aptenodytes forsteri	"	X	X	X
Gruidae	Balearica regulorum	"	Grus	X	Grus
Bucerotidae	Buceros rhinoceros	"	Tockus	Aceros	Tockus
Trochilidae	Calypte anna	Amazilia	Glaucis	Archilocus	Colibri
Caprimulgidae	Antrostomus carolinensis	"	"	Nyctibius	"
Cariamidae	Cariama cristata	"	"	X	"
Cathartidae	Cathartes aura	"	"	X	"
Apodidae	Chaetura pelagica	"	Apus	Apus	Aerodramus
Charadriidae	Charadrius vociferus	"	Haematopus	Haematopus	"
Otididae	Chlamydotis macqueenii	Afrotis	Afrotis	X	Eupodotis
Columbidae	Columba livia	"	"	Leptotila	"
Coliidae	Colius striatus	"	"	X	"
Corvidae	Corvus brachyrhynchos	"	Aphelocoma	"	"
Cuculidae	Cuculus canorus	"	"	Eudynamis	"
Ardeidae	Egretta garzetta	Ardea	Ardea	Ardea	Ardea
Eurypygidae	Eurypyga helias	"	"	X	"
Falconidae	Falco peregrinus	"	"	"	"
Procellariidae	Fulmarus glacialis	Pachyptila	Pachyptila	Thalassarche	Diomedea
Phasianidae	Gallus gallus	"	"	"	"
Gaviidae	Gavia stellata	"	"	"	"
Thraupidae	Geospiza fortis	Thraupis	X	X	Fringilla
Accipitridae	Haliaeetus albicilla	X	X	X	X
Aciipitridae	Haliaeetus leucocephalus	Buteo	Accipiter	Buteo	Buteo
Leptosomidae	Leptosomus discolor	"	"	X	"
Pipridae	Manacus vitellinus	"	Pitangus	Cnemotriccus	Pipra
Phasianidae	Meleagris gallopavo	"	"	"	X
Psittacidae	Melopsittacus undulatus	Nymphicus	"	"	Platycercus
Meropidae	Merops nubicus	"	"	Eurystomus	"
Mesitornithidae	Mesitornis unicolor	X	"	X	"
Psittacidae	Nestor notabilis	X	X	Strigops	X
Threskiornithidae	Nipponia nippon	Plegadis	Plegadis	"	Eudocimus
Opisthocomidae	Opisthocomus hoazin	"	"	X	"
Pelecanidae	Pelecanus crispus	"	"	"	"
Phalacrocoracidae	Phalacrocorax carbo	"	"	X	"
Phaethontidae	Phaethon lepturus	"	"	X	"
Phoenicopteridae	Phoenicopterus ruber	"	"	"	"
Picidae	Picoides pubescens	"	"	Dryocopus	Dryocopus
Podicipedidae	Podiceps cristatus	"	"	"	"
Pteroclidae	Pterocles gutturalis	"	"	X	"
Spheniscidae	Pygoscelis adeliae	Spheniscus	Spheniscus	Eudyptula	Eudyptula
Struthionidae	Struthio camelus	"	"	X	"
Passeridae	Taeniopygia guttata	Passer	Passer	"	Ploceus
Musophagidae	Tauraco erythrolophus	"	Corythaixoides	X	"
Tinamidae	Tinamus guttatus	Crypturellus	Eudromia	X	"

| Tytonidae | Tyto alba | " | " | " | " |

Table S7. Gene tree metatable phylogeny categories. For further details see SM7.

Category	Definition
Strong Support	All taxa of the potential clade are present in the tree, and those taxa form a monophyletic clade so that the node representing that clade (i.e. its MRCA) has at least 75% support.
Strong Support (partially missing)	At least one taxon of the potential clade is missing from the tree but at least two are present. Those present taxa form a monophyletic clade, and the node representing that clade (i.e. its MRCA) has at least 75% support.
Weak Support	All taxa of the potential clade are present in the tree, and they form a monophyletic clade; however, the node representing that clade (i.e. its MRCA) has less than 75% support.
Weak Support (partially missing)	At least one taxon of the potential clade is missing from the tree but at least two are present. Those present taxa form a monophyletic clade, and the node representing that clade (i.e. its MRCA) has less than 75% support.
Weak Rejection	All taxa of the potential clade are present in the tree, but they do not form a monophyletic clade; however, if edges with support below 75% are contracted, the result is a tree that is compatible with monophyly (i.e. there is a way of refining the polytomies in the contracted tree to make the subset a monophyletic clade).
Strong rejection	The potential clade is not monophyletic, and after contracting edges with support less than 75%, the tree does not become compatible with monophyly.
Missing	If there is at most one taxon from the clade present in the tree, it is not meaningful to study monophyly. These cases are labeled "missing".

Table S8. List of the 52 species and numbers of transcript/genes used in the phylomeDB analyses. Transcripts, the number of unique longest transcript; Genes, number of annotated genes using the method described in (44); Source and Date, data was downloaded from the avian phylogenomics data repository (http://phybirds.genomics.org.cn). The number of unique longest transcripts can be smaller than the number of genes, since the two longest transcripts with identical sequence are collapsed into a single entry. Species used as seeds for the phylome reconstruction are highlighted with light-gray background. For further details see SM8.

Species Name	Transcripts	Genes	Source	Date
Acanthisitta chloris	14,551	14,596	PhyBirds	Nov/2012
Anas platyrhynchos	15,657	16,521	PhyBirds	Nov/2012
Antrostomus carolinensis	14,589	14,676	PhyBirds	Nov/2012
Apaloderma vittatum	13,568	13,615	PhyBirds	Nov/2012
Aptenodytes forsteri	15,993	16,070	PhyBirds	Nov/2012
Balearica regulorum	14,152	14,173	PhyBirds	Nov/2012
Buceros rhinoceros	13,805	13,873	PhyBirds	Nov/2012
Calypte anna	15,823	16,000	PhyBirds	Nov/2012
Cariama cristata	14,197	14,216	PhyBirds	Nov/2012
Cathartes aura	13,495	13,534	PhyBirds	Nov/2012
Chaetura pelagica	15,257	15,373	PhyBirds	Nov/2012
Charadrius vociferus	16,507	16,860	PhyBirds	Nov/2012

Chlamydotis macqueenii	13,578	13,582	PhyBirds	Nov/2012
Columba livia	16,456	16,652	PhyBirds	Nov/2012
Colius striatus	13,502	13,538	PhyBirds	Nov/2012
Corvus brachyrhynchos	16,485	16,562	PhyBirds	Nov/2012
Cuculus canorus	15,828	15,889	PhyBirds	Nov/2012
Egretta garzetta	15,562	16,585	PhyBirds	Nov/2012
Eurypyga helias	13,858	13,974	PhyBirds	Nov/2012
Falco peregrinus	16,193	16,242	PhyBirds	Nov/2012
Fulmarus glacialis	14,280	14,306	PhyBirds	Nov/2012
Gallus gallus	16,440	16,516	PhyBirds	Nov/2012
Gavia stellata	13,449	13,454	PhyBirds	Nov/2012
Geospiza fortis	16,166	16,286	PhyBirds	Nov/2012
Haliaeetus albicilla	13,822	13,831	PhyBirds	Nov/2012
Haliaeetus leucocephalus	16,521	16,526	PhyBirds	Nov/2012
Leptosomus discolor	14,825	14,831	PhyBirds	Nov/2012
Manacus vitellinus	15,182	15,285	PhyBirds	Nov/2012
Meleagris gallopavo	16,000	16,051	PhyBirds	Nov/2012
Melopsittacus undulatus	15,383	15,470	PhyBirds	Nov/2012
Merops nubicus	13,429	13,467	PhyBirds	Nov/2012
Mesitornis unicolor	15,335	15,371	PhyBirds	Nov/2012
Nestor notabilis	14,066	14,074	PhyBirds	Nov/2012
Nipponia nippon	16,640	16,756	PhyBirds	Nov/2012
Opisthocomus hoazin	15,483	15,702	PhyBirds	Nov/2012
Pelecanus crispus	14,723	14,813	PhyBirds	Nov/2012
Phalacrocorax carbo	13,457	13,479	PhyBirds	Nov/2012
Phaethon lepturus	14,808	14,970	PhyBirds	Nov/2012
Phoenicopterus ruber	13,976	14,024	PhyBirds	Nov/2012
Picoides pubescens	15,459	15,576	PhyBirds	Nov/2012
Podiceps cristatus	13,841	13,913	PhyBirds	Nov/2012
Pterocles gutturalis	13,860	13,867	PhyBirds	Nov/2012
Pygoscelis adeliae	15,134	15,270	PhyBirds	Nov/2012
Struthio camelus	15,465	16,178	PhyBirds	Nov/2012
Taeniopygia guttata	17,384	17,471	PhyBirds	Nov/2012
Tauraco erythrolophus	15,298	15,435	PhyBirds	Nov/2012
Tinamus guttatus	15,594	15,788	PhyBirds	Nov/2012
Tyto alba	13,592	13,613	PhyBirds	Nov/2012
Anolis carolinensis	17,734	18,952	Ensemb 69	Nov/2012
Alligator mississippiensis	18,164	18,287	PhyBirds	Nov/2012
Chelonia mydas	15,936	18,971	PhyBirds	Nov/2012
Homo sapiens	19,997	21,206	QfO r2012	Jul/2012

Table S9. Numbers of indels per data partition. For further details see SM9.

			Indel Size Classes		
	All	>1bp	>10bp	>100bp	<30bp
Intron indels with non-avian outgroups					
Total Characters	4,236,411	3,206,207	1,098,283	109,568	NA
Parsimony Informative	1,023,591	755,074	193,063	14,601	NA
% Informative	24.16%	23.55%	17.58%	13.33%	NA
Intron indels without non-avian outgroups					
Total Characters	3,918,322	2,894,642	881,372	75,724	NA
Parsimony Informative	942,619	702,874	172,441	13,430	NA
% Informative	24.06%	24.28%	19.57%	17.74%	NA
UCE indels					
Total Characters	1,308,980	963,012	333,722	19,745	NA
Parsimony Informative	324,520	242,628	69,453	1,481	NA
% Informative	24.79%	25.19%	20.81%	7.50%	NA
Exon indels					
Total Characters	157,632	NA	NA	NA	157,632
Parsimony Informative	36,111	NA	NA	NA	36,111
% Informative	22.91%	NA	NA	NA	22.91%

Table S10. Comparison of nucleotide and indel retention index. Ensemble Retention Index values of MP and ML tree was reconstructed using 400 introns partitioned into the nucleotide alignment and the indel alignment generated from it. For further details see SM9.

	Nucleotide characters	Indel characters
Maximum Parsimony	0.275	0.532
Maximum Likelihood	0.310	0.527

Table S11. Percent parsimony uninformative nucleotide and indel characters in a 400 intron data set. For further details see SM9.

	Nucleotide Partition	Indel Partition
Total Characters	691,187	141,138
Parsimony Informative	469,007	33,878
% Uninformative	32.14%	76.00%

Table S12. Comparison of long and short indel retention index. For further details see SM9.

		Indel Size Classes			
	All	>1bp	>10bp	>100bp	<30bp
Intron Indels					
Parsimony Indel tree	0.524	0.515	0.589	0.837	NA
ML Indel tree	0.520	0.510	0.584	0.833	NA
EaxML TENT tree	0.521	0.513	0.587	0.834	NA
UCE Indels					
Parsimony Indel tree	0.524	0.515	0.589	0.837	NA
ML Indel tree	0.520	0.510	0.584	0.833	NA
EaxML TENT tree	0.460	0.446	0.455	0.671	NA

Exon Indels

Parsimony Indel tree	0.436	NA	NA	NA	0.436
ML Indel tree	0.434	NA	NA	NA	0.434
EaxML TENT tree	0.430	NA	NA	NA	0.430

Intron+UCE+Exon Indels

Parsimony Indel tree	0.504	0.494	0.530	0.520	NA
ML Indel tree	0.500	0.488	0.522	0.513	NA
EaxML TENT tree	0.502	0.492	0.530	0.513	NA

Table S13. **Comparison of % retention index = 1.0 in long and short indels on the EaxML TENT.** For further details see SM9.

	Indel Size Classes			
	1-10bp	11-99bp	>100bp	<30bp
Intron Indels	38.70%	51.45%	82.39%	NA
UCE indels	33.83%	35.20%	64.68%	NA
Exon Indels	NA	NA	NA	30.85%

Table S14. **Correlation statistics for tree branch length, GC content, and body mass.** * - Phylogenetic control using Independent contrast analysis. For further details see SM11.

Correlation	**Pearson r**		**P**	
	Before	**After[*]**	**Before**	**After**
GC3 vs Branch length (Low variance)	0.552	0.512	0.000048	0.00017
GC3 vs Branch length (High variance)	0.975	0.771	<0.000001	<0.000001
Body mass vs Branch length (Low variance)	0.602	-0.589	0.000006	0.000009
Body mass vs Branch length (High variance)	0.724	-0.479	<0.000001	0.000498

Table S15. Fossil calibrations used in molecular dating analyses on 7 different tree topologies. Calibration numbers refer to the list of 39 calibrations in the text. Gray, fossil calibration included. For further details see SM12.

Fossil	ExaML TENT	MP-EST* TENT	WGA-B	WGA-A	Exon c123	Intron	UCE
1							
2	■	■	■	■	■	■	■
3							
4	■	■	■	■	■	■	■
5	■	■	■	■	■	■	■
6							
7	■	■	■	■	■	■	■
8							
9	■	■	■	■	■	■	
10/11	■	■	■	■	■	■	■
12	■		■	■	■	■	■
13					■		

14							
15							
16							
17							
18							
19							
20							
21							
22							
23							
24							
25							
26							
27							
28							
29							
30							
31							
32							
33							
34							
35							
36							
37							
38							
39							
TOTAL	18	19	17	18	20	18	17

Table S16. Estimated divergence times for major avian lineages on different trees (only legend provided here, full table in a separate tab-delimited text file). Numbers are in millions of years ago (MYA). ( ) = credibility intervals. Clade names of each major group are listed and below them are the names of the clades for each of their first divergences. In column C, the outgroups are the three reptile species used (alligator, turtle, and lizard). *Dates with a decrease in the age of the alligator-bird and lizard-bird divergences to 247 and 255.9 MYA respectively. See online materials for nexus files for all dated trees. For further details see SM12.

Table S17. Genome sequence and annotation downloads (only legend provided here, full table in a separate tab-delimited text file). For further details see SM13.

Appendix A: UCE Supplementary Code

LASTZ parameters we used to map probes targeting UCE loci to each avian genome assembly.

```
LASTZ \
TARGET_GENOME[nameparse=full]
faircloth+stephen-probes.fasta[nameparse=full]
--strand=both
--seed=12of19
--transition
--nogfextend
--nochain
--gap=400,30
--xdrop=910
--ydrop=8370
--hspthresh=3000
--gappedthresh=3000
--noentropy
--coverage=83
--identity=92.5
--output=OUTPUT_FILE_NAME
--format=general-
:score,name1,strand1,zstart1,end1,length1,name2,strand2,zstart2,end2,length2,
diff,cigar,identity,continuity,coverage
```

Appendix B: SATé commands

1. SATé was executed as follows on all the datasets:

```
python run_sate.py -i [input file] -j [a name] [relevant
configuration file]
```

The relevant configuration file depends on the dataset. The following shows the exact configuration file used in each analyses:

2. **Exons; SATé-Prank**

```
[commandline]
keepalignmenttemps = False
multilocus = False
datatype = Protein
keeptemp = True

[sate]
time_limit = -1
iter_without_imp_limit = -1
time_without_imp_limit = -1.0
```

break_strategy = longest
start_tree_search_from_current = True
blind_after_iter_without_imp = -1
blind_mode_was_final = True
blind_after_time_without_imp = -1.0
max_subproblem_size = 0
merger = muscle
aligner = prank
tree_estimator = raxml
num_cpus = 1
after_blind_time_without_imp_limit = -1.0
max_subproblem_frac = 0.2
blind_after_total_time = -1.0
after_blind_time_term_limit = -1.0
output_directory = results
iter_limit = -1
blind_after_total_iter = -1
after_blind_iter_term_limit = -1
return_final_tree_and_alignment = False
move_to_blind_on_worse_score = True
after_blind_iter_without_imp_limit = 2

3. **Exons; SATé-MAFFT**

[raxml]
 model = PROTCATJTT

[commandline]
keepalignmenttemps = False
multilocus = False
datatype = Protein
keeptemp = True

[sate]
time_limit = -1
iter_without_imp_limit = -1
time_without_imp_limit = -1.0
break_strategy = longest
start_tree_search_from_current = True
blind_after_iter_without_imp = -1
blind_mode_was_final = True
blind_after_time_without_imp = -1.0
max_subproblem_size = 0
merger = muscle
aligner = mafft
tree_estimator = raxml
num_cpus = 1
after_blind_time_without_imp_limit = -1.0
max_subproblem_frac = 0.5
blind_after_total_time = -1.0
after_blind_time_term_limit = -1.0
output_directory = results
iter_limit = -1

blind_after_total_iter = -1
after_blind_iter_term_limit = -1
return_final_tree_and_alignment = False
move_to_blind_on_worse_score = True
after_blind_iter_without_imp_limit = 2

Introns; SATé-MAFFT

[raxml]
model = GTRCAT

[commandline]
keepalignmenttemps = False
multilocus = False
datatype = dna
keeptemp = True

[sate]
time_limit = -1
iter_without_imp_limit = -1
time_without_imp_limit = -1.0
break_strategy = longest
start_tree_search_from_current = True
blind_after_iter_without_imp = -1
blind_mode_was_final = True
blind_after_time_without_imp = -1.0
max_subproblem_size = 0
merger = opal
aligner = mafft
tree_estimator = raxml
num_cpus = 1
after_blind_time_without_imp_limit = -1.0
max_subproblem_frac = 0.5
blind_after_total_time = -1.0
after_blind_time_term_limit = -1.0
output_directory = results
iter_limit = -1
blind_after_total_iter = -1
after_blind_iter_term_limit = -1
return_final_tree_and_alignment = False
move_to_blind_on_worse_score = True
after_blind_iter_without_imp_limit = 2

UCEs; SATé-MAFFT

[raxml]
model = GTRCAT

[commandline]

keepalignmenttemps = False
multilocus = False
datatype = dna
keeptemp = True

[sate]
time_limit = -1
iter_without_imp_limit = -1
time_without_imp_limit = -1.0
break_strategy = longest
start_tree_search_from_current = True
blind_after_iter_without_imp = -1
blind_mode_was_final = True
blind_after_time_without_imp = -1.0
max_subproblem_size = 0
merger = opal
aligner = mafft
tree_estimator = raxml
num_cpus = 1
after_blind_time_without_imp_limit = -1.0
max_subproblem_frac = 0.2
blind_after_total_time = -1.0
after_blind_time_term_limit = -1.0
output_directory = results
iter_limit = -1
blind_after_total_iter = -1
after_blind_iter_term_limit = -1
return_final_tree_and_alignment = False
move_to_blind_on_worse_score = True
after_blind_iter_without_imp_limit = 2

References and Notes

1. C. Venditti, A. Meade, M. Pagel, Phylogenies reveal new interpretation of speciation and the Red Queen. *Nature* **463**, 349–352 (2010). Medline doi:10.1038/nature08630

2. J. B. Yoder, E. Clancey, S. Des Roches, J. M. Eastman, L. Gentry, W. Godsoe, T. J. Hagey, D. Jochimsen, B. P. Oswald, J. Robertson, B. A. Sarver, J. J. Schenk, S. F. Spear, L. J. Harmon, Ecological opportunity and the origin of adaptive radiations. *J. Evol. Biol.* **23**, 1581–1596 (2010). Medline doi:10.1111/j.1420-9101.2010.02029.x

3. A. Feduccia, Explosive evolution in tertiary birds and mammals. *Science* **267**, 637–638 (1995). Medline doi:10.1126/science.267.5198.637

4. P. Schulte, L. Alegret, I. Arenillas, J. A. Arz, P. J. Barton, P. R. Bown, T. J. Bralower, G. L. Christeson, P. Claeys, C. S. Cockell, G. S. Collins, A. Deutsch, T. J. Goldin, K. Goto, J. M. Grajales-Nishimura, R. A. Grieve, S. P. Gulick, K. R. Johnson, W. Kiessling, C. Koeberl, D. A. Kring, K. G. MacLeod, T. Matsui, J. Melosh, A. Montanari, J. V. Morgan, C. R. Neal, D. J. Nichols, R. D. Norris, E. Pierazzo, G. Ravizza, M. Rebolledo-Vieyra, W. U. Reimold, E. Robin, T. Salge, R. P. Speijer, A. R. Sweet, J. Urrutia-Fucugauchi, V. Vajda, M. T. Whalen, P. S. Willumsen, The Chicxulub asteroid impact and mass extinction at the Cretaceous-Paleogene boundary. *Science* **327**, 1214–1218 (2010). Medline doi:10.1126/science.1177265

5. N. R. Longrich, T. Tokaryk, D. J. Field, Mass extinction of birds at the Cretaceous-Paleogene (K-Pg) boundary. *Proc. Natl. Acad. Sci. U.S.A.* **108**, 15253–15257 (2011). Medline doi:10.1073/pnas.1110395108

6. D. T. Ksepka, C. A. Boyd, Quantifying historical trends in the completeness of the fossil record and the contributing factors: An example using Aves. *Paleobiology* **38**, 112–125 (2012). doi:10.1666/10059.1

7. K. M. Cohen, S. Finney, P. L. Gibbard, International Chronostratigraphic Chart v2013/01, in *International Commission on Stratigraphy* (2013); www.stratigraphy.org/ICSchart/ChronostratChart2013-01.jpg.

8. P. G. Ericson, C. L. Anderson, T. Britton, A. Elzanowski, U. S. Johansson, M. Källersjö, J. I. Ohlson, T. J. Parsons, D. Zuccon, G. Mayr, Diversification of Neoaves: Integration of molecular sequence data and fossils. *Biol. Lett.* **2**, 543–547 (2006). Medline doi:10.1098/rsbl.2006.0523

9. R. W. Meredith, J. E. Janečka, J. Gatesy, O. A. Ryder, C. A. Fisher, E. C. Teeling, A. Goodbla, E. Eizirik, T. L. Simão, T. Stadler, D. L. Rabosky, R. L. Honeycutt, J. J. Flynn, C. M. Ingram, C. Steiner, T. L. Williams, T. J. Robinson, A. Burk-Herrick, M. Westerman, N. A. Ayoub, M. S. Springer, W. J. Murphy, Impacts of the Cretaceous Terrestrial Revolution and KPg extinction on mammal diversification. *Science* **334**, 521–524 (2011). Medline doi:10.1126/science.1211028

10. W. Jetz, G. H. Thomas, J. B. Joy, K. Hartmann, A. O. Mooers, The global diversity of birds in space and time. *Nature* **491**, 444–448 (2012). Medline doi:10.1038/nature11631

11. O. Haddrath, A. J. Baker, Multiple nuclear genes and retroposons support vicariance and dispersal of the palaeognaths, and an Early Cretaceous origin of modern birds. *Proc. Biol. Sci.* **279**, 4617–4625 (2012). Medline doi:10.1098/rspb.2012.1630

12. M. S. Lee, A. Cau, D. Naish, G. J. Dyke, Morphological clocks in paleontology, and a mid-Cretaceous origin of crown Aves. *Syst. Biol.* **63**, 442–449 (2014). Medline doi:10.1093/sysbio/syt110

13. J. W. Brown, J. S. Rest, J. García-Moreno, M. D. Sorenson, D. P. Mindell, Strong mitochondrial DNA support for a Cretaceous origin of modern avian lineages. *BMC Biol.* **6**, 6 (2008). Medline doi:10.1186/1741-7007-6-6

14. M. A. Pacheco, F. U. Battistuzzi, M. Lentino, R. F. Aguilar, S. Kumar, A. A. Escalante, Evolution of modern birds revealed by mitogenomics: Timing the radiation and origin of major orders. *Mol. Biol. Evol.* **28**, 1927–1942 (2011). Medline doi:10.1093/molbev/msr014

15. B. C. Livezey, R. L. Zusi, Higher-order phylogeny of modern birds (Theropoda, Aves: Neornithes) based on comparative anatomy. II. Analysis and discussion. *Zool. J. Linn. Soc.* **149**, 1–95 (2007). Medline doi:10.1111/j.1096-3642.2006.00293.x

16. G. Mayr, Metaves, Mirandornithes, Strisores and other novelties – a critical review of the higher-level phylogeny of neornithine birds. *J. Zool. Syst. Evol. Res.* **49**, 58–76 (2011). doi:10.1111/j.1439-0469.2010.00586.x

17. S. J. Hackett, R. T. Kimball, S. Reddy, R. C. Bowie, E. L. Braun, M. J. Braun, J. L. Chojnowski, W. A. Cox, K. L. Han, J. Harshman, C. J. Huddleston, B. D. Marks, K. J. Miglia, W. S. Moore, F. H. Sheldon, D. W. Steadman, C. C. Witt, T. Yuri, A phylogenomic study of birds reveals their evolutionary history. *Science* **320**, 1763–1768 (2008). Medline doi:10.1126/science.1157704

18. R. C. Pratt, G. C. Gibb, M. Morgan-Richards, M. J. Phillips, M. D. Hendy, D. Penny, Toward resolving deep neoaves phylogeny: Data, signal enhancement, and priors. *Mol. Biol. Evol.* **26**, 313–326 (2009). Medline doi:10.1093/molbev/msn248

19. B. Nabholz, A. Künstner, R. Wang, E. D. Jarvis, H. Ellegren, Dynamic evolution of base composition: Causes and consequences in avian phylogenomics. *Mol. Biol. Evol.* **28**, 2197–2210 (2011). Medline doi:10.1093/molbev/msr047

20. O. Jeffroy, H. Brinkmann, F. Delsuc, H. Philippe, Phylogenomics: The beginning of incongruence? *Trends Genet.* **22**, 225–231 (2006). Medline doi:10.1016/j.tig.2006.02.003

21. S. Song, L. Liu, S. V. Edwards, S. Wu, Resolving conflict in eutherian mammal phylogeny using phylogenomics and the multispecies coalescent model. *Proc. Natl. Acad. Sci. U.S.A.* **109**, 14942–14947 (2012). Medline doi:10.1073/pnas.1211733109

22. J. Alföldi, K. Lindblad-Toh, Comparative genomics as a tool to understand evolution and disease. *Genome Res.* **23**, 1063–1068 (2013). Medline doi:10.1101/gr.157503.113

23. J. L. Peters, *Check-List of Birds of the World*, E. Mayr, R. A. Paynter, M. A. Traylor, J. C. Greenway, Eds. (Harvard Univ. Press, Cambridge, MA, 1937–1987).

24. C. G. Sibley, J. E. Ahlquist, *Phylogeny and Classification of Birds: A Study in Molecular Evolution* (Yale Univ. Press, New Haven, CT, 1990).

25. M. G. Fain, P. Houde, Parallel radiations in the primary clades of birds. *Evolution* **58**, 2558–2573 (2004). Medline doi:10.1111/j.0014-3820.2004.tb00884.x

26. N. Wang, E. L. Braun, R. T. Kimball, Testing hypotheses about the sister group of the passeriformes using an independent 30-locus data set. *Mol. Biol. Evol.* **29**, 737–750 (2012). Medline doi:10.1093/molbev/msr230

27. R. T. Kimball, N. Wang, V. Heimer-McGinn, C. Ferguson, E. L. Braun, Identifying localized biases in large datasets: A case study using the avian tree of life. *Mol. Phylogenet. Evol.* **69**, 1021–1032 (2013). Medline doi:10.1016/j.ympev.2013.05.029

28. J. E. McCormack, M. G. Harvey, B. C. Faircloth, N. G. Crawford, T. C. Glenn, R. T. Brumfield, A phylogeny of birds based on over 1,500 loci collected by target enrichment and high-throughput sequencing. *PLOS ONE* **8**, e54848 (2013). Medline doi:10.1371/journal.pone.0054848

29. A. Suh, M. Paus, M. Kiefmann, G. Churakov, F. A. Franke, J. Brosius, J. O. Kriegs, J. Schmitz, Mesozoic retroposons reveal parrots as the closest living relatives of passerine birds. *Nat. Commun.* **2**, 443 (2011). Medline doi:10.1038/ncomms1448

30. M. T. Mahmood, P. A. McLenachan, G. C. Gibb, D. Penny, Phylogenetic position of avian nocturnal and diurnal raptors. *Genome Biol. Evol.* **6**, 326–332 (2014). Medline doi:10.1093/gbe/evu016

31. A. Matzke, G. Churakov, P. Berkes, E. M. Arms, D. Kelsey, J. Brosius, J. O. Kriegs, J. Schmitz, Retroposon insertion patterns of neoavian birds: Strong evidence for an extensive incomplete lineage sorting era. *Mol. Biol. Evol.* **29**, 1497–1501 (2012). Medline doi:10.1093/molbev/msr319

32. J. L. Chojnowski, R. T. Kimball, E. L. Braun, Introns outperform exons in analyses of basal avian phylogeny using clathrin heavy chain genes. *Gene* **410**, 89–96 (2008). Medline doi:10.1016/j.gene.2007.11.016

33. S. Patel, R. T. Kimball, E. L. Braun, Error in the phylogenetic estimation for the bushes in the tree of life. *J. Phylogenetics Evol. Biol.* **1**, 9–10 (2013).

34. Y. I. Wolf, I. B. Rogozin, N. V. Grishin, E. V. Koonin, Genome trees and the tree of life. *Trends Genet.* **18**, 472–479 (2002). Medline doi:10.1016/S0168-9525(02)02744-0

35. A. Rokas, B. L. Williams, N. King, S. B. Carroll, Genome-scale approaches to resolving incongruence in molecular phylogenies. *Nature* **425**, 798–804 (2003). Medline doi:10.1038/nature02053

36. J. Cracraft, in *The Howard and Moore Complete Checklist of the Birds of the World*, E. C. Dickinson, J. V. Remsen, Eds. (Aves Press, Eastbourne, UK, 2013), pp. xxi–xliii.

37. E. C. Dickinson, J. V. Remsen, Eds., *The Howard and Moore Complete Checklist of Birds of the World* (Aves Press, Eastbourne, UK, 2013).

38. E. D. Jarvis, Learned birdsong and the neurobiology of human language. *Ann. N. Y. Acad. Sci.* **1016**, 749–777 (2004). Medline doi:10.1196/annals.1298.038

39. D. F. Clayton, C. N. Balakrishnan, S. E. London, Integrating genomes, brain and behavior in the study of songbirds. *Curr. Biol.* **19**, R865–R873 (2009). Medline doi:10.1016/j.cub.2009.07.006

40. L. W. Hillier, W. Miller, E. Birney, W. Warren, R. C. Hardison, C. P. Ponting, P. Bork, D. W. Burt, M. A. M. Groenen, M. E. Delany, J. B. Dodgson, A. T. Chinwalla, P. F. Cliften, S. W. Clifton, K. D. Delehaunty, C. Fronick, R. S. Fulton, T. A. Graves, C. Kremitzki, D. Layman, V. Magrini, J. D. McPherson, T. L. Miner, P. Minx, W. E. Nash, M. N. Nhan, J. O. Nelson, L. G. Oddy, C. S. Pohl, J. Randall-Maher, S. M. Smith, J. W. Wallis, S.-P. Yang, M. N. Romanov, C. M. Rondelli, B. Paton, J. Smith, D. Morrice, L. Daniels, H. G. Tempest, L. Robertson, J. S. Masabanda, D. K. Griffin, A. Vignal, V. Fillon, L. Jacobbson, S. Kerje, L. Andersson, R. P. M. Crooijmans, J. Aerts, J. J. van der Poel, H. Ellegren, R. B. Caldwell, S. J. Hubbard, D. V. Grafham, A. M. Kierzek, S. R. McLaren, I. M. Overton, H. Arakawa, K. J. Beattie, Y. Bezzubov, P. E. Boardman, J. K. Bonfield, M. D. R. Croning, R. M. Davies, M. D. Francis, S. J. Humphray, C. E. Scott, R. G. Taylor, C. Tickle, W. R. A. Brown, J. Rogers, J.-M. Buerstedde, S. A. Wilson, L. Stubbs, I. Ovcharenko, L. Gordon, S. Lucas, M. M. Miller, H. Inoko, T. Shiina, J. Kaufman, J. Salomonsen, K. Skjoedt, G. K.-S. Wong, J. Wang, B. Liu, J. Wang, J. Yu, H. Yang, M. Nefedov, M. Koriabine, P. J. deJong, L. Goodstadt, C. Webber, N. J. Dickens, I. Letunic, M. Suyama, D. Torrents, C. von Mering, E. M. Zdobnov, K. Makova, A. Nekrutenko, L. Elnitski, P. Eswara, D. C. King, S. Yang, S. Tyekucheva, A. Radakrishnan, R. S. Harris, F. Chiaromonte, J. Taylor, J. He, M. Rijnkels, S. Griffiths-Jones, A. Ureta-Vidal, M. M. Hoffman, J. Severin, S. M. J. Searle, A. S. Law, D. Speed, D. Waddington, Z. Cheng, E. Tuzun, E. Eichler, Z. Bao, P. Flicek, D. D. Shteynberg, M. R. Brent, J. M. Bye, E. J. Huckle, S. Chatterji, C. Dewey, L. Pachter, A. Kouranov, Z. Mourelatos, A. G. Hatzigeorgiou, A. H. Paterson, R. Ivarie, M. Brandstrom, E. Axelsson, N. Backstrom, S. Berlin, M. T. Webster, O. Pourquie, A. Reymond, C. Ucla, S. E. Antonarakis, M. Long, J. J. Emerson, E. Betrán, I. Dupanloup, H. Kaessmann, A. S. Hinrichs, G. Bejerano, T. S. Furey, R. A. Harte, B. Raney, A. Siepel, W. J. Kent, D. Haussler, E. Eyras, R. Castelo, J. F. Abril, S. Castellano, F. Camara, G. Parra, R. Guigo, G. Bourque, G. Tesler, P. A. Pevzner, A. Smit, L. A. Fulton, E. R. Mardis, R. K. Wilson; International Chicken Genome Sequencing Consortium, Sequence and comparative analysis of the chicken genome provide unique perspectives on vertebrate evolution. *Nature* **432**, 695–716 (2004). Medline doi:10.1038/nature03154

41. R. A. Dalloul, J. A. Long, A. V. Zimin, L. Aslam, K. Beal, L. A. Blomberg, P. Bouffard, D. W. Burt, O. Crasta, R. P. Crooijmans, K. Cooper, R. A. Coulombe, S. De, M. E. Delany, J. B. Dodgson, J. J. Dong, C. Evans, K. M. Frederickson, P. Flicek, L. Florea, O. Folkerts, M. A. Groenen, T. T. Harkins, J. Herrero, S. Hoffmann, H. J. Megens, A. Jiang, P. de Jong, P. Kaiser, H. Kim, K. W. Kim, S. Kim, D. Langenberger, M. K. Lee, T. Lee, S. Mane, G. Marcais, M. Marz, A. P. McElroy, T. Modise, M. Nefedov, C. Notredame, I. R. Paton, W. S. Payne, G. Pertea, D. Prickett, D. Puiu, D. Qioa, E. Raineri, M. Ruffier, S. L. Salzberg, M. C. Schatz, C. Scheuring, C. J. Schmidt, S. Schroeder, S. M. Searle, E. J. Smith, J. Smith, T. S. Sonstegard, P. F. Stadler, H. Tafer, Z. J. Tu, C. P. Van Tassell, A.

J. Vilella, K. P. Williams, J. A. Yorke, L. Zhang, H. B. Zhang, X. Zhang, Y. Zhang, K. M. Reed, Multi-platform next-generation sequencing of the domestic turkey (*Meleagris gallopavo*): Genome assembly and analysis. *PLOS Biol.* **8**, e1000475 (2010). [Medline](doi:10.1371/journal.pbio.1000475) doi:10.1371/journal.pbio.1000475

42. W. C. Warren, D. F. Clayton, H. Ellegren, A. P. Arnold, L. W. Hillier, A. Künstner, S. Searle, S. White, A. J. Vilella, S. Fairley, A. Heger, L. Kong, C. P. Ponting, E. D. Jarvis, C. V. Mello, P. Minx, P. Lovell, T. A. Velho, M. Ferris, C. N. Balakrishnan, S. Sinha, C. Blatti, S. E. London, Y. Li, Y. C. Lin, J. George, J. Sweedler, B. Southey, P. Gunaratne, M. Watson, K. Nam, N. Backström, L. Smeds, B. Nabholz, Y. Itoh, O. Whitney, A. R. Pfenning, J. Howard, M. Völker, B. M. Skinner, D. K. Griffin, L. Ye, W. M. McLaren, P. Flicek, V. Quesada, G. Velasco, C. Lopez-Otin, X. S. Puente, T. Olender, D. Lancet, A. F. Smit, R. Hubley, M. K. Konkel, J. A. Walker, M. A. Batzer, W. Gu, D. D. Pollock, L. Chen, Z. Cheng, E. E. Eichler, J. Stapley, J. Slate, R. Ekblom, T. Birkhead, T. Burke, D. Burt, C. Scharff, I. Adam, H. Richard, M. Sultan, A. Soldatov, H. Lehrach, S. V. Edwards, S. P. Yang, X. Li, T. Graves, L. Fulton, J. Nelson, A. Chinwalla, S. Hou, E. R. Mardis, R. K. Wilson, The genome of a songbird. *Nature* **464**, 757–762 (2010). [Medline](doi:10.1038/nature08819) doi:10.1038/nature08819

43. J. Alföldi, F. Di Palma, M. Grabherr, C. Williams, L. Kong, E. Mauceli, P. Russell, C. B. Lowe, R. E. Glor, J. D. Jaffe, D. A. Ray, S. Boissinot, A. M. Shedlock, C. Botka, T. A. Castoe, J. K. Colbourne, M. K. Fujita, R. G. Moreno, B. F. ten Hallers, D. Haussler, A. Heger, D. Heiman, D. E. Janes, J. Johnson, P. J. de Jong, M. Y. Koriabine, M. Lara, P. A. Novick, C. L. Organ, S. E. Peach, S. Poe, D. D. Pollock, K. de Queiroz, T. Sanger, S. Searle, J. D. Smith, Z. Smith, R. Swofford, J. Turner-Maier, J. Wade, S. Young, A. Zadissa, S. V. Edwards, T. C. Glenn, C. J. Schneider, J. B. Losos, E. S. Lander, M. Breen, C. P. Ponting, K. Lindblad-Toh, The genome of the green anole lizard and a comparative analysis with birds and mammals. *Nature* **477**, 587–591 (2011). [Medline](doi:10.1038/nature10390) doi:10.1038/nature10390

44. G. Zhang, C. Li, Q. Li, B. Li, D. M. Larkin, C. Lee, J. F. Storz, A. Antunes, M. J. Greenwold, R. W. Meredith, A. Ödeen, J. Cui, Q. Zhou, L. Xu, H. Pan, Z. Wang, L. Jin, P. Zhang, H. Hu, W. Yang, J. Hu, J. Xiao, Z. Yang, Y. Liu, Q. Xie, H. Yu, J. Lian, P. Wen, F. Zhang, H. Li, Y. Zeng, Z. Xiong, S. Liu, L. Zhou, Z. Huang, N. An, J. Wang, Q. Zheng, Y. Xiong, G. Wang, B. Wang, J. Wang, Y. Fan, R. R. da Fonseca, A. Alfaro-Núñez, M. Schubert, L. Orlando, T. Mourier, J. T. Howard, G. Ganapathy, A. Pfenning, O. Whitney, M. V. Rivas, E. Hara, J. Smith, M. Farré, J. Narayan, G. Slavov, M. N. Romanov, R. Borges, J. P. Machado, I. Khan, M. S. Springer, J. Gatesy, F. G. Hoffmann, J. C. Opazo, O. Håstad, R. H. Sawyer, H. Kim, K.-W. Kim, H. J. Kim, S. Cho, N. Li, Y. Huang, M. W. Bruford, X. Zhan, A. Dixon, M. F. Bertelsen, E. Derryberry, W. Warren, R. K. Wilson, S. Li, D. A. Ray, R. E. Green, S. J. O'Brien, D. Griffin, W. E. Johnson, D. Haussler, O. A. Ryder, E. Willerslev, G. R. Graves, P. Alström, J. Fjeldså, D. P. Mindell, S. V. Edwards, E. L. Braun, C. Rahbek, D. W. Burt, P. Houde, Y. Zhang, H. Yang, J. Wang, Avian Genome Consortium, E. D. Jarvis, M. T. P. Gilbert, J. Wang, Comparative genomics reveals insights into avian genome evolution and adaption. *Science* **346**, 1311–1320 (2014).

45. M. D. Shapiro, Z. Kronenberg, C. Li, E. T. Domyan, H. Pan, M. Campbell, H. Tan, C. D. Huff, H. Hu, A. I. Vickrey, S. C. Nielsen, S. A. Stringham, H. Hu, E. Willerslev, M. T. Gilbert, M. Yandell, G. Zhang, J. Wang, Genomic diversity and evolution of the head crest in the rock pigeon. *Science* **339**, 1063–1067 (2013). [Medline](doi:10.1126/science.1230422)

46. X. Zhan, S. Pan, J. Wang, A. Dixon, J. He, M. G. Muller, P. Ni, L. Hu, Y. Liu, H. Hou, Y. Chen, J. Xia, Q. Luo, P. Xu, Y. Chen, S. Liao, C. Cao, S. Gao, Z. Wang, Z. Yue, G. Li, Y. Yin, N. C. Fox, J. Wang, M. W. Bruford, Peregrine and saker falcon genome sequences provide insights into evolution of a predatory lifestyle. *Nat. Genet.* **45**, 563–566 (2013). [Medline](doi:10.1038/ng.2588)

47. Y. Huang, Y. Li, D. W. Burt, H. Chen, Y. Zhang, W. Qian, H. Kim, S. Gan, Y. Zhao, J. Li, K. Yi, H. Feng, P. Zhu, B. Li, Q. Liu, S. Fairley, K. E. Magor, Z. Du, X. Hu, L. Goodman, H. Tafer, A. Vignal, T. Lee, K. W. Kim, Z. Sheng, Y. An, S. Searle, J. Herrero, M. A. Groenen, R. P. Crooijmans, T. Faraut, Q. Cai, R. G. Webster, J. R. Aldridge, W. C. Warren, S. Bartschat, S. Kehr, M. Marz, P. F. Stadler, J. Smith, R. H. Kraus, Y. Zhao, L. Ren, J. Fei, M. Morisson, P. Kaiser, D. K. Griffin, M. Rao, F. Pitel, J. Wang, N. Li, The duck genome and transcriptome provide insight into an avian influenza virus reservoir species. *Nat. Genet.* **45**, 776–783 (2013). [Medline](doi:10.1038/ng.2657)

48. Z. Wang, J. Pascual-Anaya, A. Zadissa, W. Li, Y. Niimura, Z. Huang, C. Li, S. White, Z. Xiong, D. Fang, B. Wang, Y. Ming, Y. Chen, Y. Zheng, S. Kuraku, M. Pignatelli, J. Herrero, K. Beal, M. Nozawa, Q. Li, J. Wang, H. Zhang, L. Yu, S. Shigenobu, J. Wang, J. Liu, P. Flicek, S. Searle, J. Wang, S. Kuratani, Y. Yin, B. Aken, G. Zhang, N. Irie, The draft genomes of soft-shell turtle and green sea turtle yield insights into the development and evolution of the turtle-specific body plan. *Nat. Genet.* **45**, 701–706 (2013). [Medline](doi:10.1038/ng.2615)

49. G. Ganapathy, J. T. Howard, J. M. Ward, J. Li, B. Li, Y. Li, Y. Xiong, Y. Zhang, S. Zhou, D. C. Schwartz, M. Schatz, R. Aboukhalil, O. Fedrigo, L. Bukovnik, T. Wang, G. Wray, I. Rasolonjatovo, R. Winer, J. R. Knight, S. Koren, W. C. Warren, G. Zhang, A. M. Phillippy, E. D. Jarvis, High-coverage sequencing and annotated assemblies of the budgerigar genome. *Gigascience* **3**, 11 (2014). [Medline](doi:10.1186/2047-217X-3-11)

50. S. Li, B. Li, C. Cheng, Z. Xiong, Q. Liu, J. Lai, H. V. Carey, Q. Zhang, H. Zheng, S. Wei, H. Zhang, L. Chang, S. Liu, S. Zhang, B. Yu, X. Zeng, Y. Hou, W. Nie, Y. Guo, T. Chen, J. Han, J. Wang, J. Wang, C. Chen, J. Liu, P. J. Stambrook, M. Xu, G. Zhang, M. T. P. Gilbert, H. Yang, E. D. Jarvis, J. Yu, J. Yan, Genomic signatures of near-extinction and rebirth of the crested ibis and other endangered bird species. *Genome Biol.* 10.1186/s13059-014-0557-1 (2014).

51. C. Li, Y. Zhang, J. Li, L. Kong, H. Hu, H. Pan, L. Xu, Y. Deng, Q. Li, L. Jin, H. Yu, Y. Chen, B. Liu, L. Yang, S. Liu, Y. Zhang, Y. Lang, J. Xia, W. He, Q. Shi, S. Subramanian, C. D. Millar, S. Meader, C. M. Rands, M. K Fujita, M. J. Greenwold, T. A. Castoe, D. D. Pollock, W. Gu, K. Nam, H. Ellegren, S. Y. W. Ho, D. W. Burt, C. P. Ponting, E. D. Jarvis, M. Thomas, P. Gilbert, H. Yang, J. Wang, D. M. Lambert, J. Wang,

G. Zhang, Two Antarctic penguin genomes reveal insights into their evolutionary history and molecular changes related to the Antarctic environment. *GigaScience* **3**, 27 (2014).

52. R. E. Green, E. L. Braun, J. Armstrong, D. Earl, N. Nguyen, G. Hickey, M. W. Vandewege, J. A. St John, S. Capella-Gutiérrez, T. A. Castoe, C. Kern, M. K. Fujita, J. C. Opazo, J. Jurka, K. K. Kojima, J. Caballero, R. M. Hubley, A. F. Smit, R. N. Platt, C. A. Lavoie, M. P. Ramakodi, J. W. Finger Jr., A. Suh, S. R. Isberg, L. Miles, A. Y. Chong, W. Jaratlerdsiri, J. Gongora, C. Moran, A. Iriarte, J. McCormack, S. C. Burgess, S. V. Edwards, E. Lyons, C. Williams, M. Breen, J. T. Howard, C. R. Gresham, D. G. Peterson, J. Schmitz, D. D. Pollock, D. Haussler, E. W. Triplett, G. Zhang, N. Irie, E. D. Jarvis, C. A. Brochu, C. J. Schmidt, F. M. McCarthy, B. C. Faircloth, F. G. Hoffmann, T. C. Glenn, T. Gabaldón, B. Paten, D. A. Ray, Three crocodilian genomes reveal ancestral patterns of evolution among archosaurs. *Science* **346**, 1254449 (2014).

53. K. Liu, S. Raghavan, S. Nelesen, C. R. Linder, T. Warnow, Rapid and accurate large-scale coestimation of sequence alignments and phylogenetic trees. *Science* **324**, 1561–1564 (2009). Medline doi:10.1126/science.1171243

54. K. Liu, T. J. Warnow, M. T. Holder, S. M. Nelesen, J. Yu, A. P. Stamatakis, C. R. Linder, SATe-II: Very fast and accurate simultaneous estimation of multiple sequence alignments and phylogenetic trees. *Syst. Biol.* **61**, 90–106 (2012). Medline doi:10.1093/sysbio/syr095

55. A. Stamatakis, A. J. Aberer, C. Goll, S. A. Smith, S. A. Berger, F. Izquierdo-Carrasco, RAxML-Light: A tool for computing terabyte phylogenies. *Bioinformatics* **28**, 2064–2066 (2012). Medline doi:10.1093/bioinformatics/bts309

56. J. Zhang, A. Stamatakis, "The multi-processor scheduling problem in phylogenetics," *IEEE 26th International Parallel and Distributed Processing Symposium*, Shanghai, 21 to 25 May 2012, pp. 691–698; 10.1109/IPDPSW.2012.86.

57. A. Stamatakis, A. J. Aberer, "Novel parallelization schemes for large-scale likelihood-based phylogenetic inference," *IEEE 27th International Symposium on Parallel and Distributed Processing*, Boston, 20 to 24 May 2013, pp. 1195–1204; 10.1109/IPDPS.2013.70 .

58. S. Mirarab, M. S. Bayzid, B. Boussau, T. Warnow, Statistical binning enables an accurate coalescent-based estimation of the avian tree. *Science* **346**, 1250463 (2014).

59. T. Yuri, R. T. Kimball, J. Harshman, R. C. Bowie, M. J. Braun, J. L. Chojnowski, K. L. Han, S. J. Hackett, C. J. Huddleston, W. S. Moore, S. Reddy, F. H. Sheldon, D. W. Steadman, C. C. Witt, E. L. Braun, Parsimony and model-based analyses of indels in avian nuclear genes reveal congruent and incongruent phylogenetic signals. *Biology (Basel)* **2**, 419–444 (2013). Medline doi:10.3390/biology2010419

60. P. G. Ericson, Evolution of terrestrial birds in three continents: Biogeography and parallel radiations. *J. Biogeogr.* **39**, 813–824 (2012). doi:10.1111/j.1365-2699.2011.02650.x

61. J. Kim, Slicing hyperdimensional oranges: The geometry of phylogenetic estimation. *Mol. Phylogenet. Evol.* **17**, 58–75 (2000). Medline doi:10.1006/mpev.2000.0816

62. W. P. Maddison, Gene trees in species trees. *Syst. Biol.* **46**, 523–536 (1997). doi:10.1093/sysbio/46.3.523

63. N. A. Rosenberg, Discordance of species trees with their most likely gene trees: A unifying principle. *Mol. Biol. Evol.* **30**, 2709–2713 (2013). Medline doi:10.1093/molbev/mst160

64. J. H. Degnan, N. A. Rosenberg, Gene tree discordance, phylogenetic inference and the multispecies coalescent. *Trends Ecol. Evol.* **24**, 332–340 (2009). Medline doi:10.1016/j.tree.2009.01.009

65. A. W. Edwards, Statistical methods for evolutionary trees. *Genetics* **183**, 5–12 (2009). Medline doi:10.1534/genetics.109.107847

66. M. S. Bayzid, T. Warnow, Naive binning improves phylogenomic analyses. *Bioinformatics* **29**, 2277–2284 (2013). Medline doi:10.1093/bioinformatics/btt394

67. L. Liu, L. Yu, S. V. Edwards, A maximum pseudo-likelihood approach for estimating species trees under the coalescent model. *BMC Evol. Biol.* **10**, 302 (2010). Medline doi:10.1186/1471-2148-10-302

68. J. Huerta-Cepas, S. Capella-Gutiérrez, L. P. Pryszcz, M. Marcet-Houben, T. Gabaldón, PhylomeDB v4: Zooming into the plurality of evolutionary histories of a genome. *Nucleic Acids Res.* **42**, D897–D902 (2014). Medline doi:10.1093/nar/gkt1177

69. M. P. Simmons, H. Ochoterena, Gaps as characters in sequence-based phylogenetic analyses. *Syst. Biol.* **49**, 369–381 (2000). Medline doi:10.1093/sysbio/49.2.369

70. J. Felsenstein, *Inferring Phylogenies* (Sinauer Associates, Sunderland, MA, 2004).

71. J. C. Avise, T. J. Robinson, Hemiplasy: A new term in the lexicon of phylogenetics. *Syst. Biol.* **57**, 503–507 (2008). Medline doi:10.1080/10635150802164587

72. D. A. Ray, J. Xing, A. H. Salem, M. A. Batzer, SINEs of a nearly perfect character. *Syst. Biol.* **55**, 928–935 (2006). Medline doi:10.1080/10635150600865419

73. K. L. Han, E. L. Braun, R. T. Kimball, S. Reddy, R. C. Bowie, M. J. Braun, J. L. Chojnowski, S. J. Hackett, J. Harshman, C. J. Huddleston, B. D. Marks, K. J. Miglia, W. S. Moore, F. H. Sheldon, D. W. Steadman, C. C. Witt, T. Yuri, Are transposable element insertions homoplasy free?: An examination using the avian tree of life. *Syst. Biol.* **60**, 375–386 (2011). Medline doi:10.1093/sysbio/syq100

74. E. M. Lemmon, A. R. Lemmon, High-throughput genomic data in systematics and phylogenetics. *Annu. Rev. Ecol. Evol.* **44**, 99–121 (2013). doi:10.1146/annurev-ecolsys-110512-135822

75. C. C. Weber, B. Boussau, J. Romiguier, E. D. Jarvis, H. Ellegren, Evidence for GC-biased gene conversion as a driver of between-lineage differences in avian base composition. *Genome Biol.* **15**, 549 (2014).

76. C. C. Weber, B. Nabholz, J. Romiguier, H. Ellegren, Kr/Kc but not dN/dS correlates positively with body mass in birds, raising implications for inferring lineage-specific selection. *Genome Biol.* **15**, 542 (2014).

77. M. dos Reis, Z. Yang, Approximate likelihood calculation on a phylogeny for Bayesian estimation of divergence times. *Mol. Biol. Evol.* **28**, 2161–2172 (2011). Medline doi:10.1093/molbev/msr045

78. J. V. Smith, E. L. Braun, R. T. Kimball, Ratite nonmonophyly: Independent evidence from 40 novel loci. *Syst. Biol.* **62**, 35–49 (2013). Medline doi:10.1093/sysbio/sys067

79. P. Houde, Ostriche ancestors found in the Northern Hemisphere suggest new hypothesis of ratite origins. *Nature* **324**, 563–565 (1986). doi:10.1038/324563a0

80. G. Mayr, The age of the crown group of passerine birds and its evolutionary significance - molecular calibrations versus the fossil record. *Syst. Biodivers.* **11**, 7–13 (2013). doi:10.1080/14772000.2013.765521

81. J. A. Clarke, C. P. Tambussi, J. I. Noriega, G. M. Erickson, R. A. Ketcham, Definitive fossil evidence for the extant avian radiation in the Cretaceous. *Nature* **433**, 305–308 (2005). Medline doi:10.1038/nature03150

82. L. Salichos, A. Rokas, Inferring ancient divergences requires genes with strong phylogenetic signals. *Nature* **497**, 327–331 (2013). Medline doi:10.1038/nature12130

83. L. Salichos, A. Stamatakis, A. Rokas, Novel information theory-based measures for quantifying incongruence among phylogenetic trees. *Mol. Biol. Evol.* **31**, 1261–1271 (2014). Medline doi:10.1093/molbev/msu061

84. A. D. Twyford, R. A. Ennos, Next-generation hybridization and introgression. *Heredity (Edinb.)* **108**, 179–189 (2012). Medline doi:10.1038/hdy.2011.68

85. L. Duret, N. Galtier, Biased gene conversion and the evolution of mammalian genomic landscapes. *Annu. Rev. Genomics Hum. Genet.* **10**, 285–311 (2009). Medline doi:10.1146/annurev-genom-082908-150001

86. C. F. Mugal, P. F. Arndt, H. Ellegren, Twisted signatures of GC-biased gene conversion embedded in an evolutionary stable karyotype. *Mol. Biol. Evol.* **30**, 1700–1712 (2013). Medline doi:10.1093/molbev/mst067

87. J. Romiguier, V. Ranwez, E. J. Douzery, N. Galtier, Contrasting GC-content dynamics across 33 mammalian genomes: Relationship with life-history traits and chromosome sizes. *Genome Res.* **20**, 1001–1009 (2010). Medline doi:10.1101/gr.104372.109

88. M. K. Rudd, C. Friedman, S. S. Parghi, E. V. Linardopoulou, L. Hsu, B. J. Trask, Elevated rates of sister chromatid exchange at chromosome ends. *PLOS Genet.* **3**, e32 (2007). Medline doi:10.1371/journal.pgen.0030032

89. J. Parker, G. Tsagkogeorga, J. A. Cotton, Y. Liu, P. Provero, E. Stupka, S. J. Rossiter, Genome-wide signatures of convergent evolution in echolocating mammals. *Nature* **502**, 228–231 (2013). Medline doi:10.1038/nature12511

90. Proteome-wide analyses among the 48 bird genomes were conducted in (*44*), where it was found that vocal-learning bird species have convergent amino acid changes in a set of genes expressed in the song-learning nuclei.

91. F. Nottebohm, The origins of vocal learning. *Am. Nat.* **106**, 116–140 (1972). doi:10.1086/282756

92. V. Saranathan, D. Hamilton, G. V. Powell, D. E. Kroodsma, R. O. Prum, Genetic evidence supports song learning in the three-wattled bellbird *Procnias tricarunculata* (Cotingidae). *Mol. Ecol.* **16**, 3689–3702 (2007). [Medline](#) [doi:10.1111/j.1365-294X.2007.03415.x](#)

93. D. Kroodsma, D. Hamilton, J. E. Sánchez, B. E. Byers, H. Fandiño-Mariño, D. W. Stemple, J. M. Trainer, G. V. N. Powell, Behavioral evidence for song learning in the suboscine bellbirds (*Procnias* spp.; Cotingidae). *Wilson J. Ornithol.* **125**, 1–14 (2013). [doi:10.1676/12-033.1](#)

94. K. H. Redford, G. Peters, Notes on the biology and song of the red-legged seriema (*Cariama crostata*). *J. Field Ornithol.* **57**, 261–269 (1986).

95. H. M. F. Alvarenga, E. Hofling, Systematic revision of the Phorusrhacidae (Aves: Ralliformes). *Papeis Avulsos Zool.* **43**, 55–91 (2003).

96. G. Mayr, "Cariamae (Seriemas and Allies)" in *Paleogene Fossil Birds* (Springer, Berlin, Heidelberg, 2009), pp. 139–152.

97. P. Houde, S. L. Olson, "A radiation of coly-like birds from the Eocene of North America (Aves: Sandcoleiformes, new order)," in *Natural History Museum of Los Angeles County Science Series* (Natural History Museum of Los Angeles County, Los Angeles, 1992), vol. 36, pp. 137–160.

98. A. D. Forbes-Watson, Observations at a nest of the cuckoo-roller *Leptosomus discolor*. *Ibis* **109**, 425–430 (1967). [doi:10.1111/j.1474-919X.1967.tb04015.x](#)

99. S. L. Olson, A. Feduccia, Relationships and evolution of flamingos (Aves: Phoenicopteridae). *Smithson. Contrib. Zool.* **316**, 1–73 (1980).

100. M. A. O'Leary, J. I. Bloch, J. J. Flynn, T. J. Gaudin, A. Giallombardo, N. P. Giannini, S. L. Goldberg, B. P. Kraatz, Z. X. Luo, J. Meng, X. Ni, M. J. Novacek, F. A. Perini, Z. S. Randall, G. W. Rougier, E. J. Sargis, M. T. Silcox, N. B. Simmons, M. Spaulding, P. M. Velazco, M. Weksler, J. R. Wible, A. L. Cirranello, The placental mammal ancestor and the post-K-Pg radiation of placentals. *Science* **339**, 662–667 (2013). [Medline](#) [doi:10.1126/science.1229237](#)

101. M. dos Reis, P. C. Donoghue, Z. Yang, Neither phylogenomic nor palaeontological data support a Palaeogene origin of placental mammals. *Biol. Lett.* **10**, 20131003 (2014). [Medline](#) [doi:10.1098/rsbl.2013.1003](#)

102. M. J. Benton, The origins of modern biodiversity on land. *Philos. Trans. R. Soc. Lond. B Biol. Sci.* **365**, 3667–3679 (2010). [Medline](#) [doi:10.1098/rstb.2010.0269](#)

103. F. Gill, M. Wright, *Birds of the World: Recommended English Names* (Princeton Univ. Press, Princeton, NJ, 2006).

104. Q. Zhou, J. Zhang, D. Bachtrog, N. An, Q. Huang, E. D. Jarvis, M. T. P. Gilbert, G. Zhang, Complex evolutionary trajectories of sex chromosomes across bird taxa. *Science* **346**, 1246338 (2014).

105. A. Künstner, J. B. Wolf, N. Backström, O. Whitney, C. N. Balakrishnan, L. Day, S. V. Edwards, D. E. Janes, B. A. Schlinger, R. K. Wilson, E. D. Jarvis, W. C. Warren, H.

Ellegren, Comparative genomics based on massive parallel transcriptome sequencing reveals patterns of substitution and selection across 10 bird species. *Mol. Ecol.* **19** (suppl. 1), 266–276 (2010). Medline doi:10.1111/j.1365-294X.2009.04487.x

106. L. Almasy, J. Blangero, Multipoint quantitative-trait linkage analysis in general pedigrees. *Am. J. Hum. Genet.* **62**, 1198–1211 (1998). Medline doi:10.1086/301844

107. S. Stephen, M. Pheasant, I. V. Makunin, J. S. Mattick, Large-scale appearance of ultraconserved elements in tetrapod genomes and slowdown of the molecular clock. *Mol. Biol. Evol.* **25**, 402–408 (2008). Medline doi:10.1093/molbev/msm268

108. B. C. Faircloth, J. E. McCormack, N. G. Crawford, M. G. Harvey, R. T. Brumfield, T. C. Glenn, Ultraconserved elements anchor thousands of genetic markers spanning multiple evolutionary timescales. *Syst. Biol.* **61**, 717–726 (2012). Medline doi:10.1093/sysbio/sys004

109. R. S. Harris, "Improved pairwise alignment of genomic DNA," thesis, The Pennsylvania State University, (2007).

110. J. E. McCormack, B. C. Faircloth, N. G. Crawford, P. A. Gowaty, R. T. Brumfield, T. C. Glenn, Ultraconserved elements are novel phylogenomic markers that resolve placental mammal phylogeny when combined with species-tree analysis. *Genome Res.* **22**, 746–754 (2012). Medline doi:10.1101/gr.125864.111

111. S. Dimitrieva, P. Bucher, UCNEbase—a database of ultraconserved non-coding elements and genomic regulatory blocks. *Nucleic Acids Res.* **41**, D101–D109 (2013). Medline doi:10.1093/nar/gks1092

112. H. Ellegren, The avian genome uncovered. *Trends Ecol. Evol.* **20**, 180–186 (2005). Medline doi:10.1016/j.tree.2005.01.015

113. A. R. Quinlan, I. M. Hall, BEDTools: A flexible suite of utilities for comparing genomic features. *Bioinformatics* **26**, 841–842 (2010). Medline doi:10.1093/bioinformatics/btq033

114. K. D. Pruitt, T. Tatusova, G. R. Brown, D. R. Maglott, NCBI Reference Sequences (RefSeq): Current status, new features and genome annotation policy. *Nucleic Acids Res.* **40**, D130–D135 (2012). Medline doi:10.1093/nar/gkr1079

115. W. J. Kent, BLAT—The BLAST-like alignment tool. *Genome Res.* **12**, 656–664 (2002). Medline.

116. K. Katoh, K. Kuma, H. Toh, T. Miyata, MAFFT version 5: Improvement in accuracy of multiple sequence alignment. *Nucleic Acids Res.* **33**, 511–518 (2005). Medline doi:10.1093/nar/gki198

117. A. Löytynoja, N. Goldman, An algorithm for progressive multiple alignment of sequences with insertions. *Proc. Natl. Acad. Sci. U.S.A.* **102**, 10557–10562 (2005). Medline doi:10.1073/pnas.0409137102

118. R. C. Edgar, MUSCLE: A multiple sequence alignment method with reduced time and space complexity. *BMC Bioinformatics* **5**, 113 (2004). Medline doi:10.1186/1471-2105-5-113

119. T. J. Wheeler, J. D. Kececioglu, Multiple alignment by aligning alignments. *Bioinformatics* **23**, i559–i568 (2007). Medline doi:10.1093/bioinformatics/btm226

120. J. Castresana, Selection of conserved blocks from multiple alignments for their use in phylogenetic analysis. *Mol. Biol. Evol.* **17**, 540–552 (2000). Medline doi:10.1093/oxfordjournals.molbev.a026334

121. S. Henikoff, J. G. Henikoff, Amino acid substitution matrices from protein blocks. *Proc. Natl. Acad. Sci. U.S.A.* **89**, 10915–10919 (1992). Medline doi:10.1073/pnas.89.22.10915

122. R Core Team, R: A language and environment for statistical computing (R Foundation for Statistical Computing, Vienna, 2013); http://www.r-project.org/.

123. M. Blanchette, W. J. Kent, C. Riemer, L. Elnitski, A. F. Smit, K. M. Roskin, R. Baertsch, K. Rosenbloom, H. Clawson, E. D. Green, D. Haussler, W. Miller, Aligning multiple genomic sequences with the threaded blockset aligner. *Genome Res.* **14**, 708–715 (2004). Medline doi:10.1101/gr.1933104

124. D. Bryant, *Bioconsensus: DIMACS Working Group Meetings on Bioconsensus* (American Mathematical Society, Providence, RI, 2003).

125. A. Stamatakis, RAxML-VI-HPC: Maximum likelihood-based phylogenetic analyses with thousands of taxa and mixed models. *Bioinformatics* **22**, 2688–2690 (2006). Medline doi:10.1093/bioinformatics/btl446

126. Z. Yang, Among-site rate variation and its impact on phylogenetic analyses. *Trends Ecol. Evol.* **11**, 367–372 (1996). Medline doi:10.1016/0169-5347(96)10041-0

127. A. Stamatakis, "Phylogenetic models of rate heterogeneity: A high performance computing perspective," *20th IEEE International Parallel and Distributed Processing Symposium*, Rhodes Island, Greece, 25 to 29 April 2006, p. 278.

128. N. D. Pattengale, M. Alipour, O. R. Bininda-Emonds, B. M. Moret, A. Stamatakis, How many bootstrap replicates are necessary? *J. Comput. Biol.* **17**, 337–354 (2010). Medline doi:10.1089/cmb.2009.0179

129. S. Tavaré, Some probabilistic and statistical problems in the analysis of DNA sequences. *Lect. Math Life Sci.* **17**, 57–86 (1986).

130. R. Lanfear, B. Calcott, S. Y. Ho, S. Guindon, PartitionFinder: Combined selection of partitioning schemes and substitution models for phylogenetic analyses. *Mol. Biol. Evol.* **29**, 1695–1701 (2012). Medline doi:10.1093/molbev/mss020

131. D. T. Jones, W. R. Taylor, J. M. Thornton, The rapid generation of mutation data matrices from protein sequences. *Comput. Appl. Biosci.* **8**, 275–282 (1992). Medline

132. D. F. Robinson, L. R. Foulds, Comparison of phylogenetic trees. *Math. Biosci.* **53**, 131–147 (1981). doi:10.1016/0025-5564(81)90043-2

133. J. Gatesy, R. H. Baker, Hidden likelihood support in genomic data: Can forty-five wrongs make a right? *Syst. Biol.* **54**, 483–492 (2005). Medline doi:10.1080/10635150590945368

134. L. S. Kubatko, J. H. Degnan, Inconsistency of phylogenetic estimates from concatenated data under coalescence. *Syst. Biol.* **56**, 17–24 (2007). Medline doi:10.1080/10635150601146041

135. T. K. Seo, Calculating bootstrap probabilities of phylogeny using multilocus sequence data. *Mol. Biol. Evol.* **25**, 960–971 (2008). Medline doi:10.1093/molbev/msn043

136. J. Sukumaran, M. T. Holder, DendroPy: A Python library for phylogenetic computing. *Bioinformatics* **26**, 1569–1571 (2010). Medline doi:10.1093/bioinformatics/btq228

137. F. K. Barker, G. F. Barrowclough, J. G. Groth, A phylogenetic hypothesis for passerine birds: Taxonomic and biogeographic implications of an analysis of nuclear DNA sequence data. *Proc. Biol. Sci.* **269**, 295–308 (2002). Medline doi:10.1098/rspb.2001.1883

138. F. K. Barker, A. Cibois, P. Schikler, J. Feinstein, J. Cracraft, Phylogeny and diversification of the largest avian radiation. *Proc. Natl. Acad. Sci. U.S.A.* **101**, 11040–11045 (2004). Medline doi:10.1073/pnas.0401892101

139. F. K. Barker, K. J. Burns, J. Klicka, S. M. Lanyon, I. J. Lovette, Going to extremes: Contrasting rates of diversification in a recent radiation of new world passerine birds. *Syst. Biol.* **62**, 298–320 (2013). Medline doi:10.1093/sysbio/sys094

140. C. Pitra, D. Lieckfeldt, S. Frahnert, J. Fickel, Phylogenetic relationships and ancestral areas of the bustards (Gruiformes: Otididae), inferred from mitochondrial DNA and nuclear intron sequences. *Mol. Phylogenet. Evol.* **23**, 63–74 (2002). Medline doi:10.1006/mpev.2001.1078

141. M. G. Fain, P. Houde, Multilocus perspectives on the monophyly and phylogeny of the order Charadriiformes (Aves). *BMC Evol. Biol.* **7**, 35 (2007). Medline doi:10.1186/1471-2148-7-35

142. J. Huerta-Cepas, S. Capella-Gutierrez, L. P. Pryszcz, I. Denisov, D. Kormes, M. Marcet-Houben, T. Gabaldón, PhylomeDB v3.0: An expanding repository of genome-wide collections of trees, alignments and phylogeny-based orthology and paralogy predictions. *Nucleic Acids Res.* **39**, D556–D560 (2011). Medline doi:10.1093/nar/gkq1109

143. T. F. Smith, M. S. Waterman, Identification of common molecular subsequences. *J. Mol. Biol.* **147**, 195–197 (1981). Medline doi:10.1016/0022-2836(81)90087-5

144. K. Katoh, H. Toh, Recent developments in the MAFFT multiple sequence alignment program. *Brief. Bioinform.* **9**, 286–298 (2008). Medline doi:10.1093/bib/bbn013

145. T. Lassmann, O. Frings, E. L. Sonnhammer, Kalign2: High-performance multiple alignment of protein and nucleotide sequences allowing external features. *Nucleic Acids Res.* **37**, 858–865 (2009). Medline doi:10.1093/nar/gkn1006

146. G. Landan, D. Graur, Heads or tails: A simple reliability check for multiple sequence alignments. *Mol. Biol. Evol.* **24**, 1380–1383 (2007). Medline doi:10.1093/molbev/msm060

147. I. M. Wallace, O. O'Sullivan, D. G. Higgins, C. Notredame, M-Coffee: Combining multiple sequence alignment methods with T-Coffee. *Nucleic Acids Res.* **34**, 1692–1699 (2006). Medline doi:10.1093/nar/gkl091

148. S. Capella-Gutiérrez, J. M. Silla-Martínez, T. Gabaldón, trimAl: A tool for automated alignment trimming in large-scale phylogenetic analyses. *Bioinformatics* **25**, 1972–1973 (2009). Medline doi:10.1093/bioinformatics/btp348

149. O. Gascuel, BIONJ: An improved version of the NJ algorithm based on a simple model of sequence data. *Mol. Biol. Evol.* **14**, 685–695 (1997). Medline doi:10.1093/oxfordjournals.molbev.a025808

150. S. Guindon, J. F. Dufayard, V. Lefort, M. Anisimova, W. Hordijk, O. Gascuel, New algorithms and methods to estimate maximum-likelihood phylogenies: Assessing the performance of PhyML 3.0. *Syst. Biol.* **59**, 307–321 (2010). Medline doi:10.1093/sysbio/syq010

151. H. Akaike, "Information theory and extension of the maximum likelihood principle," in *Proceedings of the 2nd International Symposium on Information Theory*, B. N. Petrov, F. Csaki, Eds. (Akadémiai Kiadó, Budapest, 1973), pp. 267–281.

152. M. Gil, M. S. Zanetti, S. Zoller, M. Anisimova, CodonPhyML: Fast maximum likelihood phylogeny estimation under codon substitution models. *Mol. Biol. Evol.* **30**, 1270–1280 (2013). Medline doi:10.1093/molbev/mst034

153. J. Huerta-Cepas, H. Dopazo, J. Dopazo, T. Gabaldón, The human phylome. *Genome Biol.* **8**, R109 (2007). Medline

154. J. Huerta-Cepas, J. Dopazo, T. Gabaldón, ETE: A python Environment for Tree Exploration. *BMC Bioinformatics* **11**, 24 (2010). Medline doi:10.1186/1471-2105-11-24

155. L. P. Pryszcz, J. Huerta-Cepas, T. Gabaldón, MetaPhOrs: Orthology and paralogy predictions from multiple phylogenetic evidence using a consistency-based confidence score. *Nucleic Acids Res.* **39**, e32 (2011). Medline doi:10.1093/nar/gkq953

156. M. Marcet-Houben, T. Gabaldón, TreeKO: A duplication-aware algorithm for the comparison of phylogenetic trees. *Nucleic Acids Res.* **39**, e66 (2011). Medline doi:10.1093/nar/gkr087

157. D. P. Liitle, 2xread: A simple indel coding tool (2005); www.nybg.org/files/scientists/2xread.html.

158. N. D. Young, J. Healy, GapCoder automates the use of indel characters in phylogenetic analysis. *BMC Bioinformatics* **4**, 6 (2003). Medline doi:10.1186/1471-2105-4-6

159. P. A. Goloboff, J. S. Farris, K. C. Nixon, TNT, a free program for phylogenetic analysis. *Cladistics* **24**, 774–786 (2008). doi:10.1111/j.1096-0031.2008.00217.x

160. D. Swofford, *PAUP*: Phylogenetic Analysis Using Parsimony (*and Other Methods)* (Sinauer Associates, Sunderland, MA, 1999).

161. D. R. Maddison, W. P. Maddison, MacClade 4: Analysis of phylogeny and character evolution (2005); http://macclade.org.

162. J. O. Kriegs, G. Churakov, M. Kiefmann, U. Jordan, J. Brosius, J. Schmitz, Retroposed elements as archives for the evolutionary history of placental mammals. *PLOS Biol.* **4**, e91 (2006). Medline doi:10.1371/journal.pbio.0040091

163. M. A. Nilsson, G. Churakov, M. Sommer, N. V. Tran, A. Zemann, J. Brosius, J. Schmitz, Tracking marsupial evolution using archaic genomic retroposon insertions. *PLOS Biol.* **8**, e1000436 (2010). Medline doi:10.1371/journal.pbio.1000436

164. G. Churakov, J. O. Kriegs, R. Baertsch, A. Zemann, J. Brosius, J. Schmitz, Mosaic retroposon insertion patterns in placental mammals. *Genome Res.* **19**, 868–875 (2009). Medline doi:10.1101/gr.090647.108

165. H. Nishihara, S. Maruyama, N. Okada, Retroposon analysis and recent geological data suggest near-simultaneous divergence of the three superorders of mammals. *Proc. Natl. Acad. Sci. U.S.A.* **106**, 5235–5240 (2009). Medline doi:10.1073/pnas.0809297106

166. A. M. Shedlock, K. Takahashi, N. Okada, SINEs of speciation: Tracking lineages with retroposons. *Trends Ecol. Evol.* **19**, 545–553 (2004). Medline doi:10.1016/j.tree.2004.08.002

167. A. Suh, J. O. Kriegs, S. Donnellan, J. Brosius, J. Schmitz, A universal method for the study of CR1 retroposons in nonmodel bird genomes. *Mol. Biol. Evol.* **29**, 2899–2903 (2012). Medline doi:10.1093/molbev/mss124

168. A. Suh, J. O. Kriegs, J. Brosius, J. Schmitz, Retroposon insertions and the chronology of avian sex chromosome evolution. *Mol. Biol. Evol.* **28**, 2993–2997 (2011). Medline doi:10.1093/molbev/msr147

169. J. O. Kriegs, A. Matzke, G. Churakov, A. Kuritzin, G. Mayr, J. Brosius, J. Schmitz, Waves of genomic hitchhikers shed light on the evolution of gamebirds (Aves: Galliformes). *BMC Evol. Biol.* **7**, 190 (2007). Medline doi:10.1186/1471-2148-7-190

170. S. F. Altschul, W. Gish, W. Miller, E. W. Myers, D. J. Lipman, Basic local alignment search tool. *J. Mol. Biol.* **215**, 403–410 (1990). Medline doi:10.1016/S0022-2836(05)80360-2

171. C. I. Wu, W. H. Li, Evidence for higher rates of nucleotide substitution in rodents than in man. *Proc. Natl. Acad. Sci. U.S.A.* **82**, 1741–1745 (1985). Medline doi:10.1073/pnas.82.6.1741

172. A. P. Martin, S. R. Palumbi, Body size, metabolic rate, generation time, and the molecular clock. *Proc. Natl. Acad. Sci. U.S.A.* **90**, 4087–4091 (1993). Medline doi:10.1073/pnas.90.9.4087

173. J. F. Gillooly, A. P. Allen, G. B. West, J. H. Brown, The rate of DNA evolution: Effects of body size and temperature on the molecular clock. *Proc. Natl. Acad. Sci. U.S.A.* **102**, 140–145 (2005). Medline doi:10.1073/pnas.0407735101

174. J. B. J. Dunning, *CRC Handbook of Avian Body Masses* (CRC Press, Boca Raton, FL, ed. 2, 2007).

175. J. Felsenstein, Phylogenies and the comparative method. *Am. Nat.* **125**, 1–15 (1985). doi:10.1086/284325

176. J. Felsenstein, PHYLIP - Phylogeny Inference Package (version 3.2). *Cladistics* **5**, 164–166 (1989).

177. F. Ababneh, L. S. Jermiin, C. Ma, J. Robinson, Matched-pairs tests of homogeneity with applications to homologous nucleotide sequences. *Bioinformatics* **22**, 1225–1231 (2006). Medline doi:10.1093/bioinformatics/btl064

178. J. Dutheil, B. Boussau, Non-homogeneous models of sequence evolution in the Bio++ suite of libraries and programs. *BMC Evol. Biol.* **8**, 255 (2008). Medline doi:10.1186/1471-2148-8-255

179. A. J. Drummond, S. Y. Ho, M. J. Phillips, A. Rambaut, Relaxed phylogenetics and dating with confidence. *PLOS Biol.* **4**, e88 (2006). Medline doi:10.1371/journal.pbio.0040088

180. A. J. Drummond, A. Rambaut, BEAST: Bayesian evolutionary analysis by sampling trees. *BMC Evol. Biol.* **7**, 214 (2007). Medline doi:10.1186/1471-2148-7-214

181. A. J. Drummond, M. A. Suchard, D. Xie, A. Rambaut, Bayesian phylogenetics with BEAUti and the BEAST 1.7. *Mol. Biol. Evol.* **29**, 1969–1973 (2012). Medline doi:10.1093/molbev/mss075

182. S. Y. Ho, The changing face of the molecular evolutionary clock. *Trends Ecol. Evol.* **29**, 496–503 (2014). Medline doi:10.1016/j.tree.2014.07.004

183. M. J. Benton, P. C. J. Donoghue, R. J. Asher, in *The Timetree of Life*, S. B. Hedges, S. Kumar, Eds. (Oxford Univ. Press, New York, 2009), pp. 35–86.

184. P. Houde, *Paleognathous Birds from the Early Tertiary of the Northern Hemisphere* (Publications of the Nuttall Ornithological Club no. 22, Harvard Univ. Nuttall Ornithological Society, Cambridge, MA, 1988).

185. R. Secord, *The Tiffanian Land-Mammal Age (Middle and Late Paleocene) in the Northern Bighorn Basin, Wyoming* (Papers on Paleontology, Univ. of Michigan, Ann Arbor, MI, 2008), vol. 35.

186. D. C. Parris, S. Hope, in *Proceedings of the 5th Symposium of the Society of Avian Paleontology and Evolution*, Z. Zhou, F. Zhang, Eds. (Science Press, Beijing, 2002), pp. 113–124.

187. C. Mourer-Chauvire, B. Senut, M. Pickford, P. Mein, Le plus ancien représentant du genre Struthio (Aves, Struthionidae), Struthio coppensi n. sp., du Miocène inférieur de Namibie. *C. R. Acad. Sci. Paris* **322**, 325–332 (1996).

188. S. Bertelli, L. M. Chiappe, Earliest tinamous (Aves: Palaeognathae) from the Miocene of Argentina and their phylogenetic position. *Contrib. Sci.* **502**, 1–20 (2005).

189. J. I. Noriega, C. P. Tambussi, A Late Cretaceous Presbyornithidae (Aves: Anseriformes) from Vega Island, Antarctic Peninsula: paleo-biogeographic implications. *Ameghiniana* **32**, 57–61 (1995).

190. S. L. Olson, The anseriform relationships of *Anatalavis* Olson and Parris (Anseranatidae), with a new species from the Lower Eocene London Clay. *Smithson. Contrib. Paleobiol.* **89**, 231–244 (1999).

191. C. R. Eastman, New fossil bird and fish remains from the Middle Eocene of Wyoming. *Geolog. Mag. (Decade 4)* **7**, 54-58 (1900).

192. G. T. Dyke, The phylogenetic position of *Gallinuloides* Eastman (Aves: Galliformes) from the Tertiary of North America. *Zootaxa* **199**, 1–10 (2003).

193. G. Mayr, I. Weidig, The early Eocene bird *Gallinuloides wyomingensis* – A stem group representative of Galliformes. *Acta Palaeontol. Pol.* **49**, 211–217 (2004).

194. A. Milne-Edwards, *Researches Anatomiques et Paléontologiques pour Server a l'Histoire des Oiseaux Fossiles de la France* (Masson, Paris, 1867–1871).

195. C. Mourer-Chauviré, Les gangas (Aves, Columbiformes, Pteroclidae) du Paléogène et du Miocène inférieur de France. *Palaeovertebrata* **22**, 73–98 (1993).

196. C. Mourer-Chauviré, Un ganga primitif (Aves, Columbiformes, Pteroclidae) de très grande taille dans le Paléogène des Phosphorites du Quercy (France). *C. R. Acad. Sci. Paris* **314**, 229–235 (1992).

197. J. J. Becker, P. Brodkorb, "An early Miocene ground-dove (Aves: Columbidae) from Florida," in *Natural History Museum of Los Angeles County Science Series* (Natural History Museum of Los Angeles County, Los Angeles, CA, 1992), vol. 36, pp. 189–193.

198. T. H. Worthy, S. J. Hand, J. P. Worthy, A. J. D. Tennyson, R. P. Scofield, A large fruit pigeon (Columbidae) from the early Miocene of New Zealand. *Auk* **126**, 649–656 (2009). doi:10.1525/auk.2009.08244

199. G. Mayr, R. Smith, Avian remains from the lowermost Oligocene of Hoogbutsel (Belgium). *Bulletin de l'Institut Royal des Sciences Naturelles de Belgique* **72**, 139–150 (2002).

200. A. Milne-Edwards, Mémoire sur la distribution géologique des oiseaux fossiles et description de quelques espèces nouvelles. *Annales des Sciences Naturelles* **4**, 132–176 (1863).

201. P. Švec, Two new species of diving birds from the lower Miocene of Czechoslovakia. *Časopis pro Mineralogii a Geologii* **27**, 243–260 (1982).

202. P. Gervais, *Zoologie et Paléontologie Françaises (Animaux Vertébrés): Ou Nouvelles Recherches sur les Animaux Vivants et Fossiles de la France* (Arthus Bertrand, Paris, ed. 1, 1852).

203. C. J. O. Harrison, C. A. Walker, Cranial material of Oligocene and Miocene flamingos: With a description of a new species from Africa. *Bull. Br. Mus. (Nat. Hist.)* **27**, 305–312 (1976).

204. G. Mayr, R. Smith, Ducks, rails, and limicoline waders (Aves: Anseriformes, Gruiformes, Charadriiformes) from the Lowermost Oligocene of Belgium. *Geobios* **34**, 547–561 (2001). doi:10.1016/S0016-6995(01)80069-3

205. G. Mayr, A chicken-sized crane precursor from the early Oligocene of France. *Naturwissenschaften* **92**, 389–393 (2005). Medline doi:10.1007/s00114-005-0007-8

206. A. Feduccia, M. R. Voorhies, "Crowned cranes (Gruidae: *Balearica*) in the Miocene of Nebraska," in *Natural History Museum of Los Angeles County Science Series* (Natural History Museum of Los Angeles County, Los Angeles, CA, 1992), vol. 36, pp. 239–248.

207. G. Mayr, H. Alvarenga, C. Mourer-Chauviré, Out of Africa: Fossils shed light on the origin of the hoatzin, an iconic Neotropic bird. *Naturwissenschaften* **98**, 961–966 (2011). Medline doi:10.1007/s00114-011-0849-1

208. D. T. Rasmussen, S. L. Olson, E. L. Simons, Fossil birds from the Oligocene Jebel Qatrani Formation, Fayum Province, Egypt. *Smithson. Contrib. Paleobiol.* **62**, 1–20 (1987). doi:10.5479/si.00810266.62.1

209. C. W. Andrews, On the remains of a new bird from the London Clay of Sheppey. *Proc. Zool. Soc. Lond.* **67**, 776–785 (1899). doi:10.1111/j.1469-7998.1899.tb06889.x

210. C. J. O. Harrison, C. A. Walker, A reappraisal of *Prophaethon shrubsolei* Andrews (Aves). *Bull. British Mus. (Nat. Hist.) Geol.* **27**, 1–30 (1976).

211. E. Bourdon, Osteological evidence for sister group relationship between pseudo-toothed birds (Aves: Odontopterygiformes) and waterfowls (Anseriformes). *Naturwissenschaften* **92**, 586–591 (2005). Medline doi:10.1007/s00114-005-0047-0

212. E. Bourdon, B. Bouya, M. Iarochene, Earliest African Neornithine bird: A new species of Prophaethontidae (Aves) from the Paleocene of Morocco. *J. Vertebr. Paleontol.* **25**, 157–170 (2005). doi:10.1671/0272-4634(2005)025[0157:EANBAN]2.0.CO;2

213. E. Bourdon, C. Mourer-Chauviré, M. Amaghzaz, B. Bouya, New specimens of *Lithoptila abdounensis* (Aves: Prophaethontidae) from the Lower Paleogene of Morocco. *J. Vertebr. Paleontol.* **28**, 751–761 (2008). doi:10.1671/0272-4634(2008)28[751:NSOLAA]2.0.CO;2

214. R. W. Storer, The fossil loon, *Colymboides minitus*. *Condor* **58**, 413–426 (1956). doi:10.2307/1365096

215. J. Cheneval, Les oiseaux aquatiques (Gaviiformes a Anseriformes) du gisement aquatanien de Saint-Gerand-le-Puy (Allier, France): Revision systematique. *Palaeovertebrata* **14**, 33–115 (1984).

216. P. Švec, Lower Miocene birds from Dolnice (Cheb Basin), western Bohemia. *Časopis pro Mineralogii a Geologii* **25**, 377–387 (1980).

217. G. Mayr, A partial skeleton of a new fossil loon (Aves, Gaviiformes) from the early Oligocene of Germany with preserved stomach content. *J. Ornithol.* **145**, 281–286 (2004). doi:10.1007/s10336-004-0050-9

218. J. Cheneval, A fossil shearwater (Aves: Procellariiformes) from the Upper Oligocene of France and the Lower Miocene of Germany. *Courier Forschungsinstitut Senckenberg* **181**, 187–198 (1995).

219. G. Mayr, D. S. Peters, S. Rietschel, Petrel-like birds with a peculiar foot morphology from the Oligocene of Germany and Belgium (Aves: Procellariiformes). *J. Vertebr. Paleontol.* **22**, 667–676 (2002). doi:10.1671/0272-4634(2002)022[0667:PLBWAP]2.0.CO;2

220. S. L. Olson, A Lower Eocene frigatebird from the Green River Formation of Wyoming (Pelecaniformes: Fregatidae). *Smithson. Contrib. Paleobiol.* **35**, 1–33 (1977). doi:10.5479/si.00810266.35.1

221. R. A. Cushman, Palynostratigraphy and age of the Green River Formation in Fossil Basin, Wyoming. National Park Service Paleontological Research **3**, 68–72 (1998).

222. G. Mayr, A skull of a new pelecaniform bird from the Middle Eocene of Germany. *Acta Palaeontol. Pol.* **47**, 507–512 (2002).

223. G. Mayr, A small representative of the Phalacrocoracoidea (cormorants and anhingas) from the Late Oligocene of Germany. *Condor* **109**, 929–942 (2007). doi:10.1650/0010-5422(2007)109[929:ASROTP]2.0.CO;2

224. K. E. Slack, C. M. Jones, T. Ando, G. L. Harrison, R. E. Fordyce, U. Arnason, D. Penny, Early penguin fossils, plus mitochondrial genomes, calibrate avian evolution. *Mol. Biol. Evol.* **23**, 1144–1155 (2006). Medline doi:10.1093/molbev/msj124

225. A. Milne-Edwards, Sur les oiseaux fossiles des dépots éocènes de phosphate de chaux du Sud de la France. *Comptes Rendus du Second Congrès Ornithologique International Budapest* 60–80 (1892).

226. C. J. O. Harrison, "The herons (Ardeidae) of the Old World Lower Tertiary," *Tertiary Research Spec. Pap. no. 5*, 11–17 (1979).

227. P. D. Gingerich, "Early Eocene bats (Mammalia, Chiroptera) and other vertebrates in freshwater limestones of the Willwood Formation, Clark's Fork Basin, Wyoming," in *Contributions from the Museum of Paleontology* (University of Michigan, Ann Arbor, MI, 1987) vol. 27, pp. 275–320.

228. E. Wittich, Beiträge zur Kenntnis der Messeler Braunkohle und ihrer Fauna. *Abhandlungen der großherzoglich Hessischen geologischen Landesanstalt zu Darmstadt* **3**, 79–147 (1898).

229. D. S. Peters, Die "Schnepfenralle" *Rhynchaeites messelensis* Wittich 1898 ist ein Ibis. *J. Ornithol.* **124**, 1–27 (1983). doi:10.1007/BF01650658

230. G. Mayr, A contribution to the osteology of the Middle Eocene ibis *Rhynchaeites* messelensis (Aves: Threskiornithidae: Rhynchaeitinae nov. *subfam.*). *Neues Jahrb. Geol. Palaontol., Monatsh.* **8**, 501–512 (2002).

231. P. V. Rich, D. J. Bohaska, The world's oldest owl: A new strigiform from the Paleocene of southwestern Colorado. *Smithson. Contrib. Paleobiol.* **27**, 87–93 (1976).

232. C. Mourer-Chauviré, A large owl from the Palaeocene of France. *Palaeontology* **37**, 339–348 (1994).

233. G. Mayr, An owl from the Paleocene of Walbeck, Germany. Mitteilungen aus dem Museum für Naturkund in Berlin. *Geowissenschaftliche Reihe Foss. Rec.* **5**, 283–288 (2002). doi:10.5194/fr-5-283-2002

234. A. Wetmore, Another fossil owl from the Eocene of Wyoming. *Proc. U.S. Natl. Mus.* **85**, 27–29 (1938). doi:10.5479/si.00963801.85-3031.27

235. C. Mourer-Chauviré, Les Horusornithidae nov. fam., Accipitriformes (Aves) à articulation intertarsienne hyperflexible de l'Éocène du Quercy. *Geobios* **24**, 183–192 (1991). doi:10.1016/S0016-6995(66)80023-2

236. C. Mourer-Chauviré, Le gisement du Bretou (Phosphorites du Quercy), Tarn-et-Garonne, (France) et sa faune de vertébrés de l'Éocène supérieur, II. Oiseaux. *Sonder-Abdruck aus Palaeontographica. Beiträge zur Naturgeschichte der Vorzeit (A)* **205**, 29–50 (1988).

237. S. Legendre, B. Bachelet, The numerical ages: A new method of datation applied to the Paleogene mammalian localities from Southern France. *Newslett. Stratigr.* **29**, 137–158 (1993).

238. N. Schmidt-Kittler, Ed. "European reference levels and correlation tables," in *Münchner Geowischenschaftliche Abhandlungen (A): Geologie und Paläontologie* (International Symposium on Mammalian Biostratigraphy and Paleoecology of the European Paleogene, Mainz, Germany, 18 to 21 February 1987), vol. 10, pp. 13-19.

239. J. A. Allen, Description of a fossil passerine bird from the insect-bearing shales of Colorado. *Bull. U.S. Geol. Geogr. Surv. Territ.* **4**, 443–445 (1878).

240. D. T. Ksepka, J. A. Clarke, Affinities of *Palaeospiza bella* and the phylogeny and biogeography of mousebirds (Coliiformes). *Auk* **126**, 245–259 (2009). doi:10.1525/auk.2009.07178

241. G. Mayr, A new mousebird (Coliiformes: Coliidae) from the Oligocene of Germany. *J. Ornithol.* **141**, 85–92 (2000). doi:10.1007/BF01651775

242. G. Mayr, A new species of *Plesiocathartes* (Aves: Leptosomidae) from the Middle Eocene of Messel, Germany. *PaleoBios* **22**, 10–20 (2002).

243. G. Mayr, The Madagascan, "Cuckoo-roller" (Aves: Leptosomidae) is not a roller – notes on the phylogenetic affinities and evolutionary history of a "living fossil". *Acta Ornithologica* **43**, 226–230 (2008). doi:10.3161/000164508X395360

244. I. Weidig, The first New World occurrence of the Eocene bird *Plesiocathartes* (Aves? Leptosomidae). *Paläeontologische Zeitschrift* **80**, 230–237 (2006). doi:10.1007/BF02988439

245. A. V. Kristoffersen, An early Paleogene trogon (Aves: Trogoniformes) from the Fur Formation, Denmark. *J. Vertebr. Paleontol.* **22**, 661–666 (2002). doi:10.1671/0272-4634(2001)022[0661:AEPTAT]2.0.CO;2

246. G. Mayr, New trogons from the early Tertiary of Germany. *Ibis* **147**, 512–518 (2005). doi:10.1111/j.1474-919x.2005.00421.x

247. G. Mayr, A tiny barbet-like bird from the Lower Oligocene of Germany: The smallest species and earliest substantial fossil record of the Pici (woodpeckers and allies). *Auk* **122**, 1055–1063 (2005). doi:10.1642/0004-8038(2005)122[1055:ATBBFT]2.0.CO;2

248. P. Ballmann, Vögel aus der altburdigalen Spaltenfüllung von Wintershof (West). *Inst. Pal. U. Host. Geol. Univ. Munchen* **18162**, 39–89 (1967).

249. P. Brodkorb, Catalogue of Fossil Birds Part 4 (Columbiformes through Piciformes). *Bull. Fla. State Mus. Biol. Sci*. **15**, 259 (1971).

250. P. Ballmann, Vögel aus der altburdigalen Spaltebfüllung von Wintershof (West) bei Eichstätt in Bayern. *Zitteliana* **1**, 5–60 (1969).

251. G. Mayr, Tiny Hoopoe-like birds from the Middle Eocene of Messel (Germany). *Auk* **117**, 964–970 (2000). doi:10.1642/0004-8038(2000)117[0964:THLBFT]2.0.CO;2

252. G. Mayr, New specimens of the Eocene Messelirrisoridae (Aves: Bucerotes), with comments on the preservation of uropygial gland waxes in fossil birds from Messel and the phylogentic affinities of Bucerotes. *Paläeontologische Zeitschrift* **80**, 390–405 (2006). doi:10.1007/BF02990211

253. S. L. Olson, An early Eocene oilbird from the Green River Formation of Wyoming (Caprimulgiformes: Steatornithidae). *Documents des Laboratoires de Géologie de Lyon* **99**, 57–70 (1987).

254. G. Mayr, The Palaeogene Old World potoo *Paraprefica* Mayr, 1999 (Aves, Nyctibiidae): Its osteology and affinities to the New World Preficinae Olson, 1987. *J. Syst. Palaeontology* **3**, 359–370 (2005). doi:10.1017/S1477201905001653

255. G. Mayr, Caprimulgiform birds from the Middle Eocene of Messel (Hessen, Germany). *J. Vertebr. Paleontol.* **19**, 521–532 (1999). doi:10.1080/02724634.1999.10011162

256. C. J. O. Harrison, A revision of the fossil swifts (Vertebrata, Aves, suborder Apodi), with descriptions of three new genera and two new species. *Mededelingen van de Werkgroep voor Tertiaire en Kwartaire Geologie* **21**, 157–177 (1984).

257. G. Mayr, Reappraisal of *Eocypselus* – a stem group apodiform from the early Eocene of Northern Europe. *Palaeobiodiversity and Palaeoenvironments* **90**, 395–403 (2010). doi:10.1007/s12549-010-0043-z

258. G. J. Dyke, D. M. Waterhouse, A. V. Kristoffersen, Three new fossil landbirds from the early Paleogene of Denmark. *Bull. Geol. Soc. Den.* **51**, 47–56 (2004).

259. D. S. Peters, Ein neuer Segler aus der Grube Messel und seine Bedeutung fur den Status der Aegialornithidae (Aves: Apodiformes). *Senckenberg Lethaea* **66**, (1985).

260. G. Mayr, Old World fossil record of modern-type hummingbirds. *Science* **304**, 861–864 (2004). Medline doi:10.1126/science.1096856

261. G. Mayr, New specimens of the early Oligocene Old World hummingbird *Eurotrochilus inexpectatus*. *J. Ornithol.* **148**, 105–111 (2007). doi:10.1007/s10336-006-0108-y

262. D. S. Peters, *Idiornis tuberculata* n. spec., ein weiterer ungewöhnlicher Vogel aus der Grube Messel (Aves: Gruiformes: Cariamidae: Idiornithinae). *Acta Palaeornithologica. Courier Forschungsinstitut Senckenberg* **181**, 107–119 (1995).

263. C. Mourer-Chauviré, Paleogene avian localities of France. *Acta Universitatis Carolinae Geologica* **39**, 567–589 (1996).

264. G. Mayr, C. Mourer-Chauviré, Three dimensionally preserved cranial remains of *Elaphrocnemus* (Aves, Cariamae) from the Paleogene Quercy fissure fillings of France. *Neues Jahrb. Geol. Palaontol. Monatsh.* **2006**, 15–27 (2006).

265. H. M. F. Alvarenga, in *Coletânea de Trabalhos Paleontológicos: Trabalhos Apresentados no VIII Congresso Brasileiro de Paleontologia, 1983* (Ministério de Minas e Energia - Departamento Nacional de Produção Mineral, Série Geologia 27, 1985), vol. Paleontologia e Estratigrafia 2, pp. 17–20.

266. W. E. Boles, The world's oldest songbird. *Nature* **374**, 21–22 (1995). doi:10.1038/374021b0

267. W. E. Boles, Fossil Songbirds (Passeriformes) from the Early Eocene of Australia. *Emu* **97**, 43–50 (1997). doi:10.1071/MU97004

268. T. H. Worthy, S. J. Hand, J. M. T. Nguyen, A. J. D. Tennyson, J. P. Worthy, R. P. Scofield, W. E. Boles, M. Archer, Biogeographic and phylogenetic implications of an early Miocene wren (Aves: Passeriformes: Acanthisittidae) from New Zealand. *J. Vertebr. Paleontol.* **30**, 479–498 (2010). doi:10.1080/02724631003618033

269. A. Elzanowski, W. E. Boles, Australia's oldest Anseriform fossil: A quadrate from the Early Eocene Tingamarra Fauna. *Palaeontology* **55**, 903–911 (2012). doi:10.1111/j.1475-4983.2012.01166.x

270. G. Mayr, A. Manegold, The oldest European fossil songbird from the early Oligocene of Germany. *Naturwissenschaften* **91**, 173–177 (2004). Medline doi:10.1007/s00114-004-0509-9

271. P. Brodkorb, Catalogue of Fossil Birds Part 5 (Passeriformes). *Bull. Fla. State Mus. Biol. Sci.* **23**, 145 (1978).

272. P. Brodkorb, Neogene fossil jays from the Great Plains. *Condor* **74**, 347–349 (1972). doi:10.2307/1366596

273. T. Warnow, Tree compatibility and inferring evolutionary history. *J. Algorithms* **16**, 388–407 (1994). doi:10.1006/jagm.1994.1018

274. R. A. Becker, J. M. Chambers, A. R. Wilks, *The New S Language* [Wadsworth & Brooks/Cole (for S version), Pacific Grove, CA, 1988].

275. D. W. Scott, *Multivariate Density Estimation. Theory, Practice and Visualization* (Wiley, New York, 1992).

276. G. Zhang, B. Li, C. Li, M. T. P. Gilbert, E. D. Jarvis, J. Wang; The Avian Genome Consortium, Genomic data of the Avian Phylogenomics Project I. *GigaScience* **3**, 26 (2014); 10.1186/2047-217X-3-26.

277. E. D. Jarvis, S. Mirarab, A. J. Aberer, B. Li, P. Houde, C. Li, S. Y. W. Ho, B. C. Faircloth, B. Nabholz, J. T. Howard, A. Suh, C. C. Weber, R. R. da Fonseca, A. Alfaro-Núñez, N. Narula, L. Liu, D. Burt, H. Ellegren, S. V. Edwards, A. Stamatakis, D. P. Mindell, J. Cracraft, E. L. Braun, T. Warnow, W. Jun, M. T. P. Gilbert, G. Zhang; The Avian Phylogenomics Consortium, Phylogenomic analyses data of the Avian Phylogenomics Project. *GigaScience* 10.5524/101041 (2014).